CONCERNING THE ROLE OF DEFORMATION TWINNING AND DYNAMIC STRAIN AGING ON THE STRESS-STRAIN CURVES OF ALPHA TITANIUM

By

A. T. Santhanam

A Dissertation Presented to the Graduate Council
of the University of Florida
in Partial Fulfillment of the Requirements for the
Degree of Doctor of Philosophy

UNIVERSITY OF FLORIDA

1971


University of Florida
1853

ACKNOWLEDGEMENTS

The author wishes to express his sincere gratitude to Dr. R. E. Reed-Hill for his patience, guidance and encouragement, without which this dissertation would not have been possible. He also thanks Drs. C. S. Hartley, J. J. Hren and E. H. Hadlock for serving on his supervisory committee. Special thanks are due to Dr. V. Ramachandran and Mr. M. S. Ananth for their valuable assistance in computer programming. The help and encouragement received from Drs. D. H. Baldwin and R. A. Mayor, and other graduate students, S. N. Monteiro, A. M. Garde and P. R. Cetlin, have been invaluable. The author is also grateful to Dr. F. N. Rhines and all the members of the faculty and staff of the Department of Metallurgical and Materials Engineering.

The financial support of the U. S. Atomic Energy Commission is gratefully acknowledged.

A special note of appreciation is due to his wife, Mohana, for her encouragement, love and understanding during the difficult time of being the wife of a student.

TABLE OF CONTENTS

TABLE OF CONTENTS (cont.)

LIST OF TABLES

LIST OF FIGURES

LIST OF FIGURES (cont.)

LIST OF FIGURES (cont.)

LIST OF FIGURES (cont.)

LIST OF FIGURES (cont.)

Abstract of Dissertation Presented to the Graduate Council of the University of Florida in Partial Fulfillment of the Requirements for the Degree of Doctor of Philosophy

CONCERNING THE ROLE OF DEFORMATION TWINNING AND DYNAMIC STRAIN AGING ON THE STRESS-STRAIN CURVES OF ALPHA TITANIUM

By

A. T. Santhanam

August, 1971

Chairman: Dr. Robert E. Reed-Hill
Major Department: Metallurgical and Materials Engineering

The tensile behavior of commercial purity titanium is strongly influenced by the deformation temperature and the strain rate. The shapes of the stress-strain curves vary widely over the entire range of test temperatures (77° to 1073°K) and strain rates (2.7×10^{-6} to 2.7×10^{-1} sec^{-1}) employed in the present study. For example, at 77°K the true stress-true strain curve is linear to very large strains. These strains are nearly twice that observed at room temperature. A quantitative microstructure study on specimens deformed at 77°K showed a high volume fraction of twins. It is believed that the high work hardening rate that persists up to large strains at 77°K is related to twinning and that it could result from either or all of the following factors: lattice reorientation due to twinning,

the role of twinning on the Petch effect, and the effect of twinning on the dynamic recovery.

Between 550° and 850°K dynamic strain aging greatly influences the stress-strain behavior. It makes the yield stress temperature and strain rate insensitive, causes ductility anomalies similar to the blue brittle effect in steel, lowers the strain rate sensitivity, and produces maxima in the work hardening rates that are temperature and strain rate dependent. It is demonstrated that the "blue brittle" effect in titanium is not a true embrittlement phenomenon. Rather, it is a necking phenomenon that promotes necking to occur at small strains. Also, the strain associated with the neck is very small at the ductility minimum temperature. On the other hand, just above the ductility minimum temperature there is a very rapid rise in the total elongation but most of this occurs during necking, resulting in an extended or diffuse neck. The conditions that cause diffuse necks in commercial titanium just above the blue brittle temperature are different from those that produce this type of neck in superplasticity. In superplasticity the necking phenomenon is associated with a direct dependence of the flow stress on the strain rate, whereas in the present case it is primarily due to the rate dependent work hardening associated with dynamic strain aging.

Strain rate change tests also do not have the same effect on the shape of the stress-strain diagram at all temperatures. Only within rather limited temperature ranges does the flow stress change smoothly and continuously to a value characteristic of the new deformation rate. In dynamic strain aging a rate increase produces a small transient flow stress maximum similar in appearance to a yield point, while equivalent minima are observed on a decrease in rate. An analysis using a modified Johnston-Gilman approach has shown that the transients can be obtained by assuming that the mobile dislocation density increases more rapidly with increasing strain rate and similarly decreases with decreasing strain rate during a time interval at which transients are observed.

INTRODUCTION

In the past decade titanium has reversed its position in the metals field from that of a rare and expensive metal to a major structural material for a variety of applications such as airframe systems, spaceships and mass transportation vehicles. The ever-increasing technological importance of this metal has created a need for a more complete understanding of its mechanical behavior. The most widely employed test for studying mechanical behavior is the tensile test. This simple test yields data that are widely used for design purposes and also for understanding the rate controlling dislocation mechanisms associated with thermally activated deformation as well as the work hardening behavior. While studies of mechanical behavior of titanium have been carried out in the past, they have often been restricted both with regard to testing temperature interval and deformation rate, with the result that a broad picture of the deformation behavior has been difficult to obtain. Therefore, an attempt is made here to investigate the plastic deformation behavior of commercial purity titanium over the almost complete range of stability of its hexagonal close packed alpha phase and over a wide range of deformation rates.

The present work is an offshoot of a research program initiated by Reed-Hill[1] of the University of Florida to study the flow stress components during tensile deformation of alpha titanium. During the course of this investigation, it was found that if one plotted the logarithm of yield stress against absolute temperature, there was a general linear dependence except for two deviations, one centered around 250°K and the other lying between 550° and 800°K. In both these regions, anomalies were found in strain rate sensitivity, work hardening behavior and the effect of strain rate changes on the shape of the stress-strain curves. In particular, tensile specimens deformed at 673°K showed much greater work hardening when deformed at slower rates than when deformed at faster rates. The results were rationalized in terms of total and mobile dislocation densities that might become functions of strain rate, probably as a result of dynamic strain aging.[2]

The above results implied that detailed investigation of the work hardening behavior of alpha titanium might uncover some important new information. This has indeed been true since it led to the discovery of the existence of maxima in work hardening rate that are strain rate and temperature dependent. It will be shown that the work hardening maxima, together with other observations like a low strain rate sensitivity, the Portevin-Le Chatelier effect and a temperature and strain rate insensitive yield stress in the

temperature range between 550° and 800°K, are strong manifestations of dynamic strain aging. The role of dynamic strain aging on other aspects of plastic deformation of titanium will be discussed. In particular, the shapes of the stress-strain curves as affected by dynamic strain aging and dynamic recovery will be discussed.

Attention will also be given to the important role played by deformation twinning in the plastic deformation of titanium at low temperatures. An analysis will be presented that will bring out the possible close connection between deformation twinning and the high ductility observed at the temperature of liquid nitrogen.

It is also the purpose of this dissertation to develop a consistent theory that will explain the various shapes of the stress-strain curves obtained upon a strain rate change. The experimental observations at various temperatures will be compared to the theoretical curves calculated from the theory of dislocation dynamics to determine what values of the various parameters such as dislocation multiplication rate and dislocation velocity exponent are needed to reproduce the experimentally observed results.

CHAPTER I

PREVIOUS INVESTIGATIONS

1.1. Deformation Modes of Alpha Titanium

Titanium slips primarily on the $\{10\bar{1}0\}$ planes in the $[11\bar{2}0]$ direction. Slip on the $\{10\bar{1}1\}\langle 11\bar{2}0\rangle$ system also occurs, but it is less important, and in coarse grained specimens of commercial titanium, used by Rose, Dubé and Alexander,[3] occurred only when all three $\{10\bar{1}0\}$ systems were operative. Anderson, Jillson and Dunbar,[4] using large titanium crystals, found prismatic slip $\{10\bar{1}0\}\langle 11\bar{2}0\rangle$ to be the most active, but did not observe $\{10\bar{1}1\}$. However, they reported basal slip for a limited range of orientations. Slip on the basal plane in the $[11\bar{2}0]$ direction has also been reported by Churchman[5] for the single crystals of commercial pure titanium. Churchman also reported that the critical resolved shear stress for slip on the basal plane is greater than that for $\{10\bar{1}1\}$ slip, which in turn is greater than that for $\{10\bar{1}0\}$ slip.

Rosi, Perkins and Seigle[6] studied the deformation mechanisms of coarse grained iodide titanium specimens and found that at 77°K slip takes place only on $\{10\bar{1}0\}$ planes in a $[11\bar{2}0]$ direction and that at 773° and 1073°K prismatic slip was still the primary form with $\{10\bar{1}1\}$ pyramidal slip

being of secondary importance. The work of McHargue and Hammond[7] on iodide titanium specimens at 1088°K also showed that slip on the $\{10\bar{1}0\}$ planes was still the predominant mode of deformation although $\{10\bar{1}1\}$ pyramidal slip occurred much more frequently than at room temperature. Cass[8] and Williams and Blackburn[9] studied dislocation substructures in deformed commercial purity titanium and identified dislocations with $\vec{c}+\vec{a}$ Burgers vectors.

Deformation twinning also plays an important role in the plastic deformation of titanium, particularly at low temperatures. Thus, Rosi, Dubé and Alexander[3] and Rosi, Perkins and Seigle[6] have identified twins on $\{10\bar{1}2\}$, $\{11\bar{2}1\}$, $\{11\bar{2}2\}$, $\{11\bar{2}3\}$, and $\{11\bar{2}4\}$ planes. More recently, Lii, Ramachandran and Reed-Hill[10] reported twins on $\{11\bar{2}2\}$ and $\{11\bar{2}4\}$ planes. Occasionally $\{10\bar{1}2\}$ twins were also found by these authors. The volume fraction of twins was found to decrease with increasing temperature. The work of Kula and DeSisto[11] also showed the presence of deformation twins in coarse grained commercial purity titanium specimens deformed at 4°K. On the other hand, Orava, Stone and Conrad[12] have reported that in very fine grained commercial purity titanium, twinning was not observed even after strains beyond 10 percent at 77°K. This disagreement in the literature concerning the existence and importance of twinning in the low temperature deformation of titanium has very recently been resolved by Garde and Reed-Hill[13] who showed

metallographically that deformation twinning occurs significantly and is important in the low temperature deformation of swaged high purity titanium specimens even at a grain size of 2.4μ.

1.2. Low Temperature Deformation

The preceding paragraph showed that twinning is an important deformation mode in titanium below room temperature. That twinning not only occurs in titanium at low temperatures, but has a significant effect on the mechanical behavior of this metal, can be seen in the early work of Rosi and Perkins[14] and the later work of Wasilewski.[15] In the experiments of Rosi and Perkins,[14] cylindrical tensile specimens of commercial purity titanium became elliptical in cross-section after deformation. The observed ellipticity decreased with decreasing deformation temperature, suggesting a shift in the deformation mode. Lii, Ramachandran and Reed-Hill[10] have demonstrated from quantitative microstructure studies that the observed variation of strain anisotropy with temperature in titanium can be accounted for by variations in the volume fraction of the twinned material.

There is also evidence that deformation twinning could affect the shape of the stress-strain curves at low temperatures. Wasilewski[15] reported that when a titanium specimen is deformed in tension at 77°K, a linear true stress-true

strain curve results. He suggested that this "laminar flow" could result from a combination of slip and twinning. Wasilewski further concluded that the large uniform elongation observed at 77°K was related to the ease with which twinning occurred in this metal. Recent results in our laboratory at the University of Florida have also confirmed the close connection between deformation twinning and linear stress-strain curve in transverse zirconium specimen deformed at 77°K.

1.3. Elevated Temperature Properties

The short-time tensile characteristics of alpha titanium have been under study for nearly two decades. Among these early studies,the first systematic investigation was made by Rosi and Perkins[14] on commercial titanium (0.05 wt. % C, 0.08 wt. % N, 0.10 wt. % Fe). Their results indicated the occurrence of strain again phenomena in this metal. Yield drops were observed in a narrow temperature interval, 390° to 555°K. The total elongation to failure decreased between 500° and 725°K. A slight depression in the stress-strain curve near the ultimate stress at 725°K was referred to as discontinuous yielding. A higher work hardening rate at this temperature compared to that at a lower temperature, 625°K, was reported. But its significance was not analyzed.

The work of Kiessel and Sinnott[16] on commercial titanium confirmed the findings of Rosi and Perkins that titanium

exhibits strain aging characteristics. Yield points and serrations in the stress-strain curve were observed in a temperature range of 373° to 615°K and the elongation decreased in the range of 590° to 700°K. Kiessel and Sinnott[14] also observed strain aging effects in creep tests using titanium containing 0.037 wt. % carbon. Following an initial decrease between 20° and 100°C, the stress required to maintain a chosen creep rate increased to a maximum at approximately 200°C. Turner and Roberts[17] attributed a peak in the fatigue limit to ultimate tensile strength ratio of titanium at 523°K to a weak dynamic aging effect. On the other hand, Suiter[18] expressed doubts about the occurrence of strain aging in titanium, although his commercial purity metal and a wide variety of solid solutions containing oxygen, nitrogen, carbon, aluminum, tin and zirconium all showed pronounced ductility minima similar to the blue brittle effect in steel. Then, in 1966, Orava, Stone and Conrad[12] published an extensive set of tensile data on fine grained titanium specimens of commercial purity, but the role of strain aging was largely ignored. In a recent review paper on strain aging of metals, Baird[19] points out that the yield point and strain aging effects in titanium are consistent with a relatively weak interaction between interstitial atoms and dislocations in titanium. There thus exist in literature conflicting opinions about the role of dynamic strain aging in titanium. It will

be shown in the following chapters that contrary to the popular belief dynamic strain aging plays a very significant role in the plastic deformation of commercial purity titanium.

It will be well at this point to consider the general theory of flow stress components and their relation to dynamic strain aging.

1.4. The Flow Stress of Metals

Recent advances in dislocation theory make it possible to define the stress required to deform a metal in terms of experimentally determined parameters. The flow stress of a nearly pure metal can thus be divided into two basic components. One component is that required to force dislocations past obstacles, whose stress field interactions with moving dislocations are short-range in character. This involves thermal activation. The other flow stress component is the stress required to move dislocations against the opposing long-range stress fields inside the metal. This is not believed to be directly controlled by thermal activation. This component of flow stress is temperature independent except for a small indirect dependence through the temperature variation of shear modulus. Monteiro et al.[20] proposed that these two flow stress components be called σ_s and σ_ℓ in conformity with their short- and long-range

character. Thus,

$$\sigma = \sigma_s + \sigma_\ell \tag{1}$$

The studies of Johnston and Gilman,[21] Johnston[22] and Hahn[23] have helped to more clearly define the thermally activated component. Thus σ_s may be expressed in the form

$$\sigma_s = D \left[\frac{\dot{\varepsilon}}{\rho_m b}\right]^{1/m} \tag{2}$$

where $\dot{\varepsilon}$ is the strain rate, ρ_m is the mobile dislocation density, b is the Burgers vector, m is the dislocation velocity exponent, and D is a constant. σ_s is not a strong function of dislocation density and does not vary appreciably with strain. On the other hand, thin film electron microscopy studies have shown that the long-range flow stress component, σ_ℓ, is largely determined by the total dislocation density developed as a result of deformation in the metal. For example, Dingley and McLean's[24] data on 99.97 percent pure iron have shown the following functional relationship between σ and ρ, the total dislocation density.

$$\sigma = \sigma_o + k\rho^{1/2} \tag{3}$$

where σ_o and k are constants. In this equation, the second term, $k\rho^{1/2}$, can be considered to represent the long-range flow stress component, σ_ℓ. Then σ_o must represent the short-range component, σ_s. Reed-Hill[1] has demonstrated

that this is nearly true in commercial purity titanium.

1.5. The Temperature Dependence of Flow Stress

Reed-Hill[1] has pointed out, citing evidence from at least six papers,[15,25-29] that the flow stress at small strains in metals measured at a constant strain rate tends to vary exponentially with the absolute temperature according to the equation

$$\sigma_s = \sigma_{s_o} e^{-BT} \tag{4}$$

or

$$\ln \frac{\sigma_s}{\sigma_{s_o}} = -BT \tag{5}$$

where σ_s is the flow stress at small strains, σ_{s_o} is the flow stress at 0°K, B is a constant, and T is the absolute temperature. The subscript, s, has been added to σ to indicate that the measured flow stress at very small strains in coarse grained metals probably conforms to the thermally activated stress component. An excellent example of such a relationship can be seen in Carreker's data[25] on coarse grained high purity platinum wires. This is shown in Fig. 1 which gives the stress to produce several strain rates at a strain of 0.01 as a function of temperature. The strain rates vary from 10^{-6} to 10^{0} sec^{-1}. Note that the data conform very well to Eq. (5). The slope B decreases with

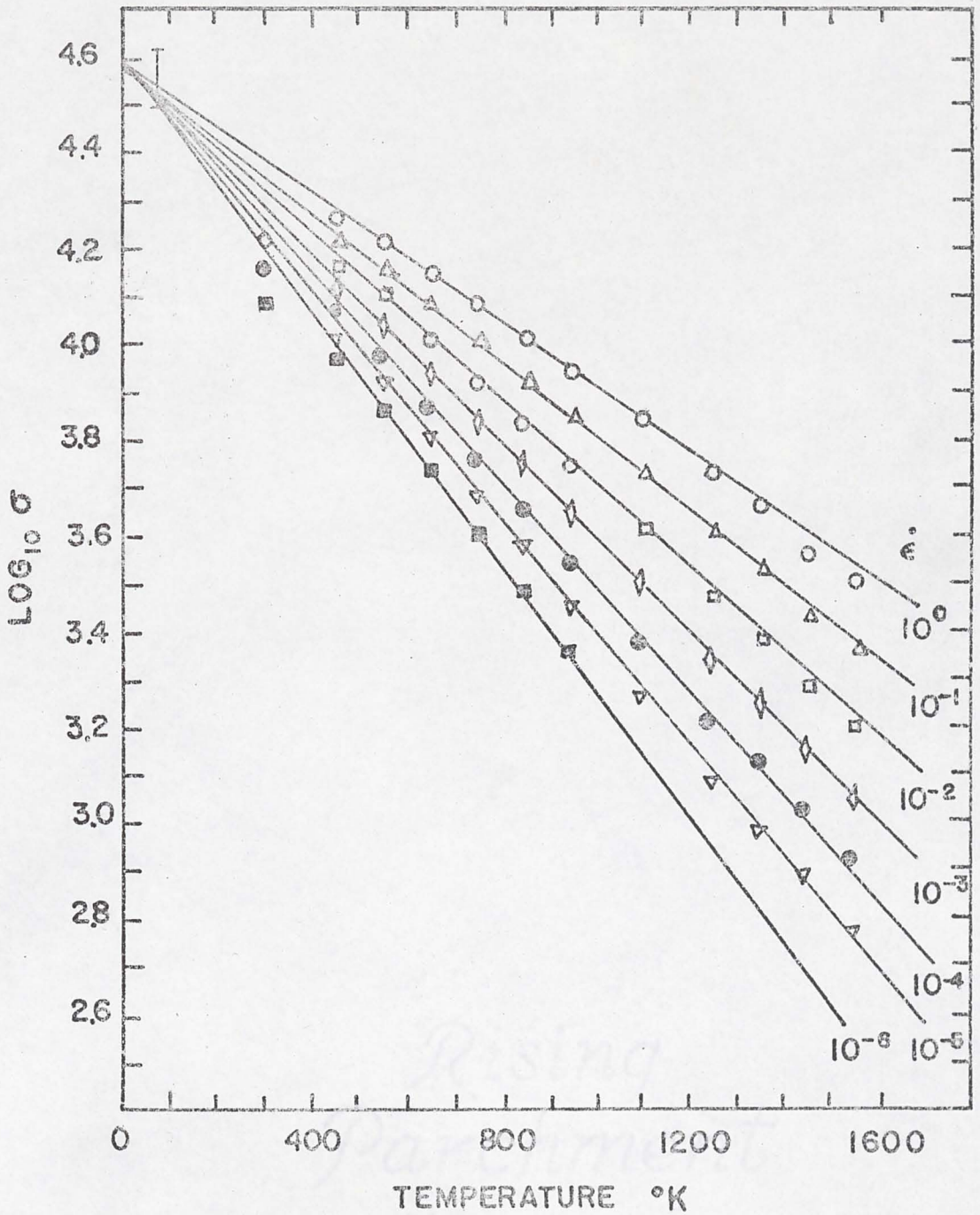

Fig. 1. The stress to produce several strain rates at a strain of 0.01 as a function of temperature for platinum. Data of Carreker.[25]

increasing strain rate, but all seven straight lines meet at zero degree absolute.

Equation (5) has also been found to be valid for low interstitial titanium by Wasilewski.[15] However, his data cover only a small temperature interval, from 77° to 623°K.

1.6. The Activation Energy for Plastic Flow

Let us assume that the thermal activation involved in the plastic flow of metals can be described by ordinary rate theory with an activation energy, H. The strain rate is then given by

$$\dot{\varepsilon} = A \exp(-H/RT) \tag{6}$$

where A includes a frequency factor that depends on the nature of the obstacle, the mobile dislocation density and the Burgers vector, and R is the universal gas constant. Solving Eq. (6) for H,

$$H = -RT \ln(\dot{\varepsilon}/A) \tag{7}$$

Comparing Eqs. (5) and (7), we can write

$$H = H_o \ln\left[\frac{\sigma_{s_o}}{\sigma_s}\right] \tag{8}$$

1.7. The Temperature Dependence of the Strain Rate Sensitivity Parameter

Substitution of Eq. (8) into Eq. (6) gives

$$\dot{\varepsilon} = A \exp\left[-\frac{H_o}{RT} \ln \frac{\sigma_{s_o}}{\sigma_s}\right] = A\left[\frac{\sigma_s}{\sigma_{s_o}}\right]^{H_o/RT} \tag{9}$$

The applied strain rate is related to the thermally activated flow stress component through a power law. If we now assume that A is independent of temperature and strain rate, Eq. (9) leads to

$$\frac{\dot{\varepsilon}_2}{\dot{\varepsilon}_1} = \left(\frac{\sigma_{s_2}}{\sigma_{s_1}}\right)^{H_o/RT} \tag{10}$$

where $\dot{\varepsilon}_2$ and $\dot{\varepsilon}_1$ are two different strain rates and σ_{s_2} and σ_{s_1} are the corresponding thermally activated flow stress components.

The strain rate sensitivity parameter, n, is defined as

$$n = \left(\frac{\partial \ln \sigma_s}{\partial \ln \dot{\varepsilon}}\right)_{\varepsilon,T} \tag{11}$$

This can be measured by direct strain rate change experiments at small strains where the long-range flow stress component would be expected to be small. The parameter n is computed from the following equation.

$$n = \frac{\ln \sigma_2/\sigma_1}{\ln \dot{\varepsilon}_2/\dot{\varepsilon}_1} \tag{12}$$

A comparison of Eq. (12) with Eq. (10) shows that the strain rate sensitivity parameter should be a linear function of temperature.

$$n = RT/H_o \tag{13}$$

This is in very good agreement with Carreker's data[25] on platinum shown in Fig. 2.

1.8. Dynamic Strain Aging

In recent years it is becoming increasingly apparent that the mechanical behavior of most commercial metals is affected by a process known as "strain aging." The term "strain aging" refers to an increase in flow stress on aging after or during straining. If aging occurs after straining, the phenomenon is called "static strain aging," and if aging occurs concurrently with straining it is referred to as "dynamic strain aging." Here we are primarily interested in the latter.

A classic example of manifestation of dynamic strain aging is "blue brittleness" in steel.[30] The name is derived from the fact that when steel is heated to about 200°C, it acquires an oxide coating that is bluish in color and is brittle when worked. Numerous investigators[31-38] have studied the dynamic strain aging phenomenon and have come to the conclusion that the loss of ductility is only one of

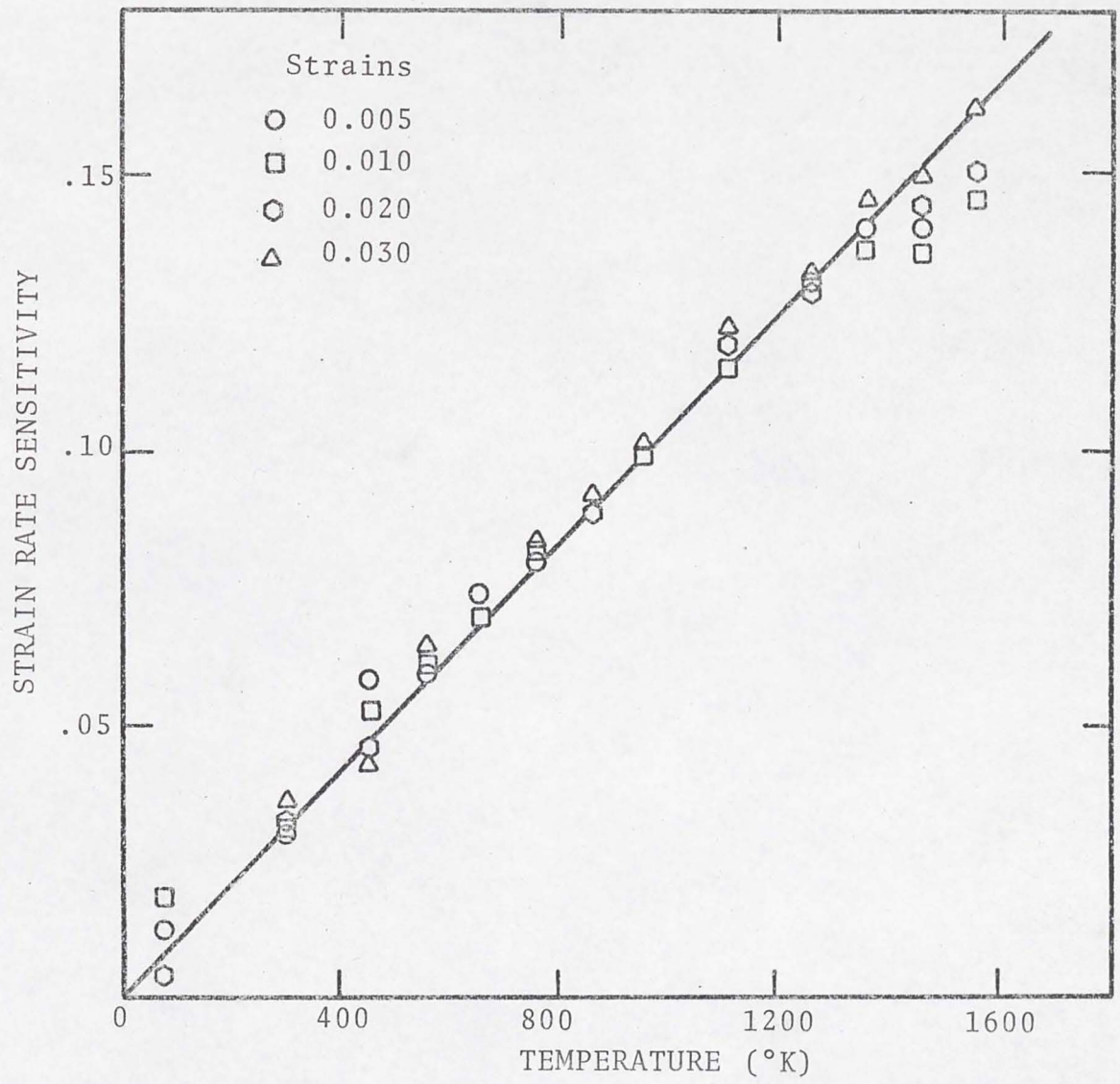

Fig. 2. Strain rate sensitivity of platinum as a function of absolute temperature. Data of Carreker.[25]

several aspects associated with dynamic strain aging. The other aspects of dynamic strain aging that have been identified are: 1) peaks or plateaus in flow stress-temperature diagrams, 2) abnormally low strain rate sensitivity, 3) discontinuous yielding or Portevin-Le Chatelier[39] phenomenon (serrated stress-strain curves), and 4) increased work hardening rates.

Excellent review papers[19,38] have been written on the subject and only the broad aspects will be considered here. Most of the effects observed in dynamic strain aging are qualitively explained as arising from the segregation of solute atoms to dislocations, pinning the latter or by providing increased frictional resistance to the motion of unpinned dislocations.[19] Both interstitial and substitutional solutes may be involved, but the high diffusion coefficients of the interstitial solutes and their high interaction energies with dislocations are believed to produce marked strain aging effects at comparatively low temperatures.

The temperature interval over which dynamic strain aging effects are most pronounced depends on the deformation rate. In mild steel, for example, at normal strain rates (10^{-4} sec^{-1}) it occurs near 200°C.[24,35,36] It can be made to occur at room temperature at very slow deformation rates (10^{-6} sec^{-1})[40,41] or at as high a temperature as 500°C when the strain rate is raised to 600 sec^{-1}.[32]

In the hexagonal close packed metal, zirconium, Ramachandran and Reed-Hill[42] observed a hardening peak at 675°K when the deformation rate was 1.3×10^{-5} sec^{-1}. This peak shifted to 875°K at a strain rate of 1.3×10^{-2} sec^{-1}. At a still higher rate comparable to that used in hot rolling, Simcoe and Thomas[43] have shown a flow stress peak in zirconium at 1073°K. Dynamic strain aging effects are therefore very significant over an extremely wide range of temperatures in metals in which strain aging has an important effect on the work hardening rate.

Although much work has been done on the Portevin-Le Chatelier[39] effect associated with dynamic strain aging, very little attention has been paid to the nature of the work hardening maxima, especially their dependence on the deformation rate. Furthermore, the shapes of the stress-strain curves obtained in the dynamic strain aging region have never been analyzed in detail. In the present investigation on the commercial purity titanium, attention is given to the above points and the role they play on other aspects of the plastic deformation of titanium.

CHAPTER II

EXPERIMENTAL METHODS

2.1. Material

Hot rolled and annealed commercial purity polycrystalline alpha titanium plate, obtained from Reactive Metals, Inc., was used as the base material in the present investigation. The plate texture was uniform with basal planes of the grains predominantly parallel to the rolling plane. The chemical analysis of the metal is as follows: carbon 200 ppm; nitrogen 100 ppm; oxygen 1,360 ppm; hydrogen 54-92 ppm; iron 1,600 ppm; and balance titanium. The average grain size, determined by the linear intercept method, was 16 microns. The microstructure of the as-received material is shown in Fig. 3.

2.2. Specimen Preparation

Only longitudinal (parallel to the rolling direction) specimens were used for the current study. Pieces 3/8 by 3/8 by 3 inches were sawed off from the plate as shown in Fig. 4. The direction of the rolling plane normal was marked on one end of each piece so that the former could be identified on the finished specimen. The pieces were

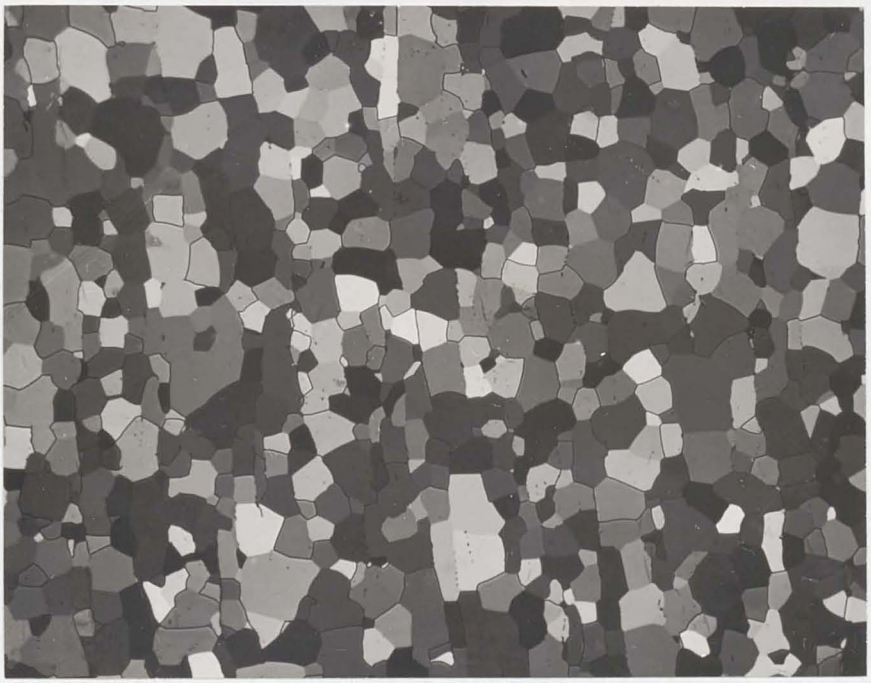

Fig. 3. Microstructure of the as-received annealed titanium. Magnification 250 times.

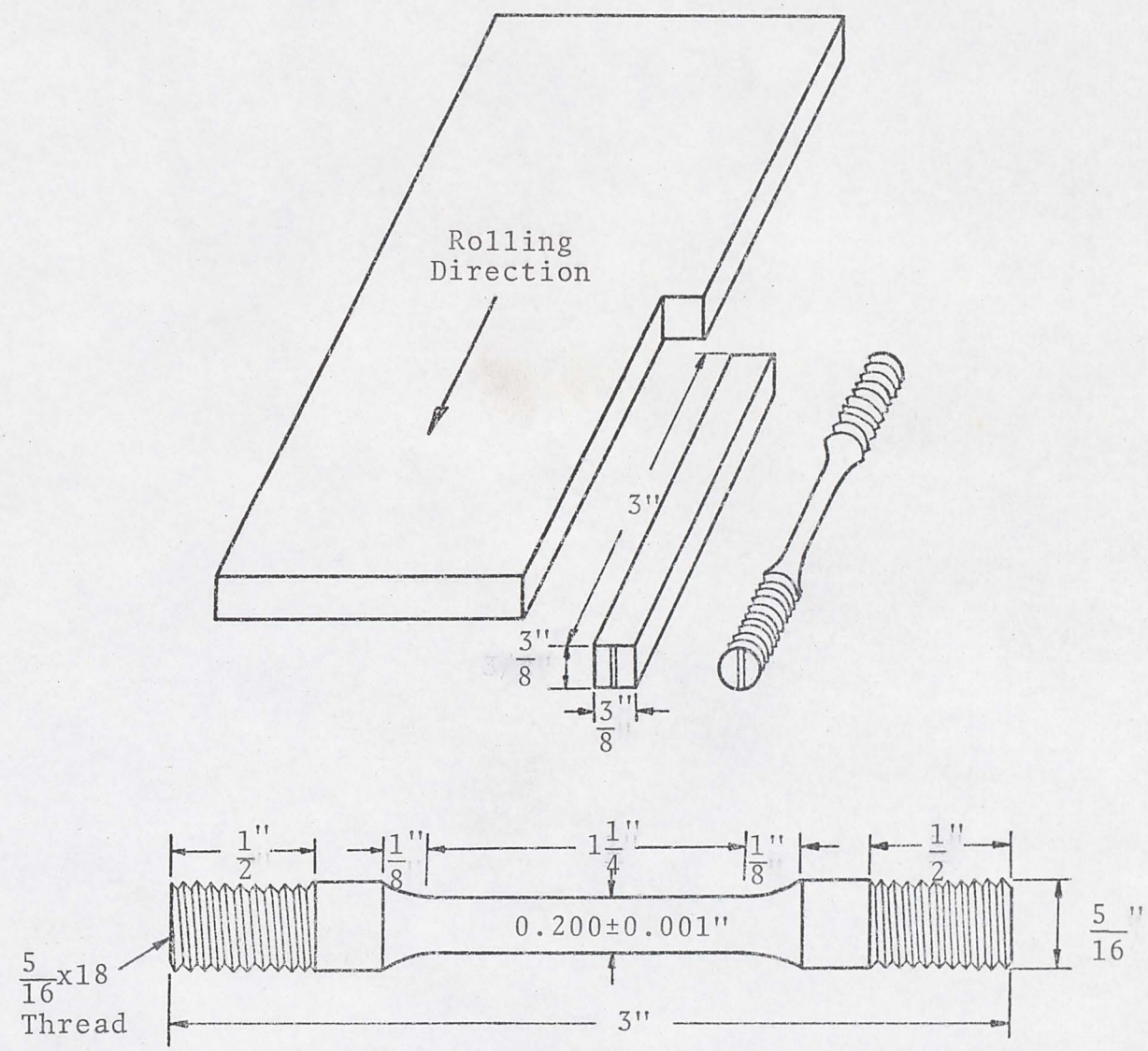

Fig. 4. Specimen cut procedure and specimen dimensions.

machined into cylindrical tensile specimens with a 1.25-inch by 0.20-inch gage section and 5/16-18 threads at either end. The specimen geometry is also shown in Fig. 4. The gage section of each specimen was polished with 600-grit emory paper to remove the tool marks introduced during machining. All specimens were tested in the as-machined condition, since no difference was observed in the plastic behavior between the as-machined and chemically machined specimens.

2.3. Apparatus and Testing Procedure

Two basic types of tensile tests were performed.

1) Strain rate change tests, involving rate changes between 2.7×10^{-5} and 2.7×10^{-4} sec^{-1}, at temperatures over the range 77° to 1073°K.

2) Tests in which the temperature and strain rate were maintained constant throughout the test. The strain rates varied from 2.7×10^{-6} to 2.7×10^{-1} sec^{-1} and temperatures from 77° to 1073°K.

All tests were carried out in an Instron Testing Machine, model TTC, of 10,000 pounds capacity. The strain rate changes were made instantaneously by an electronic switching mechanism. The machine had a load weighing accuracy of ±0.5 percent of the indicated load. Elongations were measured from the crosshead motion with a sensitivity of about 10^{-4} inch. Below room temperature, tests were

conducted in baths of liquid nitrogen (77°K), dry ice and acetone (193°K) and ice water (273°K). Temperatures between 193° and 273°K were obtained by mixing the cold acetone used for the 193°K test with fresh acetone. The low temperature test accessories are shown in Fig. 5. The specimen was mounted inside a perforated stainless steel tube attached to the bottom surface of the Instron crosshead. The purpose of the perforations was to allow the liquid of the low temperature bath to flow around the specimen and the grips. The top end of the specimen was attached to a long stainless steel rod which was in turn connected to the load cell. The other end of the specimen was attached to the bottom of the perforated tube by means of a collar with hemispherical head. The assembly mounted on the Instron Testing Machine is shown in Fig. 6. After mounting the specimen in the manner indicated above, a Dewar flask filled with suitable refrigerant was raised by means of a jack so that the specimen and the grips were completely immersed in the bath. The specimens were soaked for half an hour before testing. The temperature was measured by a low temperature thermometer and was maintained to within ±1°K throughout the test.

For the tests above room temperature, a kanthal wound furnace, shown in Fig. 7, was used. The specimen was mounted inside a high temperature vacuum capsule which was suitably modified to pass inert gas throughout the test. The

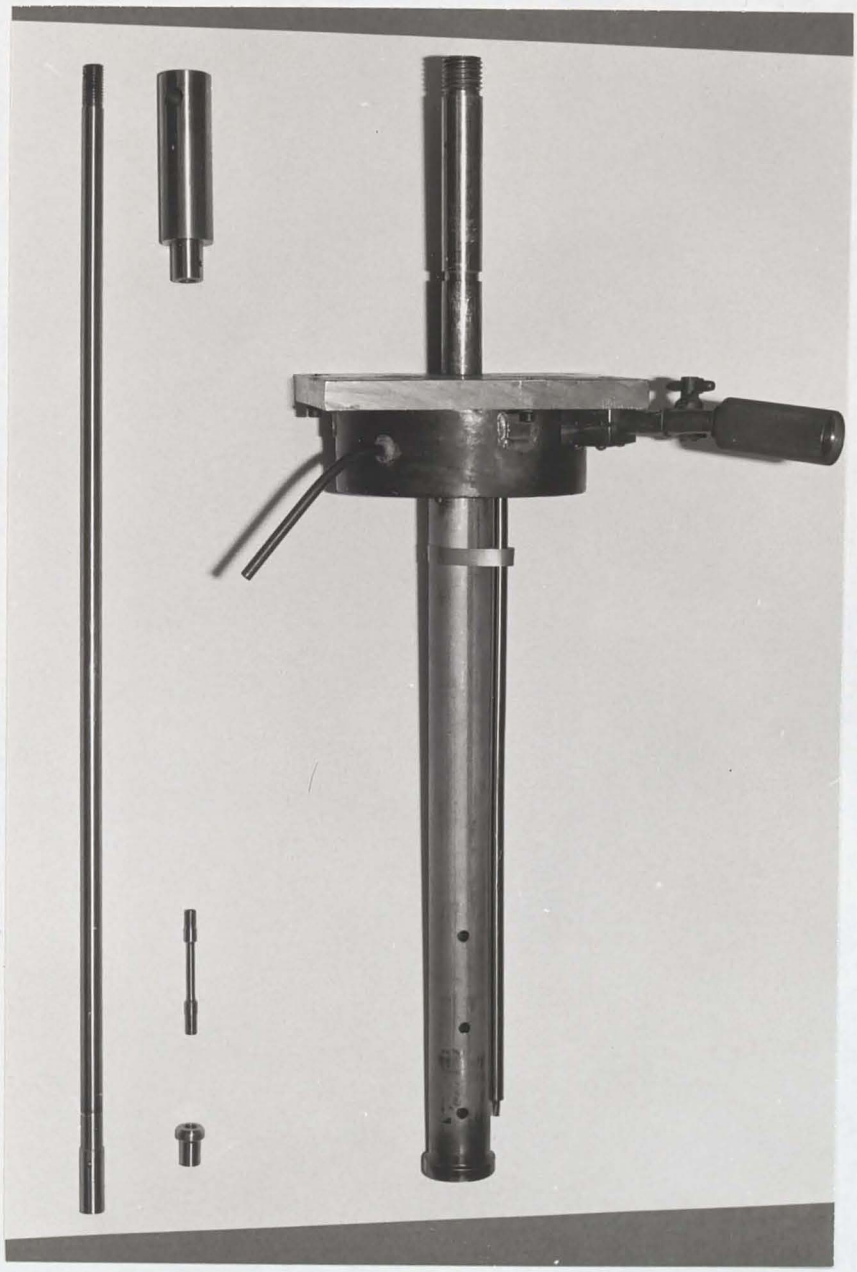

Fig. 5. Low temperature test accessories: pull rod, perforated pulling tube, specimen and bottom grip.

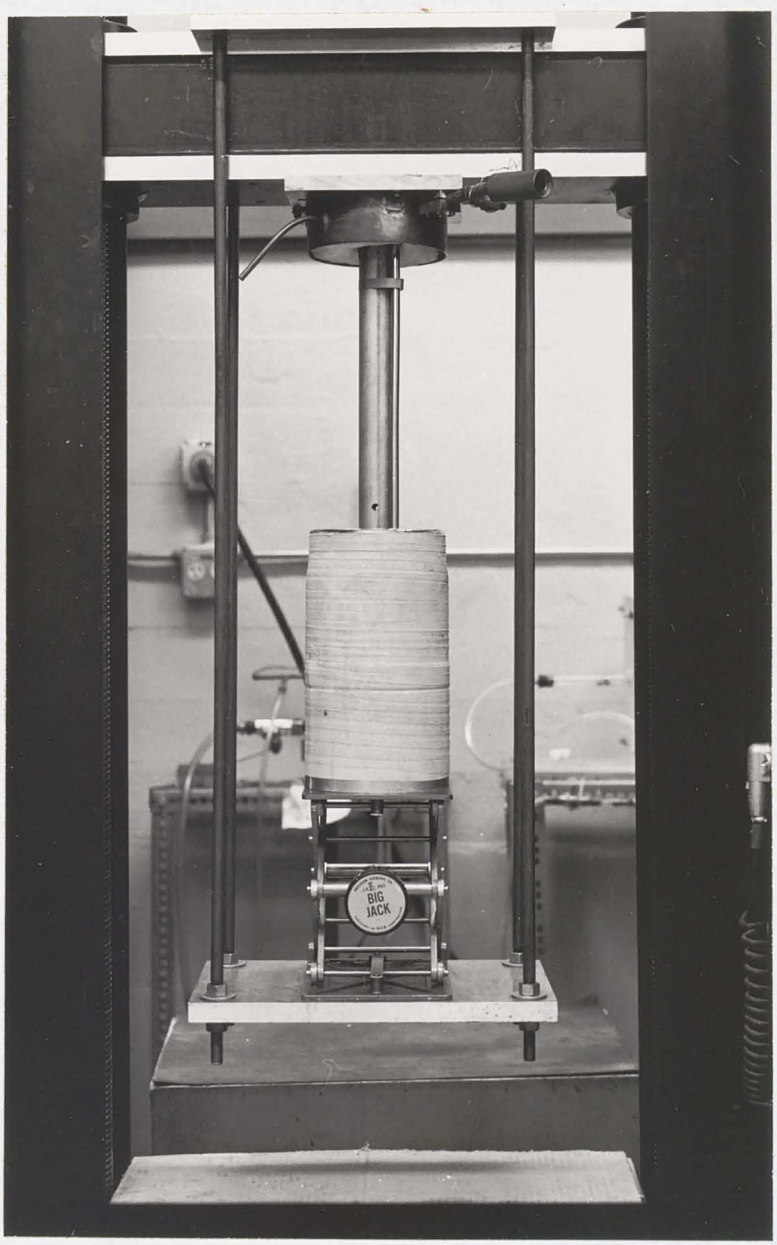

Fig. 6. Low temperature test assembly mounted on the Instron machine.

Fig. 7. High temperature tensile test assembly.

pull rod assembly and the capsule are shown in Fig. 8. The specimens were protected from surface oxidation by pure argon gas which was first desiccated through concentrated sulphuric acid and anhydrous calcium sulphate and gettered by passing through hot zirconium and copper chips. Additional protection from surface oxidation was obtained by placing pure dry zirconium chips in a tantalum tube surrounding the specimen. The temperature was controlled by two variacs set for high and low voltages and a switching mechanism. The specimen temperature was measured by a chromel-alumel thermocouple placed near the center of the gage section. The maximum variation in temperature along the gage length was ±2°K. The specimens were soaked at test temperature at least one-half hour before starting the test.

Some specimens deformed at 77°K were sectioned and mounted in epoxy cold mount for metallographic examination. Care was taken to view a plane perpendicular to the rolling plane, since the extinction under polarized light is sharper on these planes. The specimen was metallographically polished and etched electrolytically in a solution containing 118 ml methanol, 70 ml butanol and 12 ml perchloric acid. The temperature of the bath was maintained below -40°C. Electrolytic etching was carried out for 6 minutes. The specimen was thoroughly washed with water and immediately anodized. The purpose of the anodizing was to increase

Fig. 8. Accessories for high temperature tensile test: pull rod, grips, specimen, capsule and tantalum tube.

the sensitivity of the specimen surface to polarized light. Anodizing was carried out for about 5 seconds in a bath consisting of 120 ml ethyl alcohol, 70 ml distilled water, 40 ml glycerine, 20 ml lactic acid, 10 ml orthophosphoric acid and 4 g. citric acid. A stainless steel cathode was used and the potential was kept at 24 volts. Using a polarized light microscope, the volume fraction of twins was measured by the standard point count method.

2.4. Computation of the Test Data

A computer program was set up to convert the load-time data obtained from the Instron chart into true stress-true strain data up to the point of maximum load. Care was taken to remove the effect of machine stiffness in the stress-strain curves. The output from the IBM 360 computer contained the following information: engineering stress, engineering strain, true stress, true strain, flow stress and slope at specified values of plastic strains.

CHAPTER III

EXPERIMENTAL RESULTS

The results reported in this chapter have been obtained on commercial purity titanium of 16μ grain size over a temperature interval of 77° to 1073°K and over a strain rate interval from 2.7×10^{-6} to 2.7×10^{-1} sec^{-1}.

3.1. The Temperature and Strain Rate Dependence of the Yield Stress and the Ultimate Tensile Strength

As shown by several investigators,[12,14,17,44] the yield stress of commercial purity titanium is strongly temperature dependent below about 600°K. Figure 9 shows the variation of yield stress with temperature for four different strain rates, each varying from the other by an order of magnitude. Note that there is a rapid decrease in yield stress with increasing temperature up to about 600°K for all the strain rates investigated. Between 600° and 723°K, however, the yield stress becomes effectively temperature independent. There is also a negligible strain rate dependence in this temperature range. Similar temperature and strain rate independent yield stress phenomena have been observed in many metals and are usually referred to as yield stress plateaus. It is a common practice to consider the

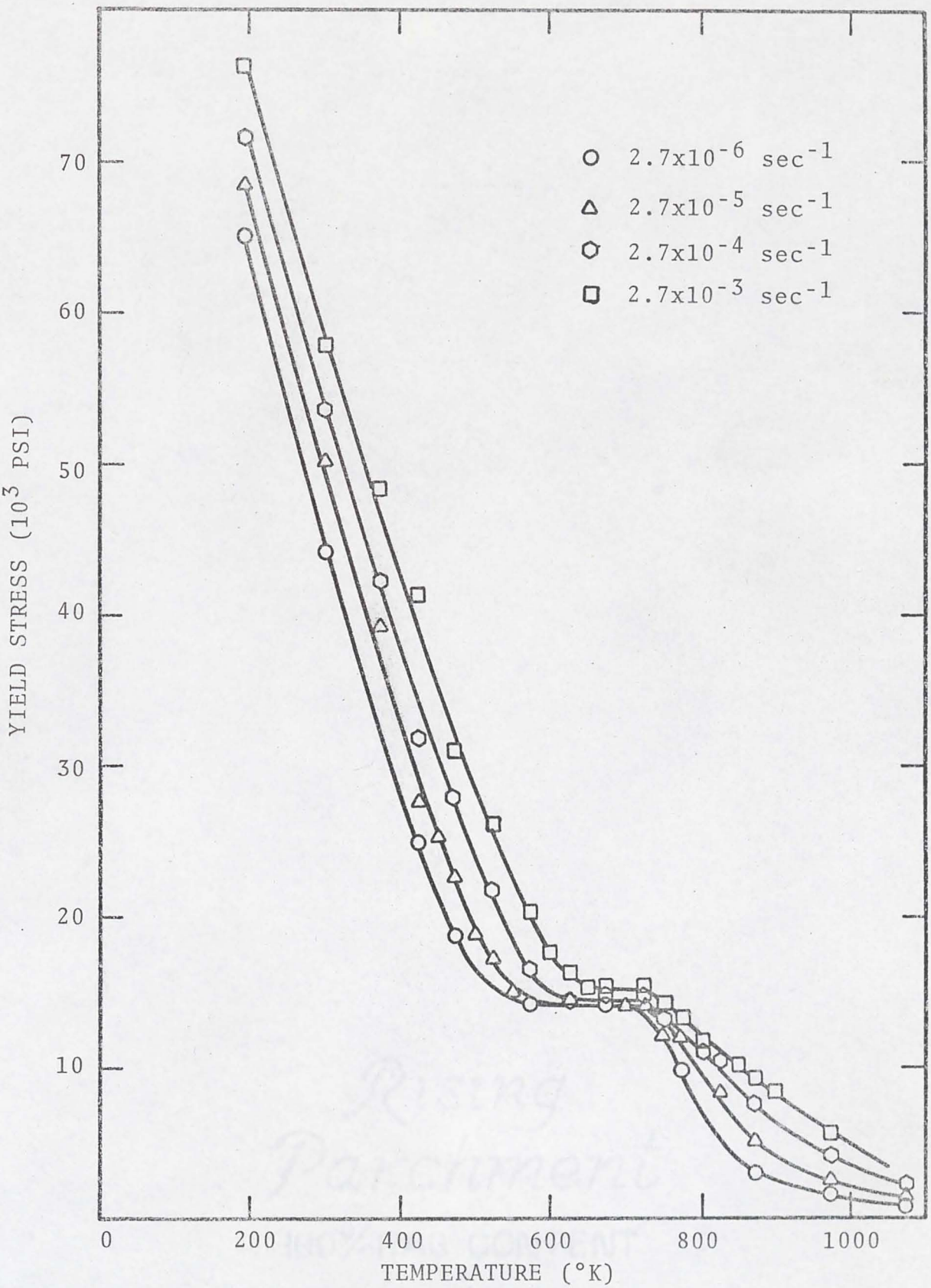

Fig. 9. The yield stress-temperature data for titanium deformed at four strain rates differing by factors of ten.

flow stress in this temperature interval to be representative of the athermal component of flow stress.[12] In other words, the thermally activated component is assumed to be zero inside the plateau. A further assumption is made that the thermally activated component at temperatures below the yield plateau can be obtained by subtracting the plateau value of the yield stress from the measured flow stress.[12] It will be shown that this view may be questionable. In this regard, note that the yield stress falls again above 723°K although somewhat less rapidly at faster strain rates.

When the same yield stress data are replotted on semi-logarithmic coordinates as in Fig. 10, the data points do not fall on straight lines as the high purity platinum data of Carreker shown in Fig. 1. There is, however, a general tendency for the yield stress to decrease with increasing temperatures. Figure 10 also shows that at each strain rate there are two regions where the $\ell n\sigma$ - T curve deviates positively from a linear relationship. At the slowest strain rate, these regions are centered at temperatures near 300° and 675°K respectively. With increasing strain rate, there is a tendency for the centers of the inflected regions to move to higher temperatures. Similar deviations from a linear relationship between $\ell n\sigma$ and temperature have been reported for reactor grade zirconium by Ramachandran and Reed-Hill[42] and are also evident in the data of Rosi and

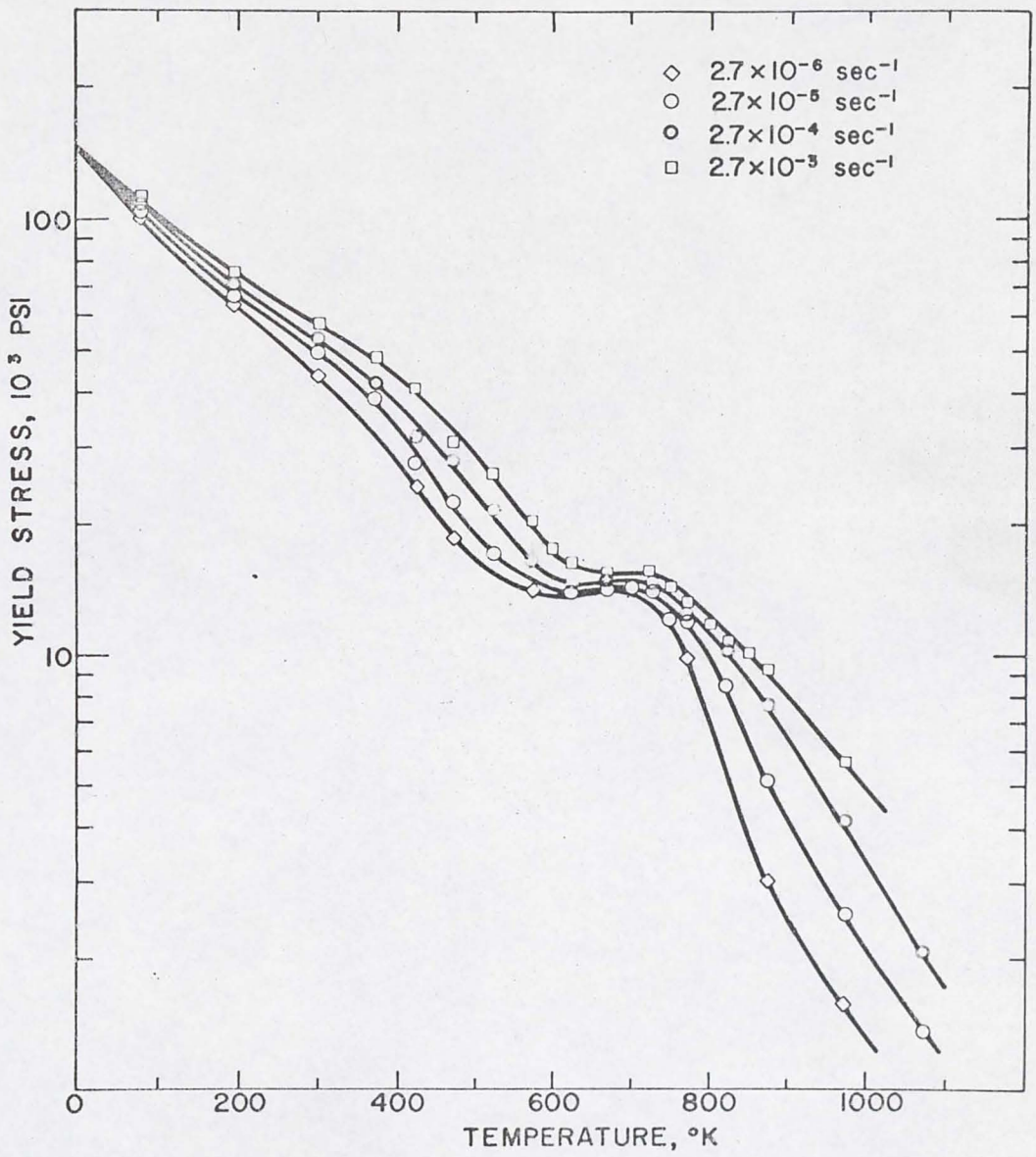

Fig. 10. This diagram shows the yield stress-temperature data of Fig. 9 plotted on semi-logarithmic coordinates. Note that there are two temperature intervals in which the curves deviate from linearity. In these regions dynamic strain aging phenomena are observed.

Perkins[14] and those of Orava, Stone and Conrad[12] when plotted on semi-logarithmic coordinates.[1]

Figure 11 shows the ultimate stress as a function of temperature for three strain rates, 2.7×10^{-5}, 2.7×10^{-4} and 2.7×10^{-3} sec^{-1}. A well defined peak occurs at each deformation rate, the peak becoming less marked at faster strain rates. Also, the peak moves to higher temperatures with increasing strain rate. Similar shifts of peaks in ultimate tensile strength with strain rate have been reported for mild steel by Nadai and Manjoine[34] and more recently by Ohmori and Yoshinaga.[45] Since no maximum occurs in the yield stress-temperature plot, the peak in the ultimate stress implies that the specimen work hardens to a greater extent in this temperature interval. In order to demonstrate this more clearly, the true flow stress has been plotted in Fig. 12 as a function of temperature at various strain levels for one strain rate, 2.7×10^{-5} sec^{-1}. This figure demonstrates that the work hardening rate increases above about 650°K and reaches a maximum at 723°K. It will be shown that the temperature of this maximum strongly depends on the deformation rate.

3.2. The Stress-Strain Curves

Like mild steel,[36,38] commercial purity titanium exhibits stress-strain curves whose shapes vary significantly with deformation temperature. This will be demonstrated

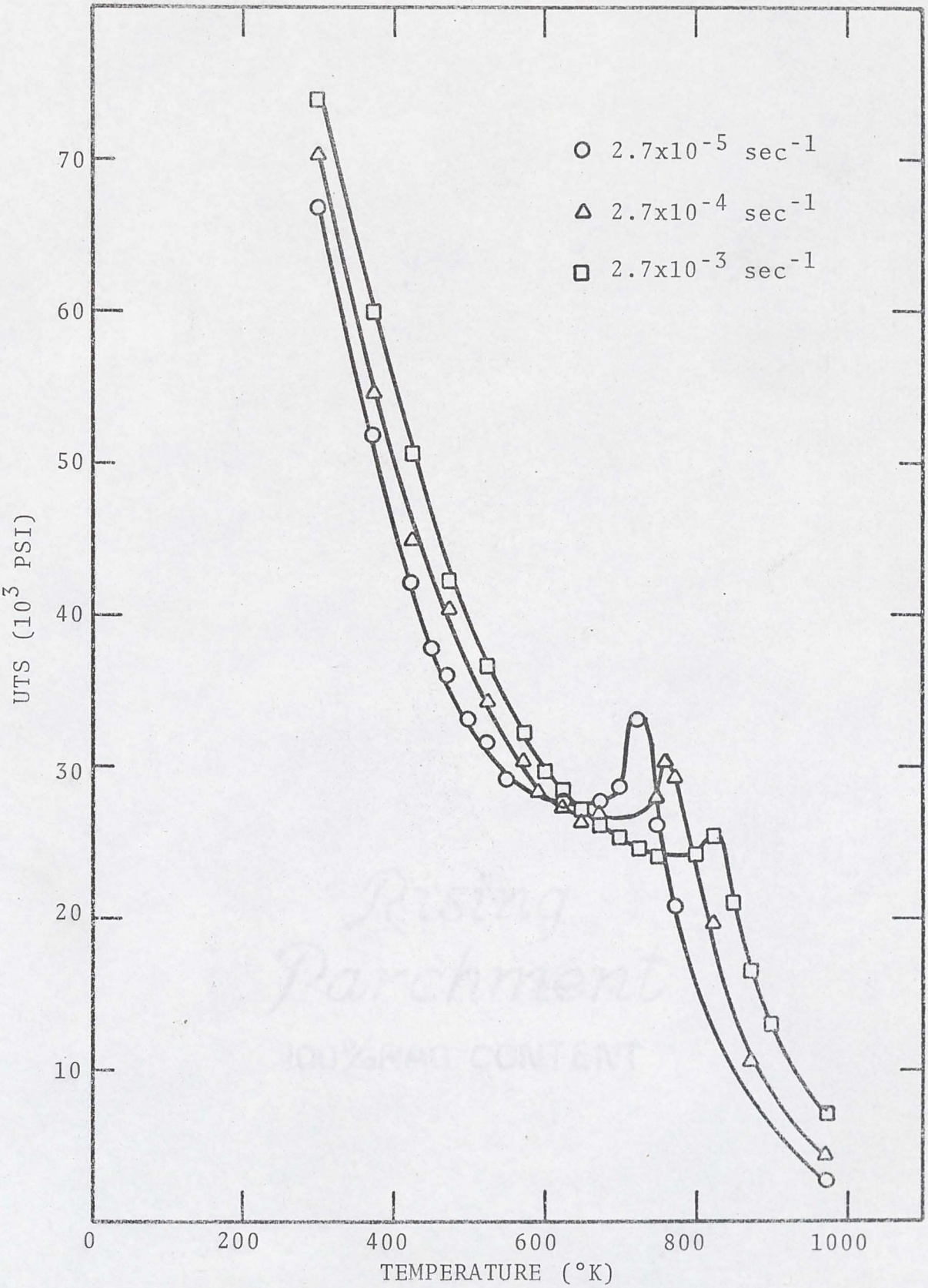

Fig. 11. Variation of ultimate tensile strength with temperature for commercial purity titanium.

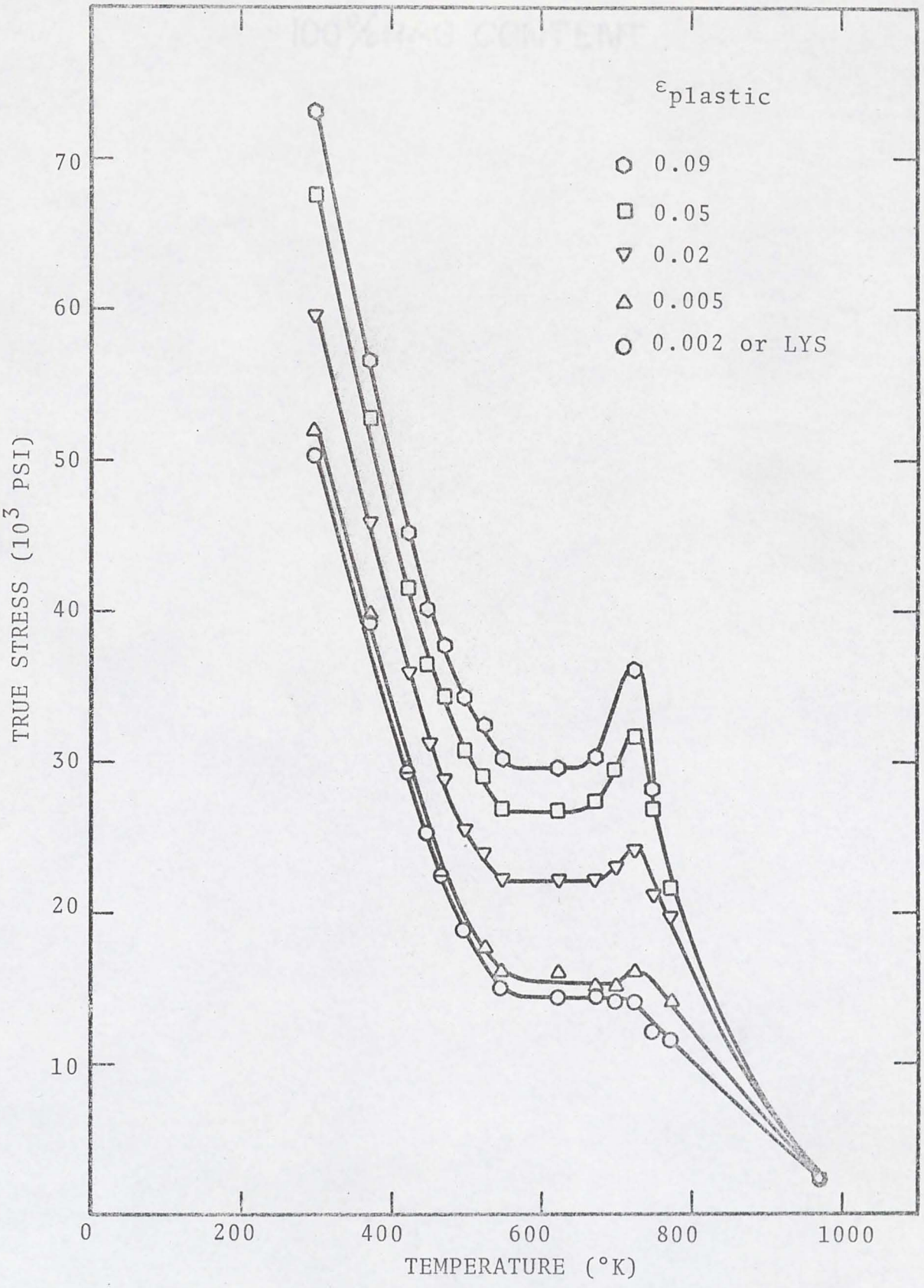

Fig. 12. Temperature dependence of lower yield stress and flow stresses of commercial purity titanium deformed at a strain rate of 2.7×10^{-5} sec^{-1}.

for specimens deformed at a strain rate of 2.7×10^{-5} sec^{-1}. Attention will be focussed on that temperature interval where the yield stress is nearly temperature independent and the work hardening behavior changes drastically.

Seven engineering stress-strain curves corresponding to specimens deformed between 550° and 773°K are given in Fig. 13. The specimen is ductile at 550°K. Serrations are observed at 623°K and the total elongation starts decreasing. With the appearance of serrations, the work hardening rate increases. At 700°K the stress-strain curve is smooth except for an instability near the maximum stress. The total elongation reaches a minimum at this temperature. However, the work hardening rate continues to rise with further increase in deformation temperature and maximizes at 723°K. At 750°K and above, necking begins at small strains but the specimen is drawn to a chisel edge (total strain nearly 120 percent). A similar stress-strain behavior was observed at faster strain rates, although displaced to higher temperatures. In other words, all the phenomena observed at one strain rate could be reproduced almost exactly at other strain rates by proper choice of deformation temperature.

We have so far considered the stress-strain curves for specimens deformed at a constant strain rate but at different temperatures. If, on the other hand, the deformation temperature is kept constant but the crosshead speed varied,

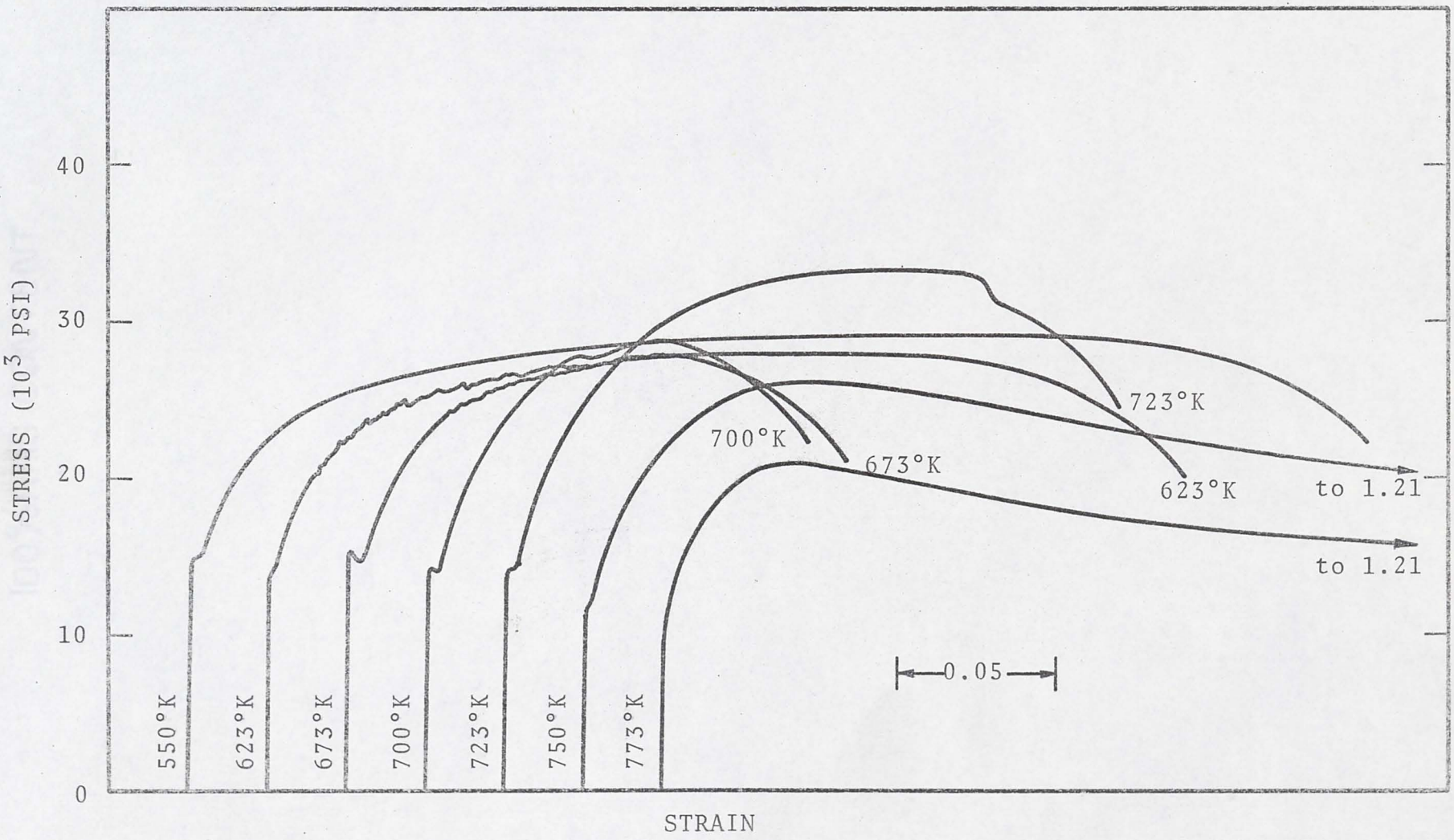

Fig. 13. Stress-strain curves for commercial purity titanium. Strain rate: 2.7×10^{-5} sec^{-1}.

the resulting shapes of the stress-strain curves may vary depending on the choice of the test temperatures. Thus, at 723°K Fig. 14 shows that the specimen deformed at a slower rate has a greater work hardening and a smaller total elongation that the one deformed at two orders of magnitude faster. This is an anomalous behavior. One would generally expect a greater work hardening to occur at a faster deformation rate if the shape of the stress-strain curve is solely determined by dynamic recovery.

When the deformation temperature is raised to 773°K, the stress-strain curves are still more interesting as may be seen in Fig. 15. This figure shows that the specimen deformed at a slower rate starts necking at smaller strains but the strain associated with necking is very large. With the faster rate of deformation,there is a greater work hardening but the necking strain is very small. It is amazing that a mere order of magnitude change in strain rate should produce such a large difference in the stress-strain behavior. As will be shown in the subsequent sections, it is possible to rationalize all these phenomena if a complete documentation of the work hardening rates and ductility is available over a wide range of temperature and strain rate.

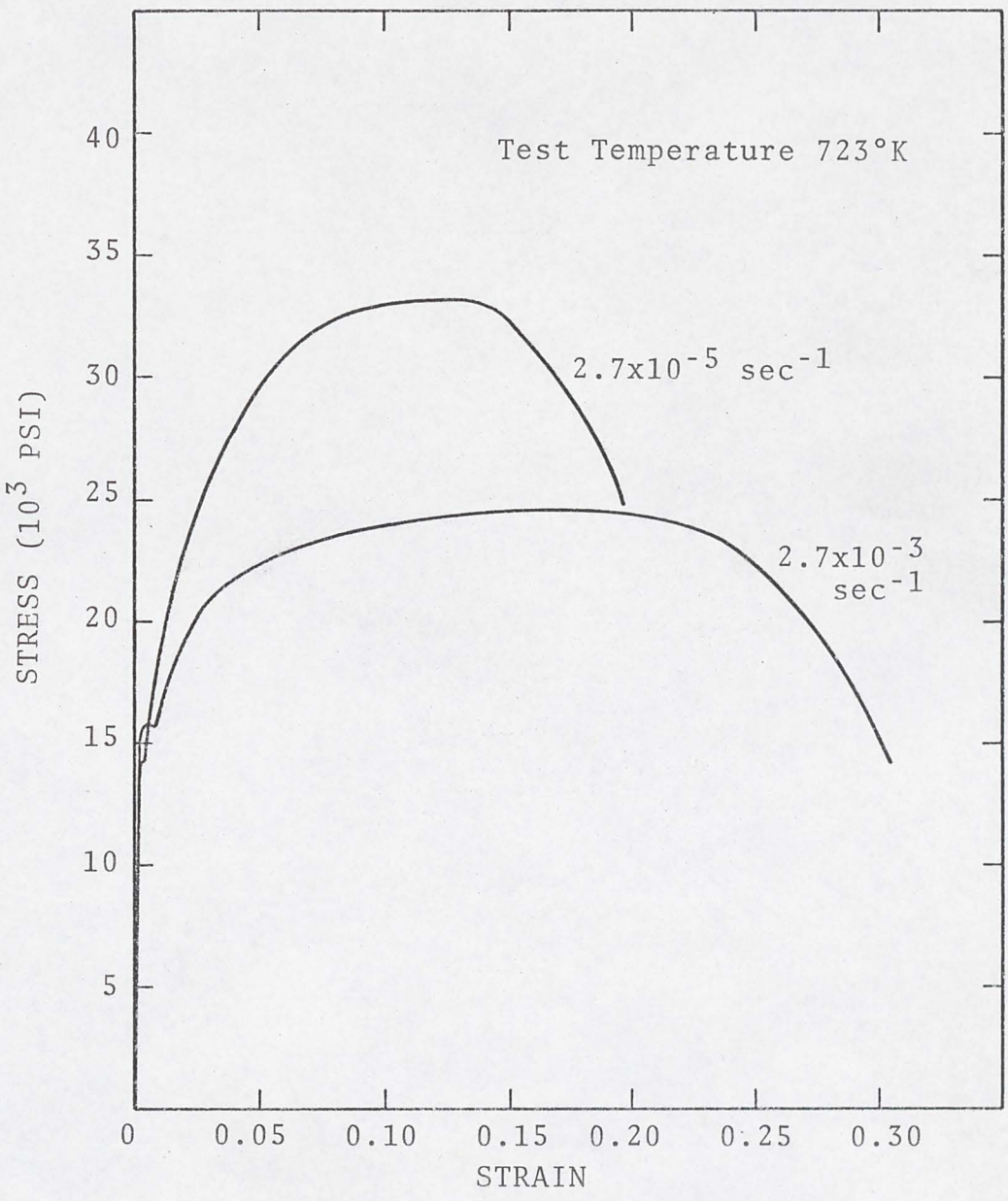

Fig. 14. The anomalous effect of strain rate on the stress-strain curves due to dynamic strain aging (commercial purity titanium deformed at 723°K).

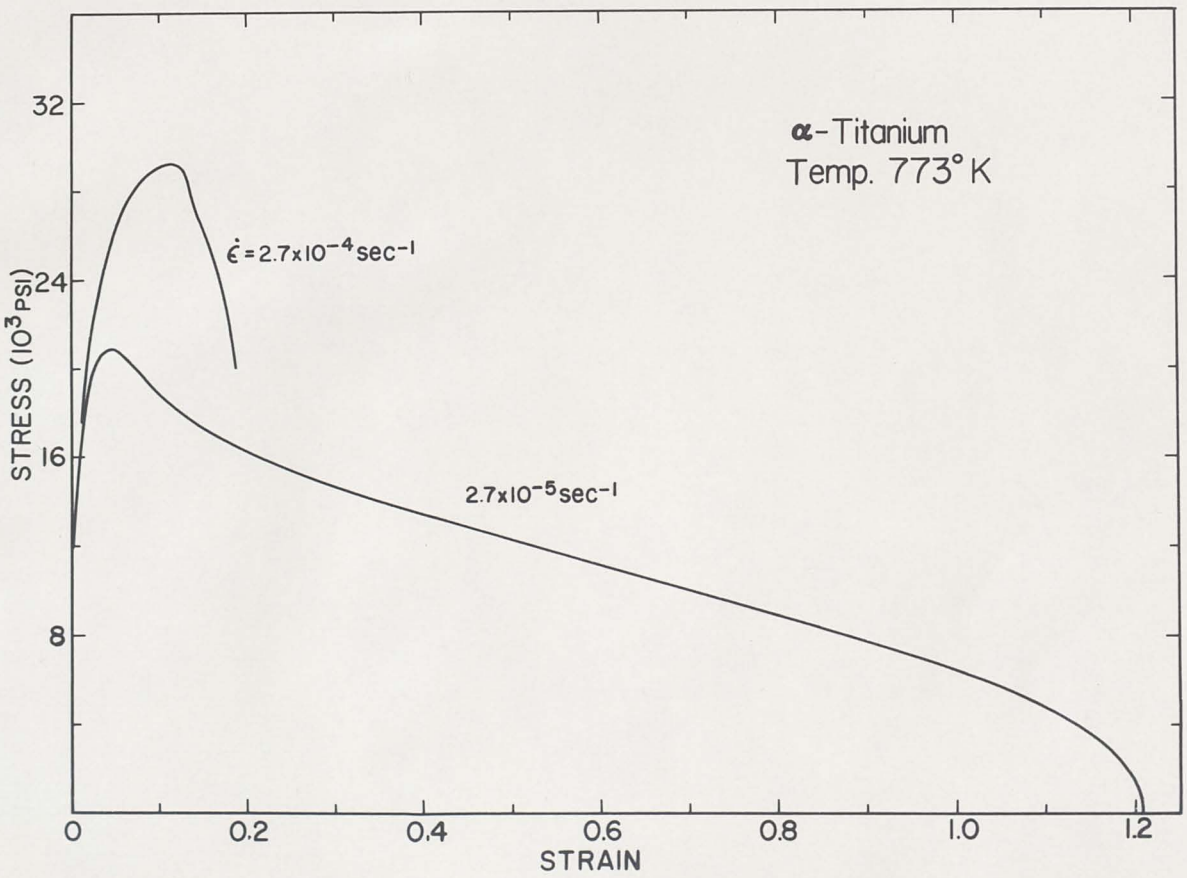

Fig. 15. The strong role played by dynamic strain aging in determining the shape of the titanium stress-strain curve is shown in this curve. At 773°K the specimen deformed at the slower strain rate shows a smaller uniform strain but a very large necking strain compared with that deformed at the faster rate.

3.3. The Nature of Serrations

It was shown in the previous section that the phenomenon of jerky flow (also known as serrated yielding or Portevin-LeChatelier effect[37]) was observed in titanium over a narrow temperature interval at each deformation rate. For example, at a strain rate of 2.7×10^{-5} sec^{-1} serrations were observed only between 600° and 673°K. This interval moved to higher temperatures with increasing strain rate. The phenomenon is generally attributed to dynamic strain aging. It is therefore of interest to compare the nature of serrations observed in the present study with those reported in other metals and alloys.

Figure 16 shows a set of serrated stress-strain curves drawn schematically for commercial purity titanium, mild steel,[36] copper-indium[46] and Al 6061 alloy.[47] The test conditions that produced these serrations were very different. Our primary concern here is the appearance of serrations. First, it should be noted that serrations in titanium are not as pronounced as in steel. It is perhaps because of this reason that several investigators have ignored the strain aging effect in titanium completely. Secondly, the serrations in the present study are somewhat similar to the so-called Type A serrations observed in the Cu-In alloy.[46] The characteristics of these serrations are that they rise above the general level of the stress-strain curve and are periodic in nature. Mild steel,[36] on the

other hand, shows serrations that either oscillate about the general level of the stress-strain curve in rapid succession (Type B) or fall below the general level of the stress-strain curve (Type C). No Type B or Type C serrations were observed in titanium at any temperature or strain rate. Another significant aspect of the serrations in titanium is that the apparent slope of each serration when it rises above the general level of the stress-strain curve decreases with increasing strain. This is indicated in the titanium curve of Fig. 16.

3.4. The Strain Rate Dependence of Flow Stress

The nature of the variation of the yield and flow stresses with strain rate depends on the deformation temperature. At room temperature Fig. 17 shows that the yield stress and flow stress at larger strains increase in a "normal" way with increase in strain rate. The curves at different strain levels are nearly parallel, indicating that the increase in flow stress due to work hardening is nearly independent of the strain rate in the range shown in Fig. 17. On the other hand, the curves in Fig. 18 show that at 723°K only the lower yield stress increases slightly with increasing deformation rate, whereas the flow stresses at larger strains decrease. Such an "inverse" strain rate dependence of flow stress merely implies that the amount of work

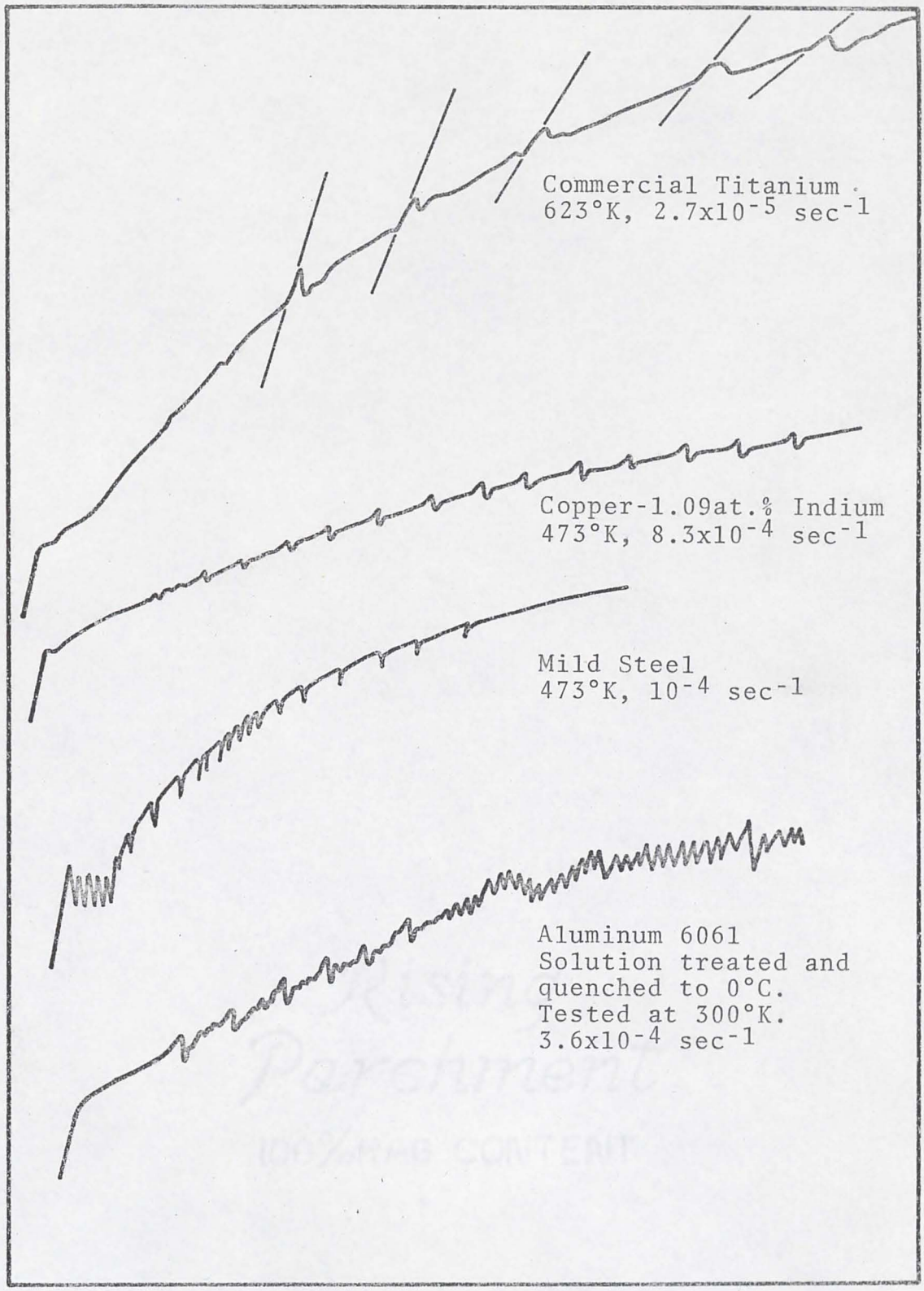

Fig. 16. The nature of serrations in the stress-strain curves of commercial purity titanium, Cu-In alloy,[46] mild steel[36] and Al 6061.[47]

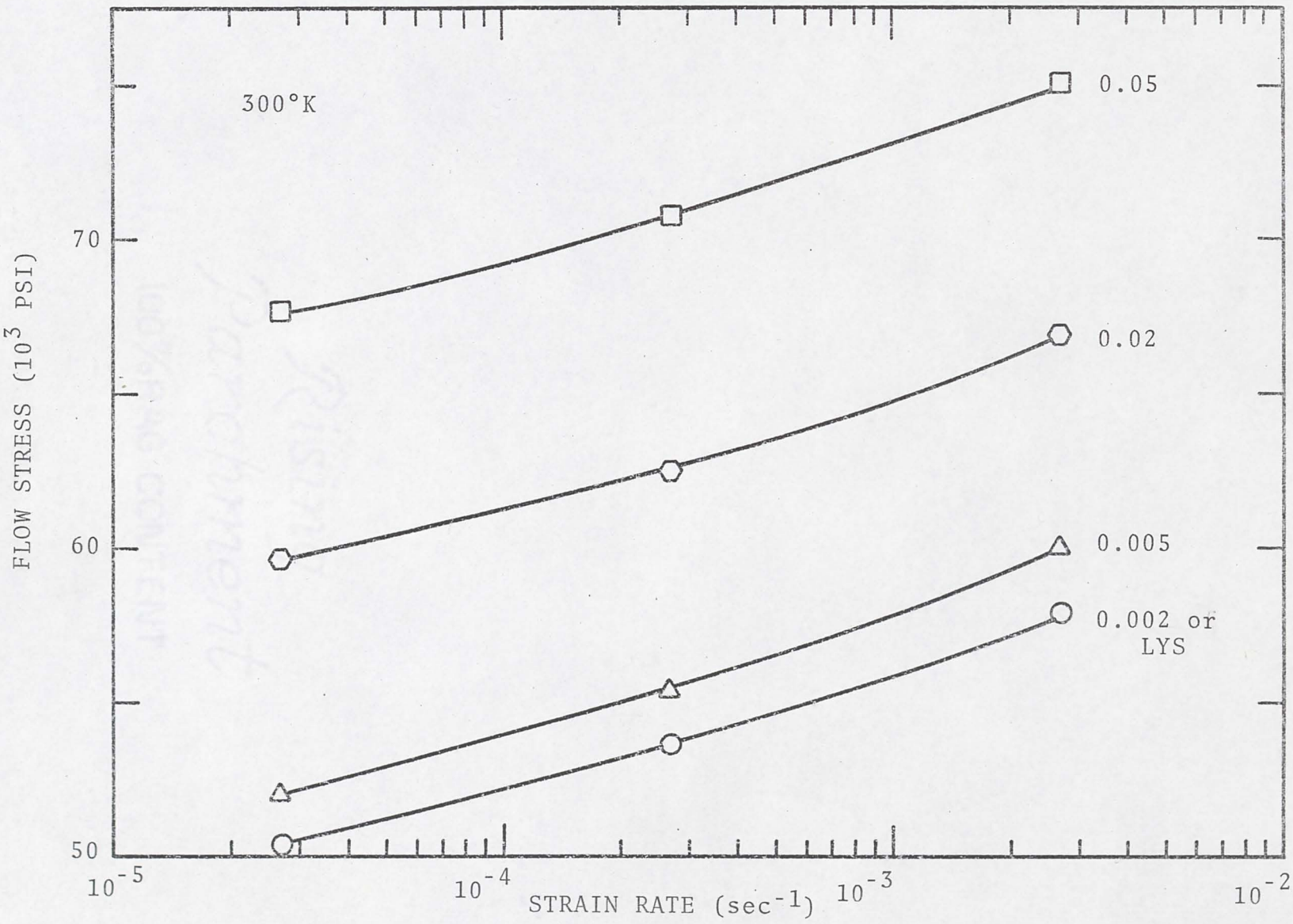

Fig. 17. Strain rate dependence of yield and flow stresses of commercial purity titanium deformed at 300°K.

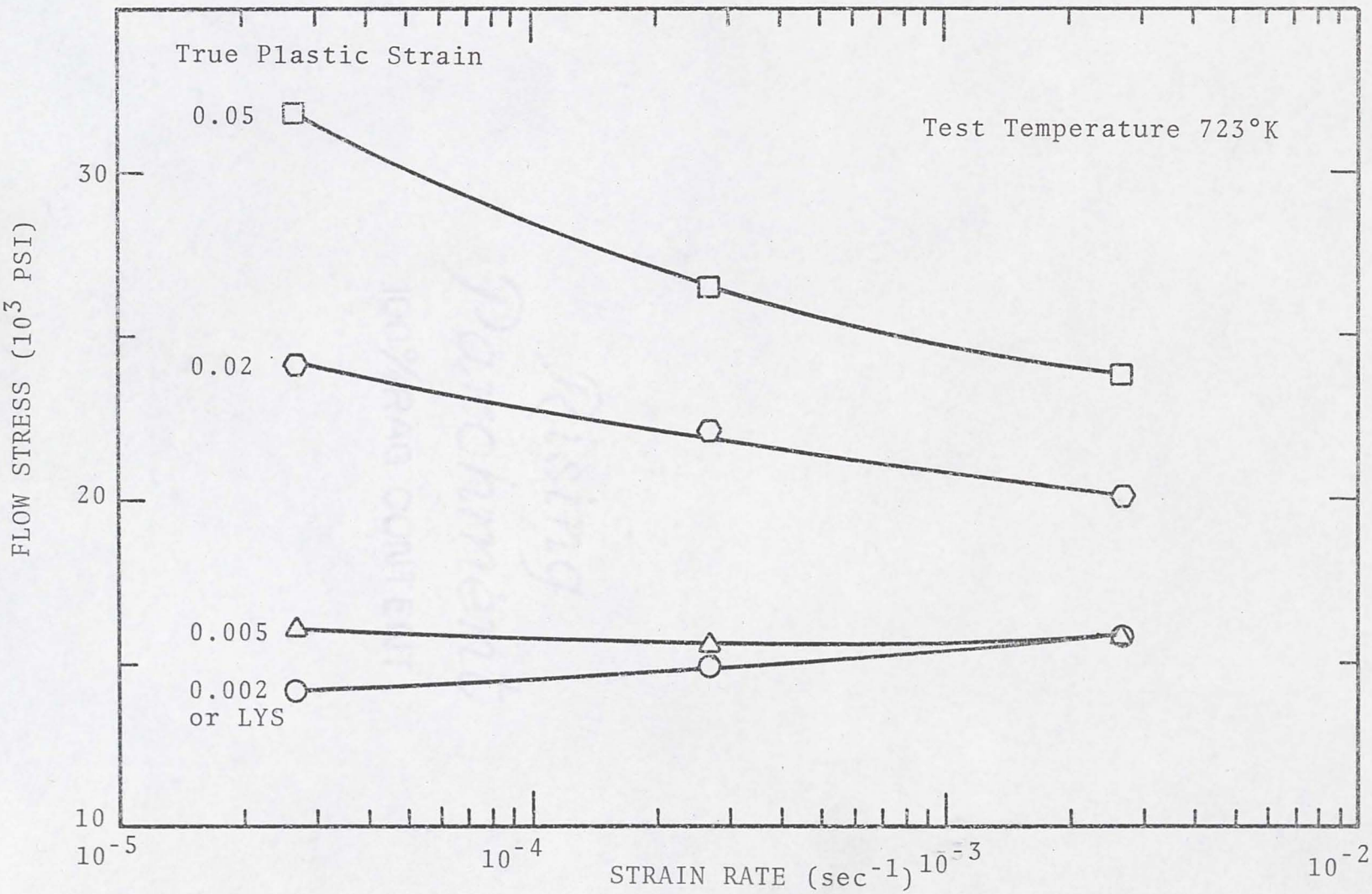

Fig. 18. Strain rate dependence of yield and flow stresses of commercial purity titanium deformed at 723°K.

hardening obtained at this temperature varies with strain rate, and is larger at slower strain rates. At a still higher temperature, namely 760°K, the yield stress again shows a normal strain rate dependence but the flow stress at moderate strains shows a maximum. See Fig. 19.

Let us now consider the nature of the variation of the flow stress over a much larger interval of strain rate. In Fig. 20(a) the flow stress values at some moderate strain are schematically plotted against temperature for a range of strain rates. At a temperature marked T_1, values of flow stress at different strain rates are read off and plotted against the strain rate in a schematic fashion in Fig. 20(b). Note that when six or seven orders of magnitude in strain rate are chosen, the general pattern of the flow stress variation with strain rate is as follows: first, an increase in flow stress with increasing strain rate followed by a decrease to a minimum before assuming a normal strain rate dependence (increase). It is interesting to note that in regions where the flow stress variation is abnormal (flow stress decrease with increasing strain rate), other effects associated with dynamic strain aging are also pronounced.

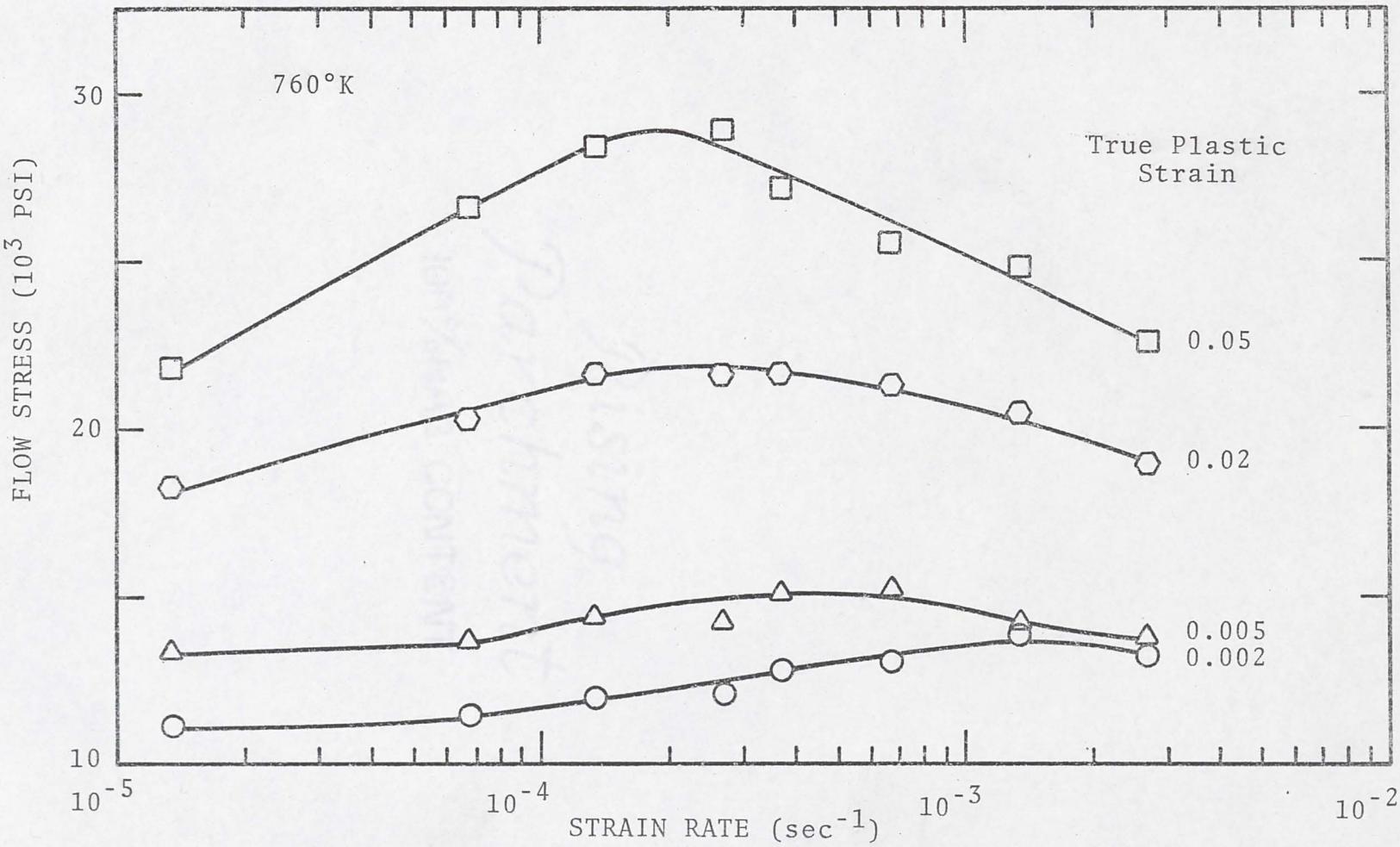

Fig. 19. Strain rate dependence of yield and flow stresses of commercial purity titanium deformed at 760°K.

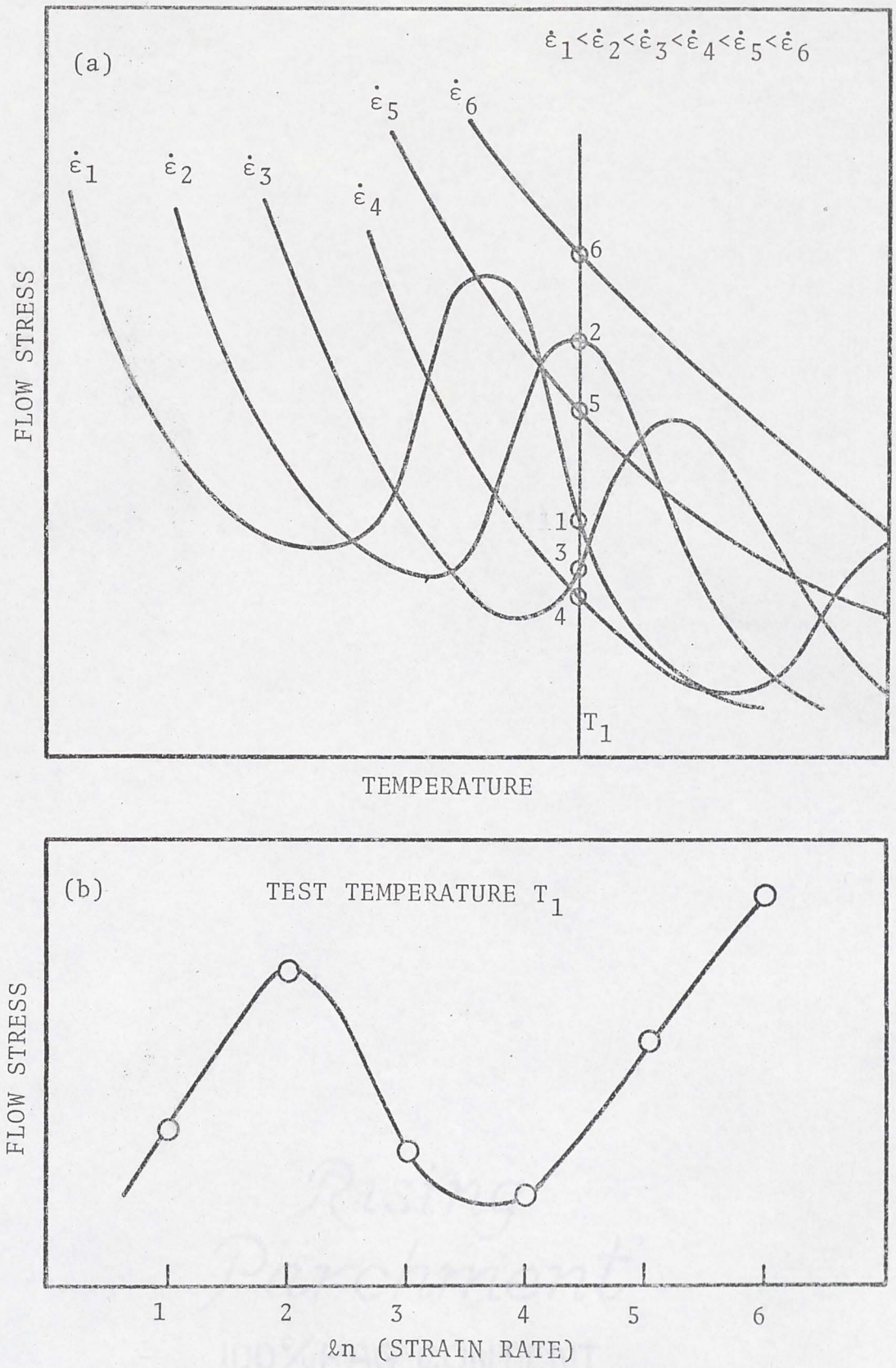

Fig. 20. (a) Schematic flow stress-temperature curves showing strain rate dependent flow stress peaks.
(b) σ-$\ell n\dot{\varepsilon}$ curve at temperature T_1.

3.5. Work Hardening Characteristics

The variation of the work hardening behavior with temperature and strain rate can be illustrated explicitly if a suitable work hardening parameter is selected. A frequently used parameter is due to Hollomon,[48] who assumed that the stress-strain curve could be approximated by the relation

$$\sigma = C\varepsilon^{\eta} \tag{14}$$

where σ is the true flow stress, ε is the true plastic strain, and C and η are constants. The parameter η was assumed to represent the work hardening rate.

There are certain difficulties in using η as a work hardening parameter. It is now generally recognized that work hardening is primarily related to changes in the dislocation structure of the metal that influence only the long-range flow stress component. The Hollomon method[48] involves plotting the logarithm of total flow stress against the logarithm of true plastic strain and computing the slope of the resulting curve.

$$\eta = \frac{d\ \ell n\ \sigma}{d\ \ell n\ \varepsilon_{pl}} \tag{15}$$

Since the total flow stress consists of two basic components, σ_s and σ_ℓ, what is actually measured is the slope of $\ell n(\sigma_s+\sigma_\ell)-\ell n\varepsilon_{pl}$ curve. In metals that have a large thermally

activated component, σ_s, in comparison to the long-range component, σ_ℓ, the above method would give numbers for η which may not be representative of the work hardening process. This is particularly true in commercial purity titanium and will be demonstrated presently.

Let us consider two metals of nearly equal moduli, titanium and copper. At 77°K the values for the Hollomon work hardening parameter η, as computed from Eq. (15), are about 0.10 and 0.60 for titanium and copper respectively. If the value of η is taken as representative of the work hardening rate, the above numbers imply that the work hardening rate in copper is six times larger than that in titanium at 77°K. That this conclusion is incorrect may be seen in Fig. 21, which shows the 77°K true stress-true strain curves for titanium and copper. Note that the two stress-strain curves are not very different in shape and the increase in flow stress over a large strain interval is nearly the same (22,000 psi between 5 and 15 percent strain) in both metals. Reed-Hill[49] has pointed out that the basic cause for the difference in the Hollomon work hardening parameters does not lie so much in the metals themselves as in the use of Eq. (15) for titanium and copper which have widely different proportional limits (105,000 psi for titanium and 10,000 psi for copper). This large difference in the two proportional limits, Reed-Hill[49] continues, probably reflects a basic difference in the corresponding thermally

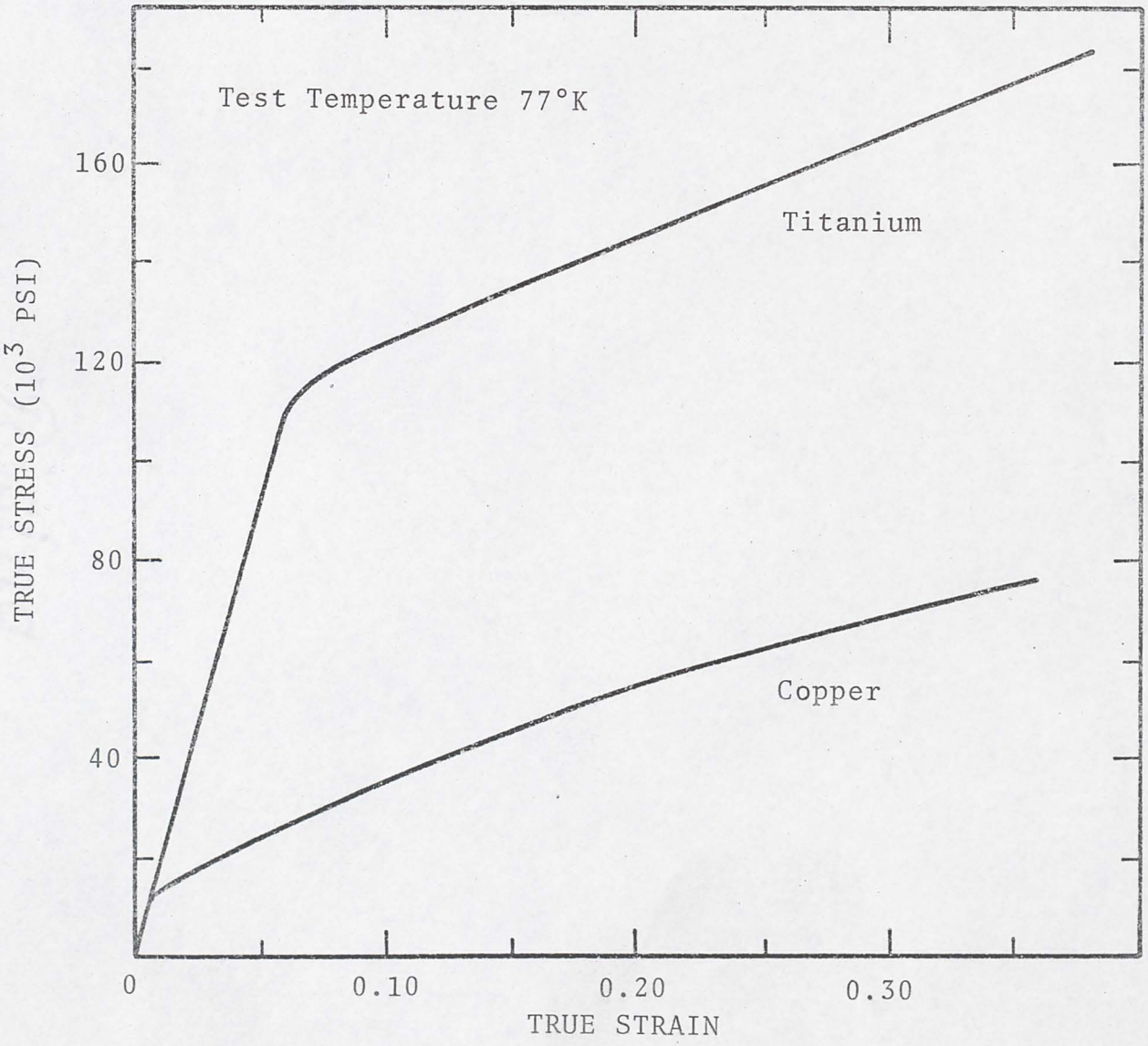

Fig. 21. True stress-true plastic strain curves for titanium and copper both deformed at 77°K. Strain rate ~10^{-4} sec^{-1}. Data from Reed-Hill.[49]

activated or short-range component of flow stress. Therefore, the use of η as a work hardening parameter is questionable, particularly in metals like titanium with a high yield stress.

Orava, Stone and Conrad[12] analyzed their commercial purity titanium stress-strain data in terms of the equation

$$\sigma = \sigma(o) + h\varepsilon^{1/2} \qquad (16)$$

where $\sigma(o)$ and h are constants. They reported that their experimental curves fitted with the above equation at all temperatures (from 77° to 795°K) and assigned h as the work hardening parameter. However, while computing the h values, these authors ignored their stress-strain data below about 2.5 percent strain. Such a procedure would lead to inconsistent values of the work hardening rate if a greater part of the increase in flow stress due to the work hardening occurs within the first 2 or 3 percent plastic strain as in zirconium at 77°K or as in titanium at temperatures between about 600° and 800°K.

Several authors[50,51] have used $d\sigma/d\varepsilon$, measured at a fixed strain, as a work hardening parameter. However, its slope at a specific strain is not generally descriptive of a stress-strain curve over a range of strain. Also, two curves with the same slope at a given strain will not necessarily have equal slopes at a later strain, because the slopes of stress-strain curves generally decrease with strain

and the second derivative, $d^2\sigma/d\varepsilon^2$, may follow different functions of the temperature, the strain rate and the strain. For this reason, the average work hardening rate over a finite strain interval was selected to represent the work hardening. The limits of the true plastic strain interval, 0.5 and 5.0 percent, were selected to avoid yield drops or the onset of necking in any specimen. When $\Delta\sigma/\Delta\varepsilon$ is plotted against temperature, a set of maxima and minima is obtained at each strain rate (see Fig. 22). In order to ascertain that the maxima in $\Delta\sigma/\Delta\varepsilon$ values are not the result of the choice of the strain interval, the average work hardening rate was computed for several smaller strain intervals. This is shown in Fig. 23 for one strain rate. Note that the shapes of all the curves are similar and that the positions of the maxima are consistent. If the temperature variation of the modulus is also taken into consideration by dividing the work hardening rate by the modulus, E, the work hardening rate maxima at the higher temperature are accentuated and the two lower temperature maxima are subdued as shown in Fig. 24. This procedure of dividing the work hardening rate by the modulus enables one to compare the work hardening rates of different metals. Figure 24 also shows that the sharp work hardening rate maxima above 600°K are strongly dependent on the deformation rate, moving to higher temperatures with increase in strain rate. A direct result of such shifts in the work hardening peaks

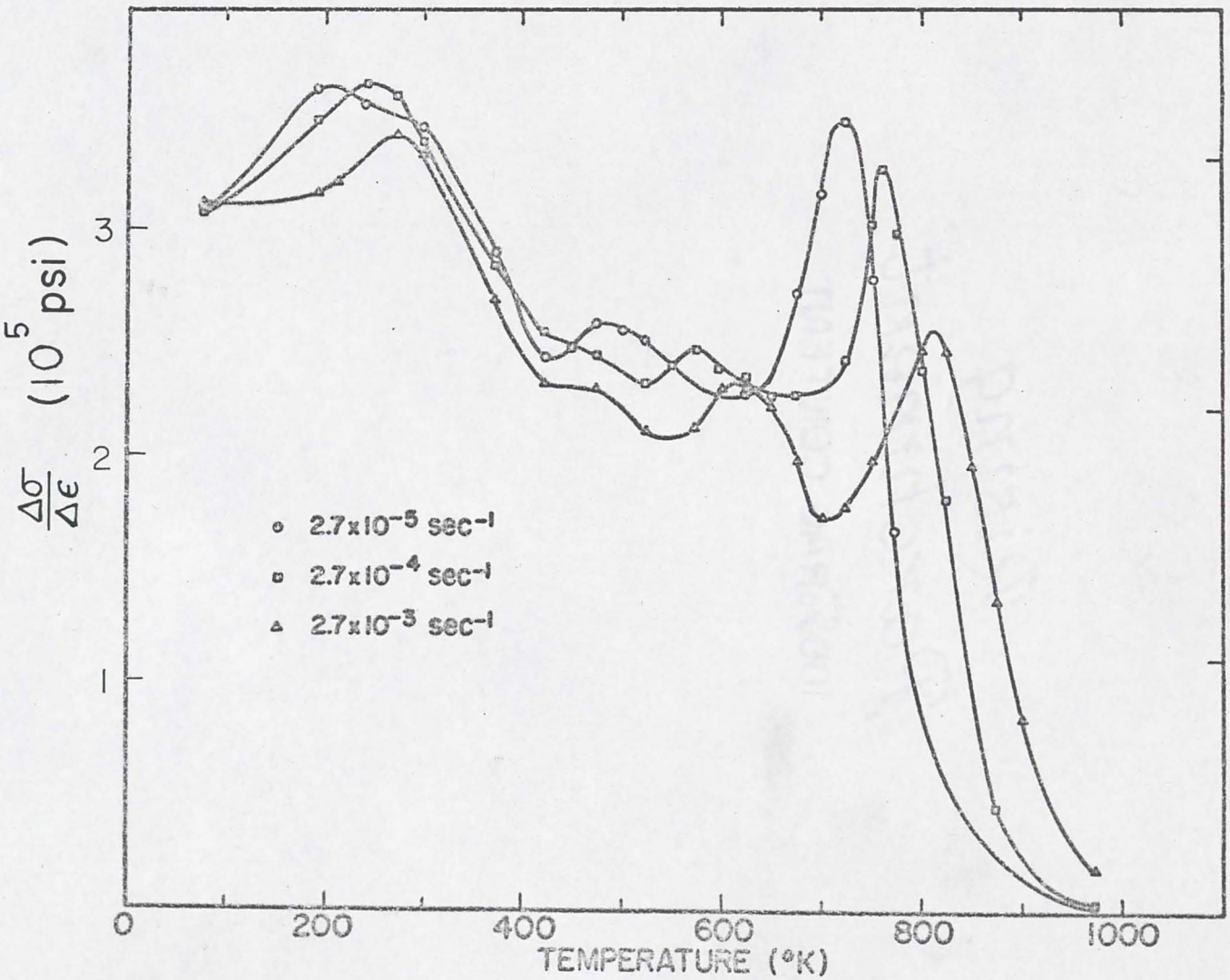

Fig. 22. The effect of temperature on the average work hardening rate between 0.5 and 5.0 percent true plastic strains for commercial purity titanium.

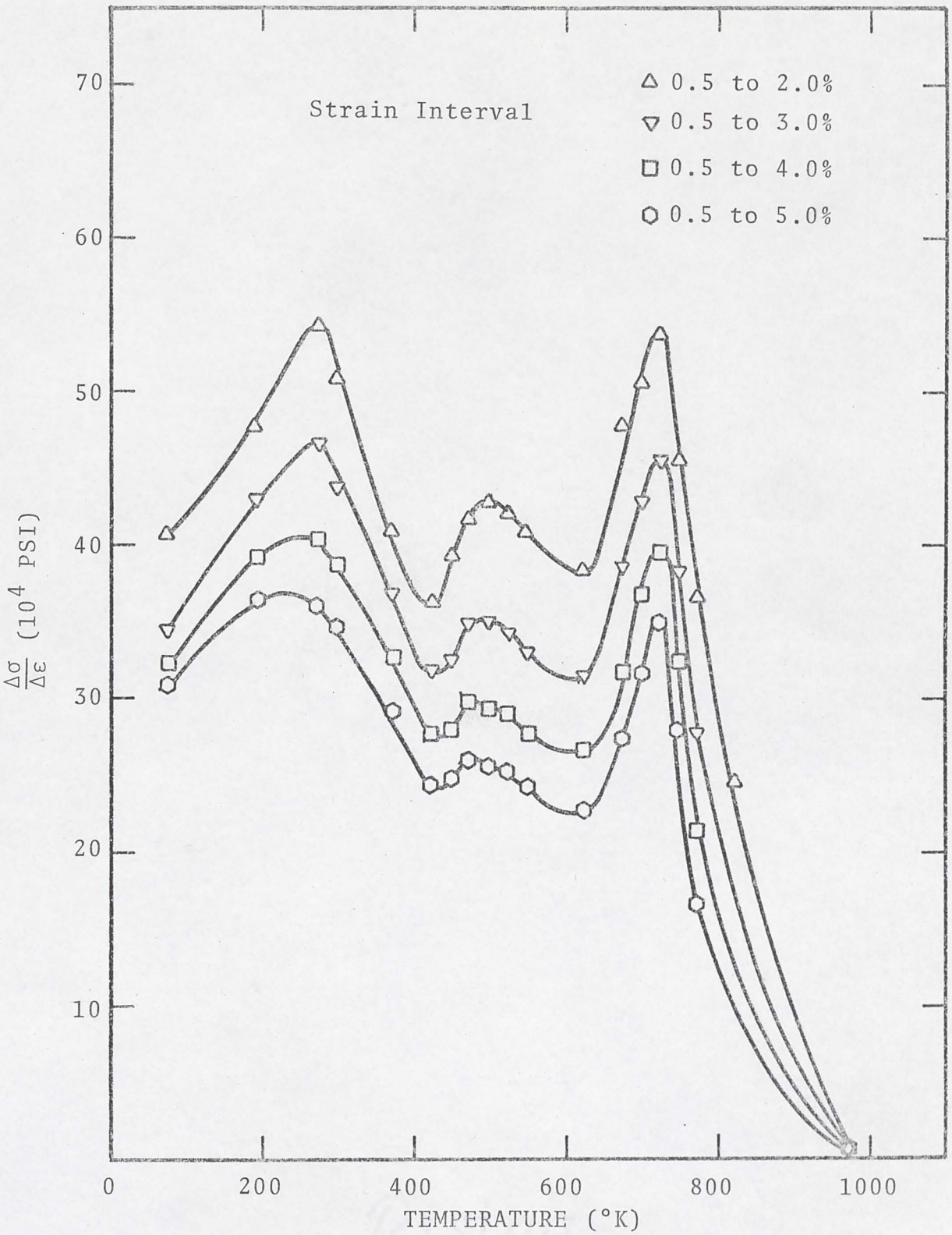

Fig. 23. When the average work hardening rate is computed for smaller strain intervals, the general shape of the curve is similar to that in Fig. 22. Strain rate 2.7×10^{-5} sec^{-1}.

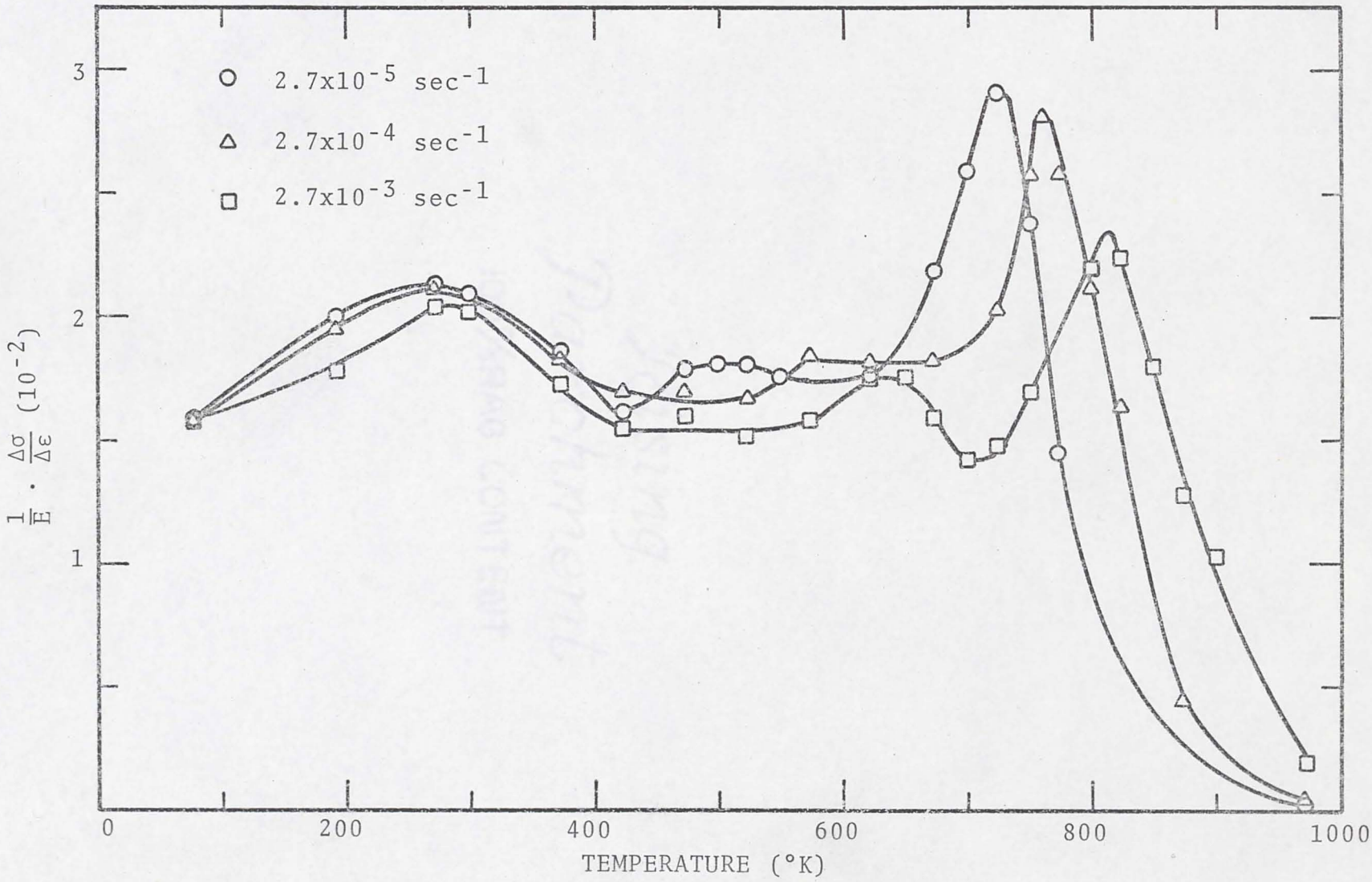

Fig. 24. The average work hardening rate divided by the elastic modulus for titanium. Note that the highest temperature peaks are accentuated while the lower temperature peaks are subdued.

is that, depending on the deformation temperature, the work hardening rate may either decrease or increase continuously with increasing strain rate, or it may show a maximum at some intermediate strain rate. This is demonstrated in Fig. 25 in which the average work hardening rate as determined over a strain interval from 0.5 to 5.0 percent is plotted against strain rate for a specimen deformed at 760°K. Note that the strain rate covers four orders of magnitude and the work hardening rate maximizes at a strain rate of 2.7×10^{-4} sec^{-1}.

It is interesting to compare the work hardening rate of commercial purity titanium with that of a pure face centered cubic metal. Figure 26 gives the average work hardening rate (divided by the modulus) as a function of temperature for copper (data of Carreker[52]) and also for commercial purity titanium deformed at the same rate (10^{-4} sec^{-1}). While the work hardening rate of copper falls continuously with increasing temperature, that of titanium remains nearly constant between about 77° and 600°K. Also note that the copper curve does not show any maximum like that of titanium.

3.6. Elongation

The variation of elongation to fracture with temperature is illustrated in Fig. 27. A well defined minimum, that depends on strain rate, may be seen to occur at

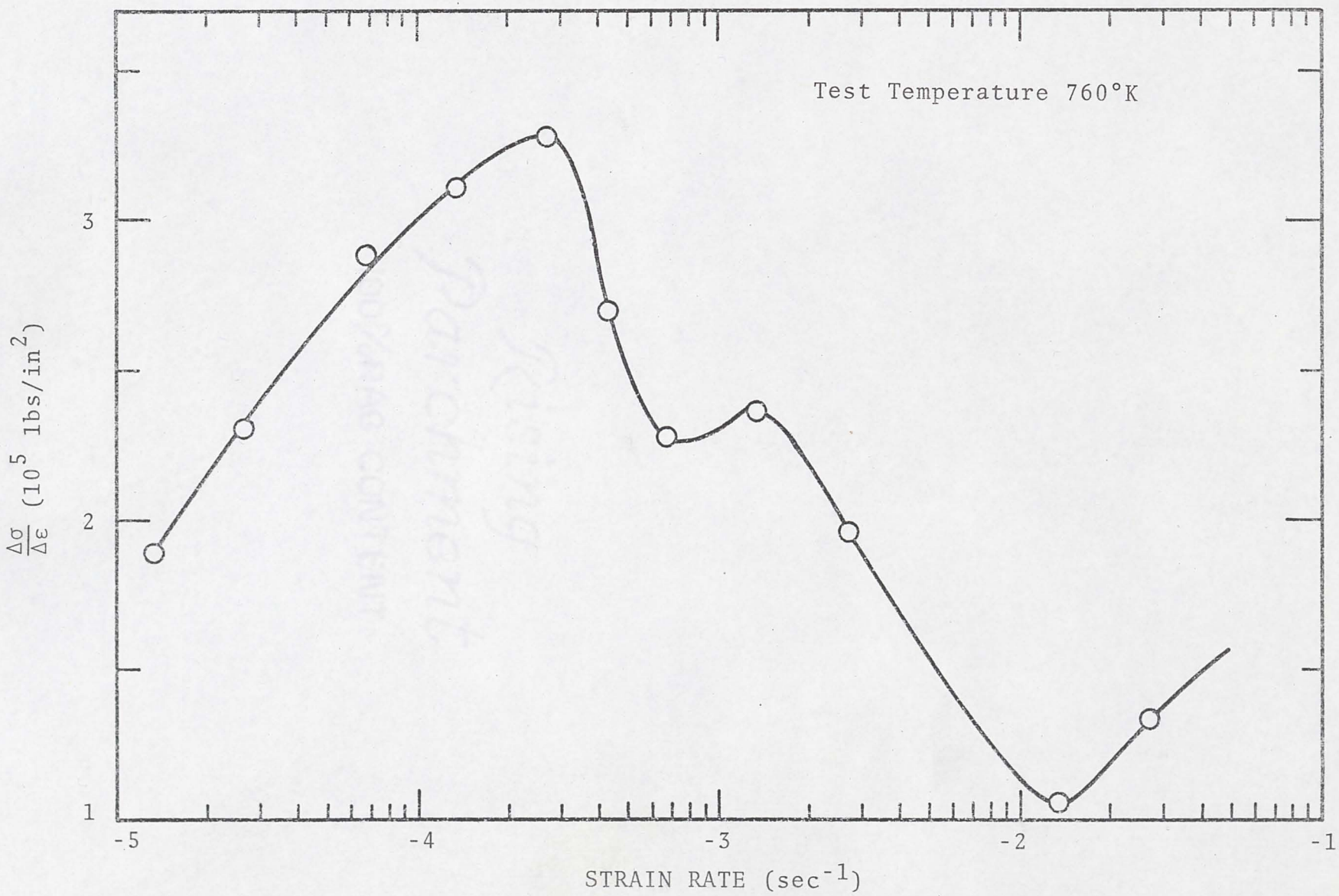

Fig. 25. The effect of strain rate on the average work hardening rate for titanium deformed at 760°K.

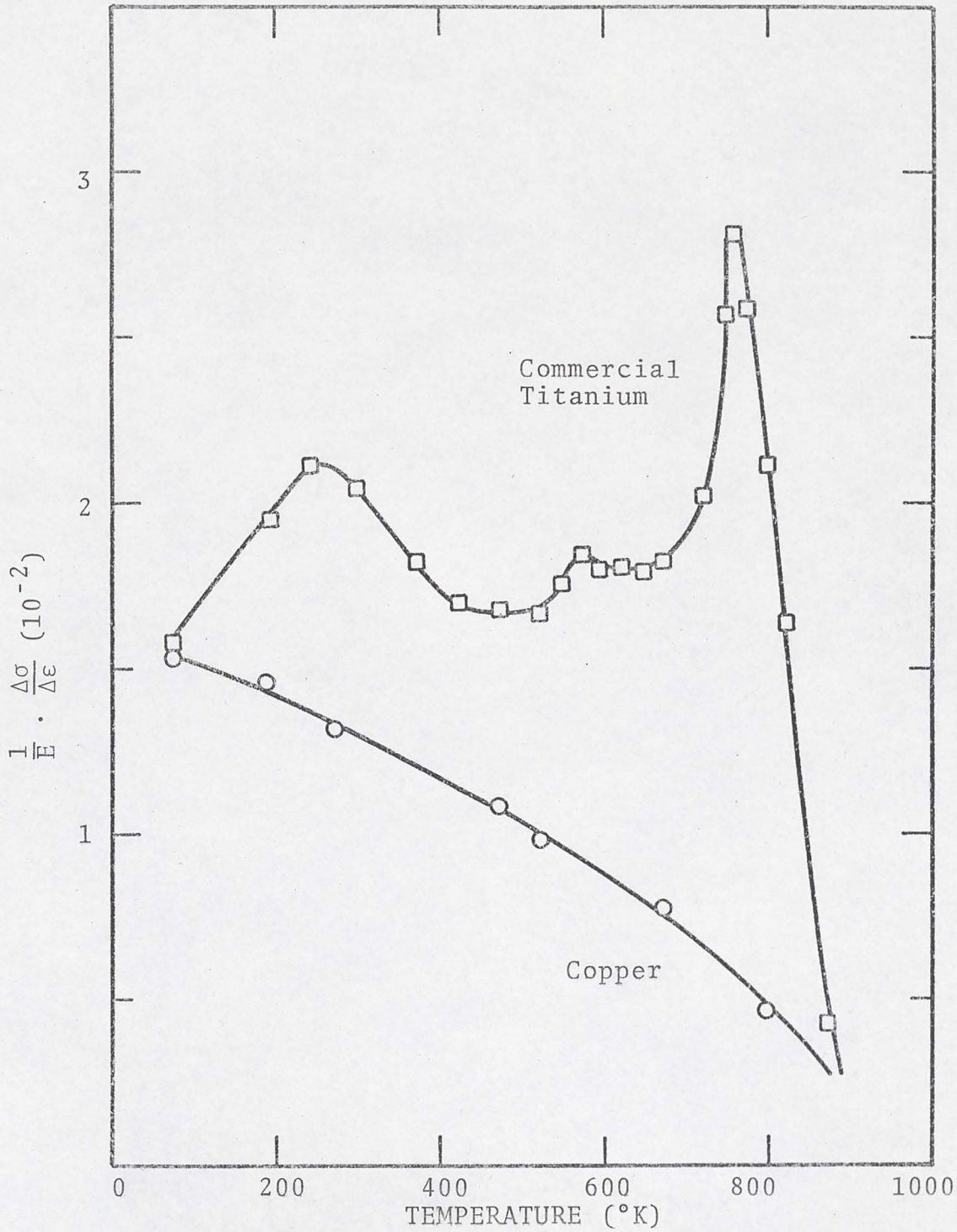

Fig. 26. A comparison of the temperature dependence of the average work hardening rate between 0.5 and 5.0 percent true plastic strains for titanium and copper. To make this comparison more meaningful the work hardening rate has in each case been divided by the elastic modulus. Copper data from Carreker.[52]

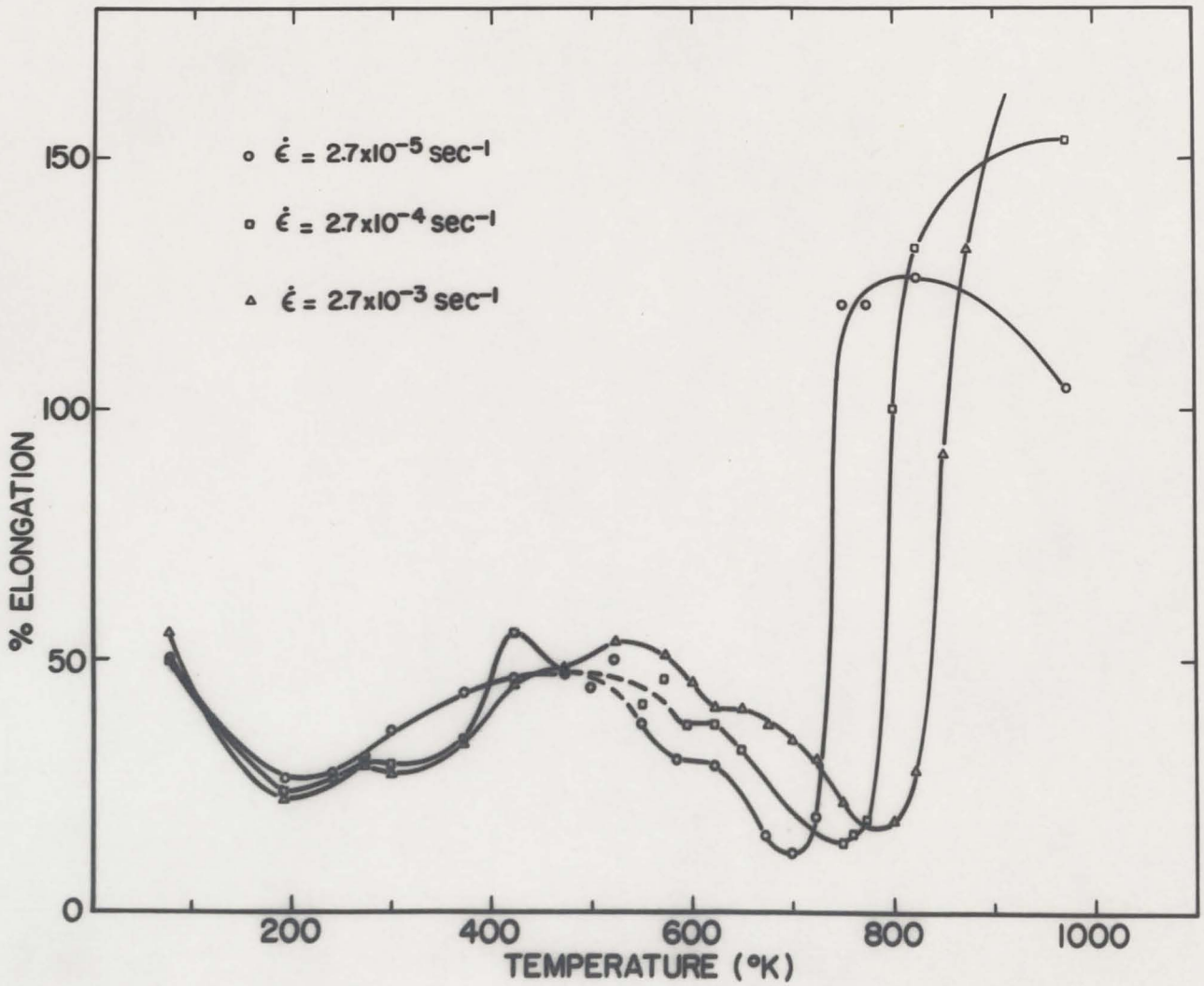

Fig. 27. Variation of the total tensile elongation with temperature for commercial purity titanium.

temperatures above 600°K. This is very similar to the "blue brittle" effect in steels. The elongation minimum in titanium is displaced by about 50°K for every order of magnitude increase in strain rate. There is also another elongation minimum that occurs near 200°K. But the temperature of this elongation minimum is not a function of the deformation rate. The metal shows increased ductility below this temperature. It will be shown that this increased ductility at subambient temperatures is directly related to the ease with which titanium twins in this temperature interval.

Figure 27 is significant in another respect because it demonstrates that the total elongation climbs very rapidly above the ductility minimum temperature. For example, the elongation increases from a low of 10 percent at the ductility minimum to over 120 percent at a temperature only 50°K higher. Correspondingly, there is a change in the necking behavior. At the temperature of minimum elongation, the neck in the tensile specimen is very sharply defined [see Fig. 28(a)]. Above the blue brittle temperature the neck is diffuse or spreads over the entire gage length of the specimen as shown in Fig. 28(b). It is interesting to note that the titanium data of Suiter[18] as well as those of Orava, Stone and Conrad[12] show a similar rapid rise in tensile elongation over a narrow temperature interval but the significance of the phenomenon was not analyzed.

(a)

(b)

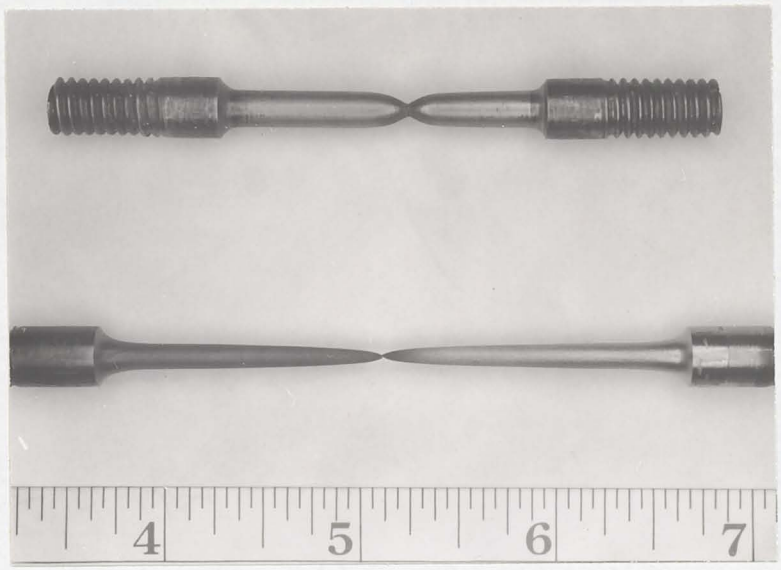

Fig. 28. Fractured tensile specimen profiles showing the two distinct types of neck observed in commercial purity titanium; a) sharp, localized neck, and b) extended or diffuse neck.

The elongation in a tensile test can be divided into two components, that occurring before the neck forms (point of maximum load) and that after it has formed. It should be pointed out, however, that necking may not always start at the point of maximum load. Figure 29 gives the total strain and the necking strain as a function of temperature for one strain rate, 2.7×10^{-5} sec^{-1}. Note that above the minimum ductility temperature (700°K) the major component of the strain is the necking strain. A similar rapid increase in necking strain was observed at all three strain rates. See Fig. 30. As can be seen by comparing Figs. 30 and 24, there is a very close correspondence between the temperature at which the necking strain increases abruptly and the temperature at which the maximum rate of work hardening is observed.

3.7. The Reduction in Area

While the loss in tensile elongation between 600° and 800°K is appreciable in titanium (from 30 percent at 600°K to about 11 percent at 700°K at a strain rate of 2.7×10^{-5} sec^{-1}), the corresponding loss in reduction in area at the same strain rate is much less pronounced. This can be seen in Fig. 31 in which the percent reduction in area at fracture is plotted as a function of temperature. Not only is the loss in reduction in area less marked, but the lowest value recorded is still above 50 percent. With increasing

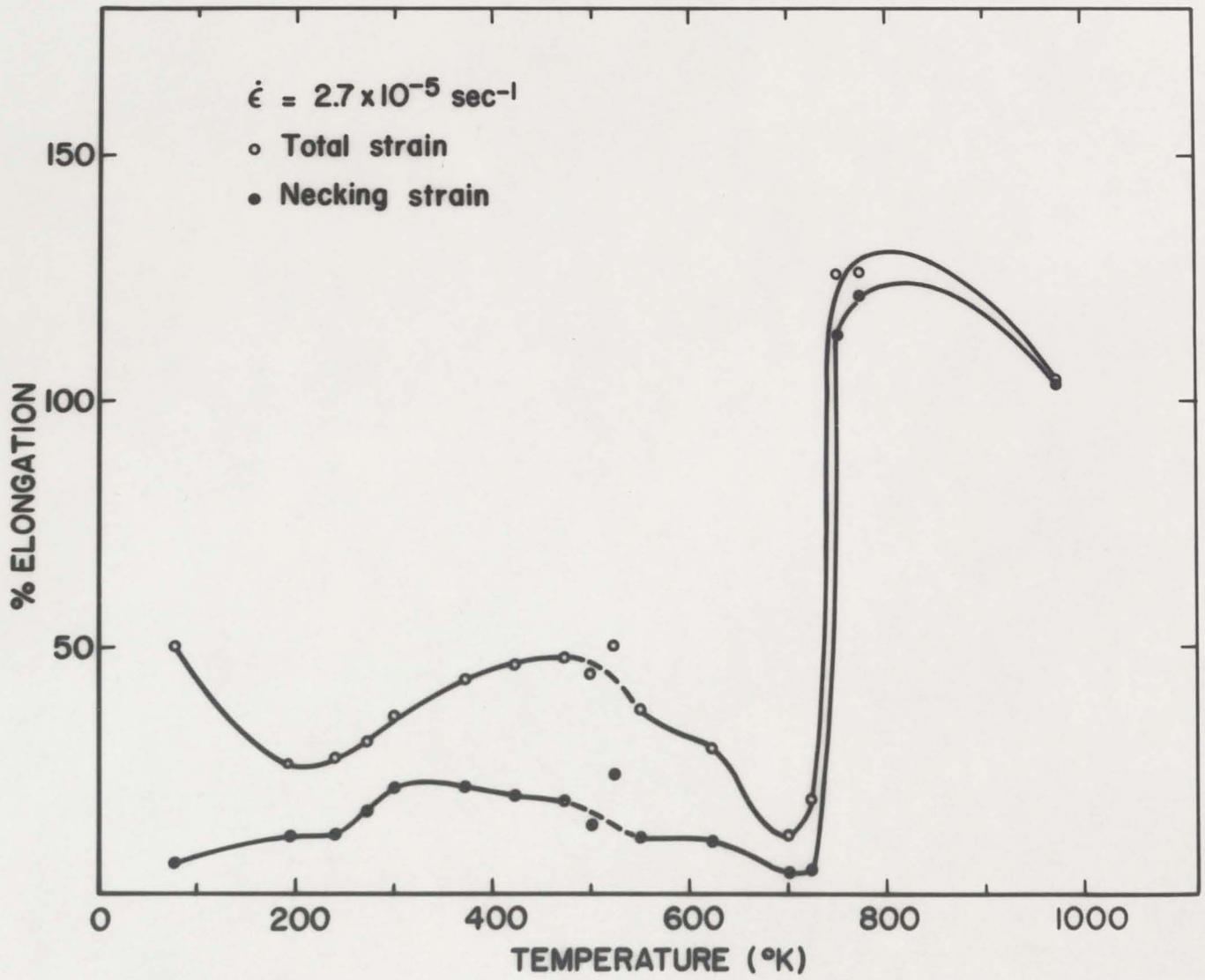

Fig. 29. Variation of the total tensile strain and the necking strain with temperature for titanium deformed at 2.7x10^{-5} sec^{-1}.

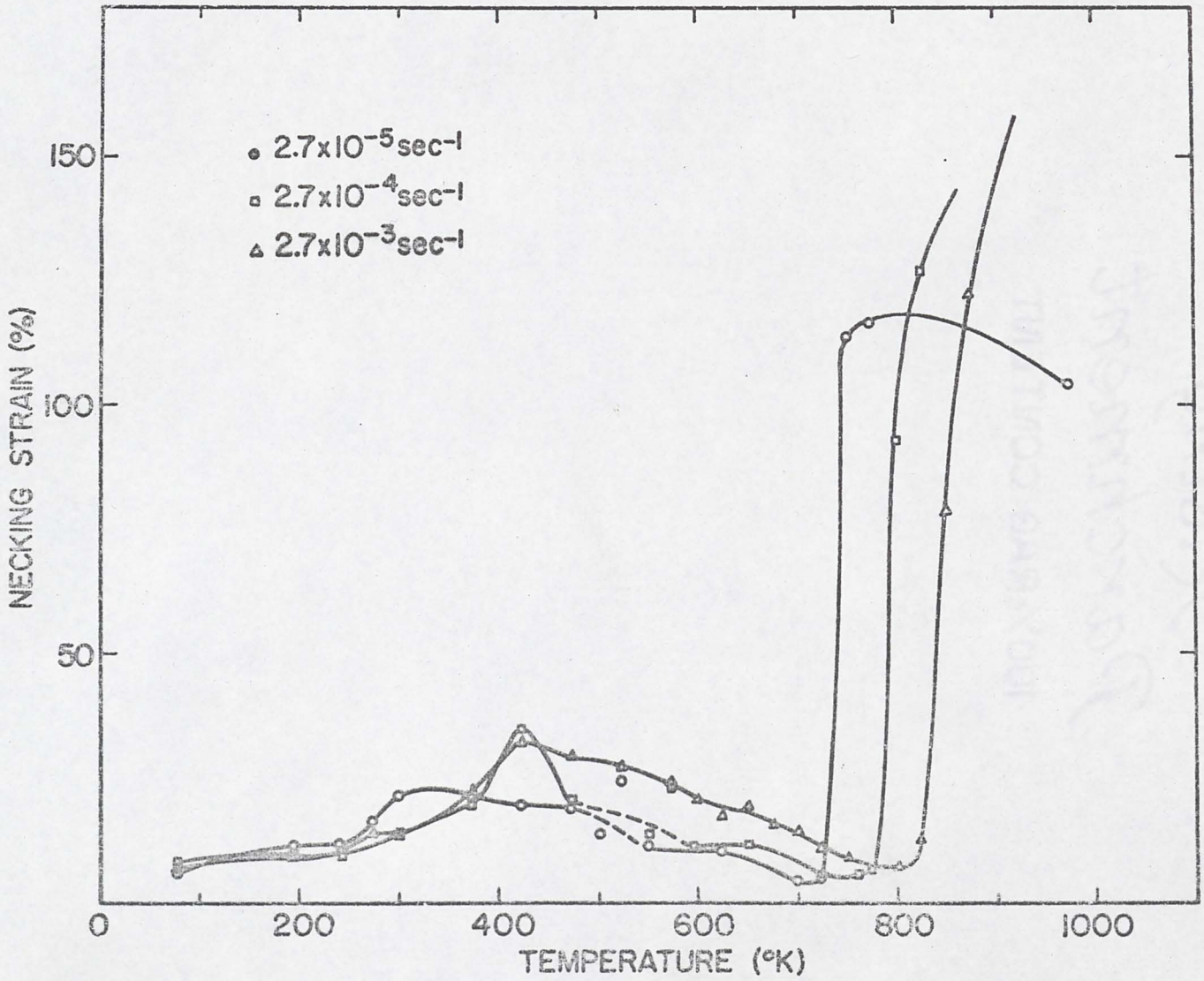

Fig. 30. Variation of the necking strain with temperature for commercial purity titanium deformed at three strain rates.

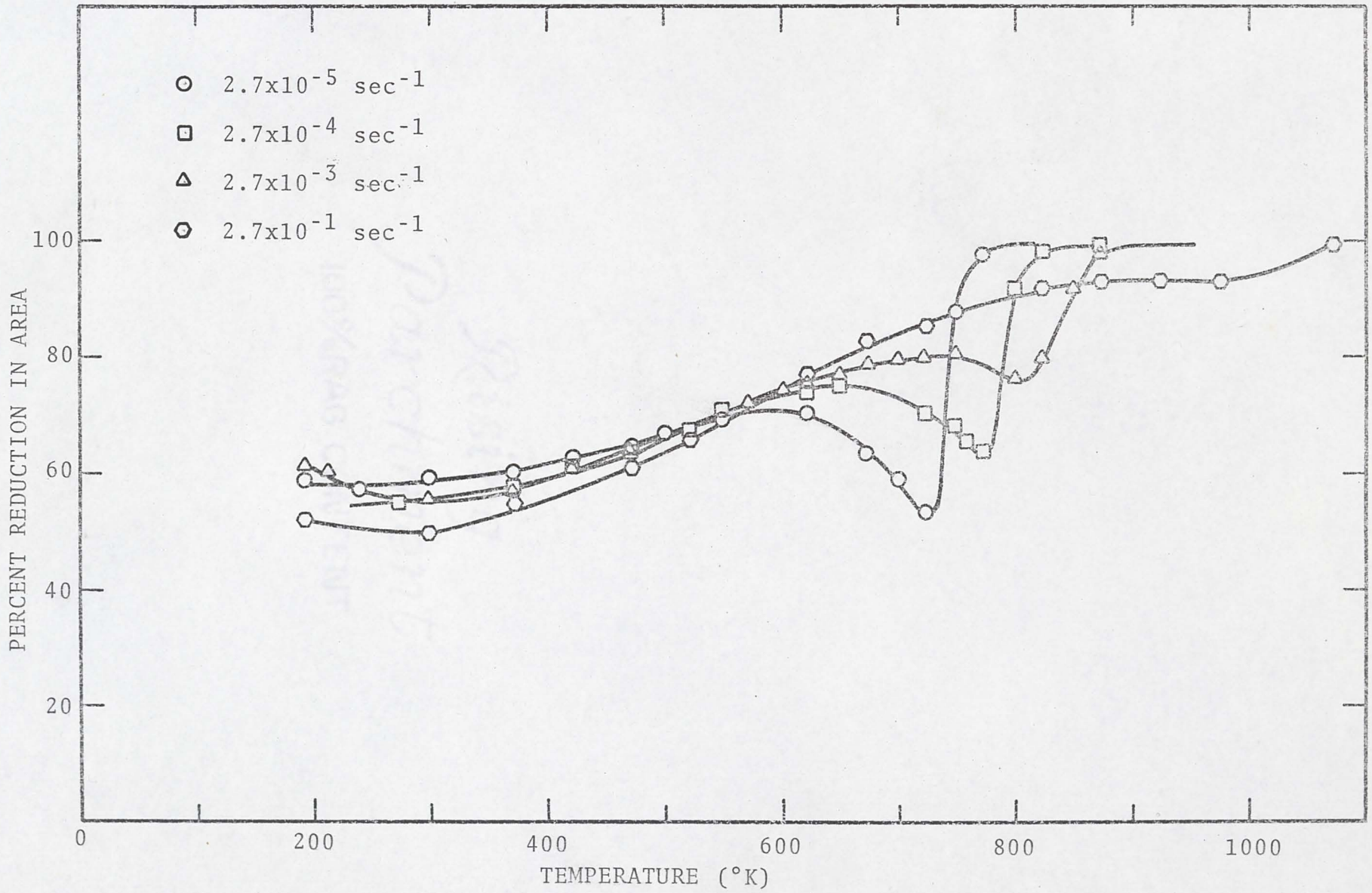

Fig. 31. The temperature dependence of the percent reduction in area for commercial purity titanium.

strain rate the loss in reduction in area gradually disappears.

An adjunct study of the fracture surfaces was made with a Cambridge Scanning Electron Microscope. Figures 32 and 33 show the fractured surfaces of specimens deformed at a strain rate of 2.7×10^{-5} sec^{-1}. The specimen of Fig. 32 was deformed at the temperature of minimum elongation (700°K) and that of Fig. 33 was deformed at the temperature of minimum reduction in area (723°K). Note that there are nearly equiaxed dimples characteristic of a ductile fracture[53] in both specimens.

3.8. Deformation at 77°K

It was shown in Fig. 27 that the total elongation to fracture for commercial purity titanium increases significantly below 200°K. Of particular significance is the deformation behavior at 77°K. Five specimens were deformed at this temperature at strain rates ranging from 2.7×10^{-5} to 2.7×10^{-1} sec^{-1}. The data obtained in these tests are given in Table I. This table clearly shows the large ductility of the metal at subambient temperature. It also shows that there is not much variation in the values of total elongation between the four lower strain rates. Furthermore, most of the strain occurs before necking starts. The specimen deformed at the faster rate, 2.7×10^{-1} sec^{-1}, however, shows poor ductility.

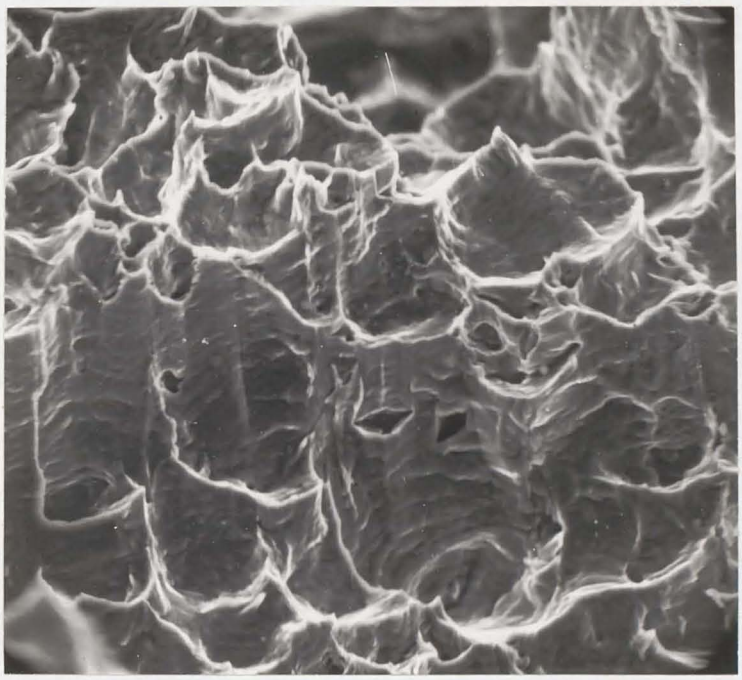

Fig. 32. Scanning electron micrograph of fracture surface of titanium deformed at the "blue brittle" temperature (700°K, strain rate 2.7×10^{-5} sec^{-1}). Magnification 600 times.

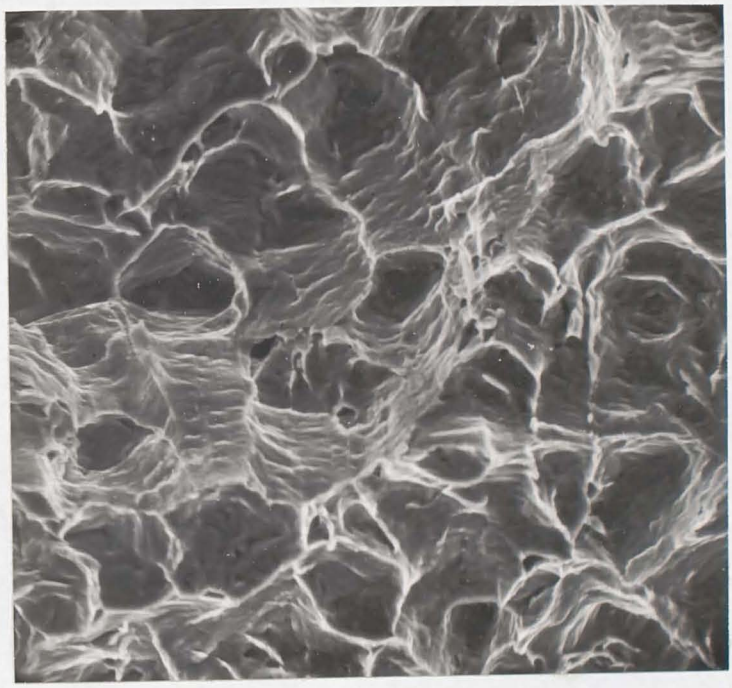

Fig. 33. Scanning electron micrograph of fracture surface of titanium deformed at the temperature of minimum reduction in area (723°K, strain rate 2.7×10^{-5} sec^{-1}). Magnification 575 times.

Table I

Elongation Data for Commercial Purity Titanium at 77°K

	Strain Rate (sec^{-1})				
	$2.7x10^{-5}$	$2.7x10^{-4}$	$2.7x10^{-3}$	$2.7x10^{-2}$	$2.7x10^{-1}$
Total Strain (%)	50	50	55	42	12
Uniform Strain (%)	44	41	48	40	7
Necking Strain (%)	6	9	7	2	5

The shapes of the stress-strain curves are also peculiar at 77°K. Figure 34 shows true stress-true strain curves up to the point of maximum load for all the five specimens. Note that the curves are linear for the entire range of uniform strain. Linear true stress-true strain curves in nearly pure metals are an exception rather than the rule. Risebrough and Teghtsoonian[54] reported linear hardening in cadmium below room temperature. But even in this metal, the linear stress-strain behavior was limited to a small strain interval. In general, most pure metals show enough dynamic recovery to give their stress-strain curves a continuously decreasing slope. This is shown in Fig. 35 for the case of a longitudinal zirconium[55] specimen deformed at 77°K. While the curvature of the zirconium curve is not discernible in the figure, the instantaneous slope, $d\sigma/d\varepsilon$, plotted on the same diagram clearly shows that the work hardening rate of the zirconium specimen falls continuously with increasing strain. Contrast this work hardening behavior with that of the titanium shown in the same diagram. In this latter case, the work hardening rate, after the first 1 percent plastic strain, remains nearly constant to a true strain of about 35 percent. The constancy of $d\sigma/d\varepsilon$ over such a large strain interval implies that the work hardening rate in titanium is abnormally large at large strains. An important consequence of such a behavior is that the Considère condition for the beginning of

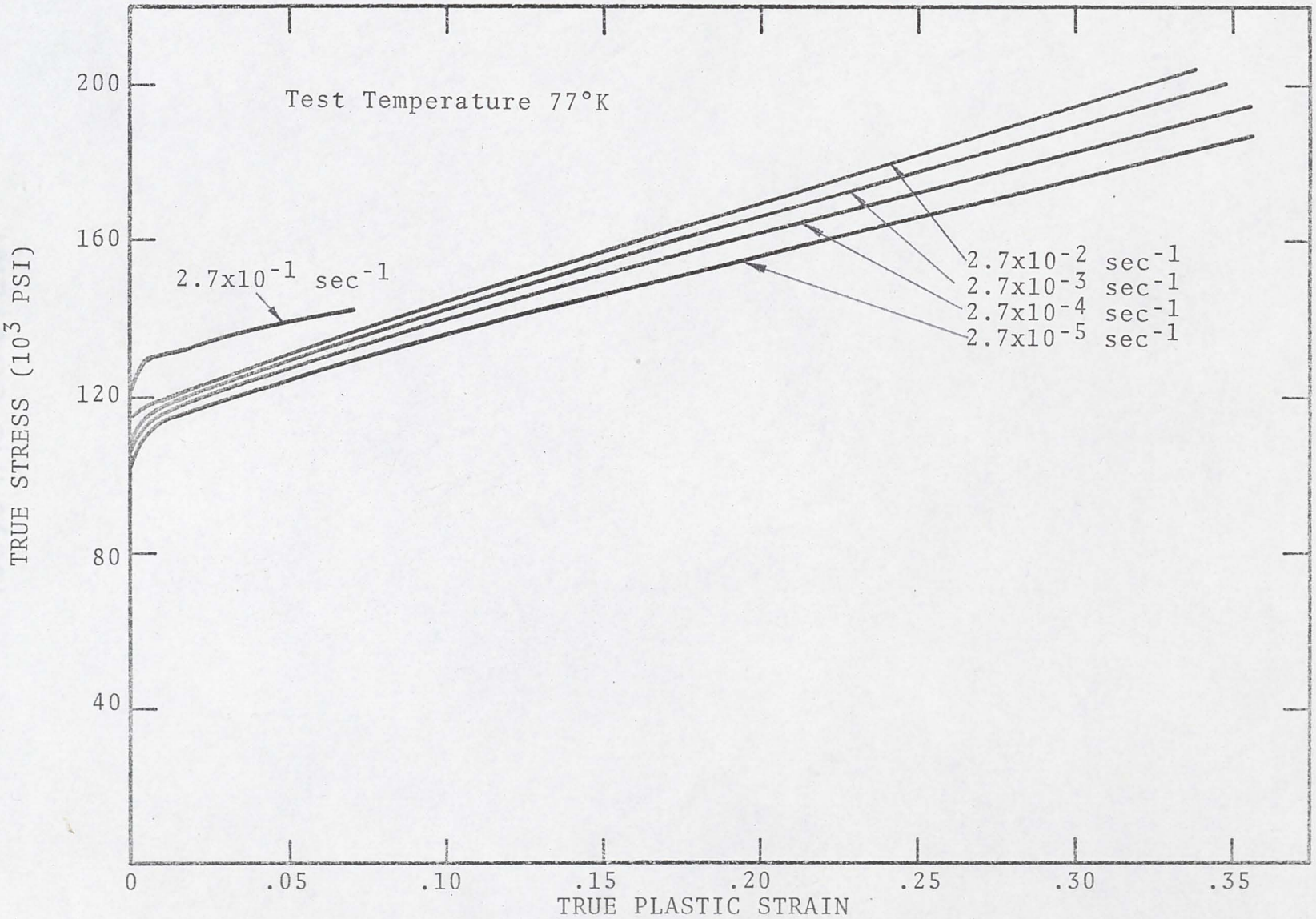

Fig. 34. True stress-true plastic strain curves for titanium deformed at 77°K. Note the low tensile elongation of the specimen deformed at the fastest rate 2.7×10^{-1} sec^{-1}.

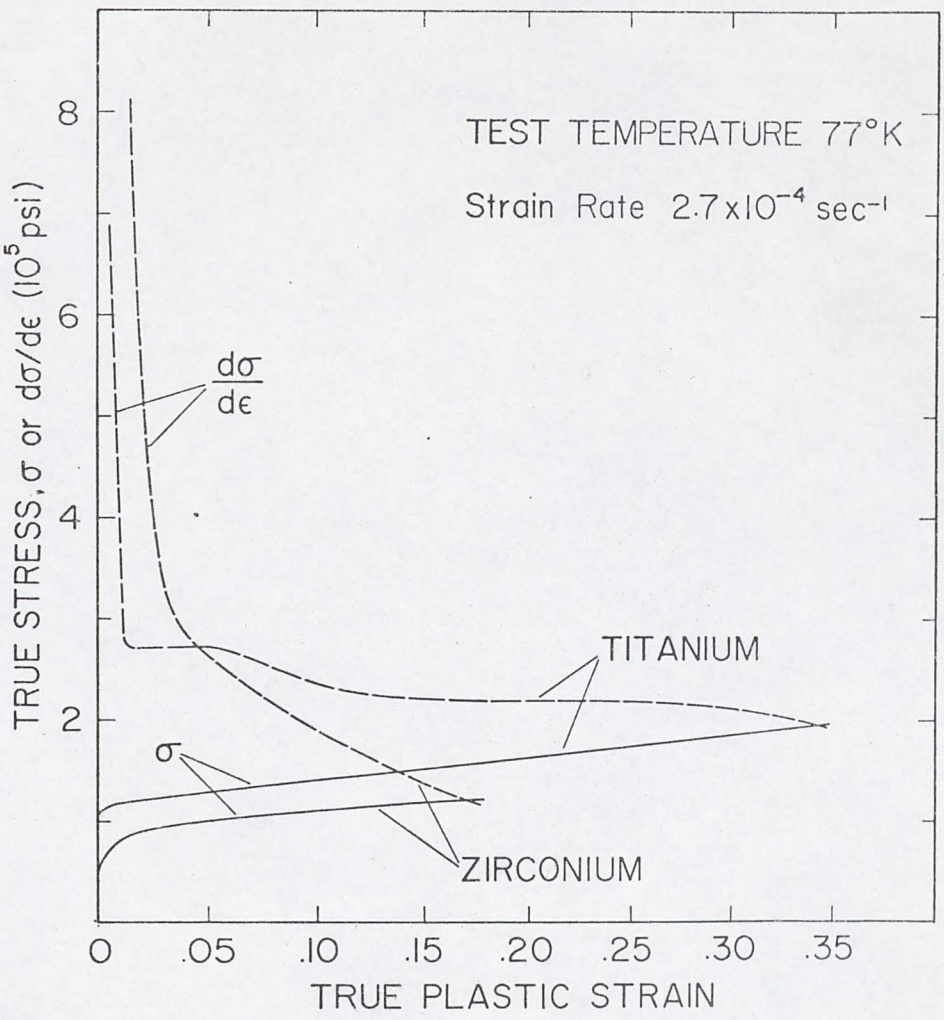

Fig. 35. The large difference between the stress-strain curves of longitudinal titanium and zirconium specimens at 77°K is best shown by comparing the variation of the slopes of the two curves with strain. Note that the work hardening rate of the titanium specimen remains effectively constant for strains greater than 1 percent, whereas that of the zirconium specimen falls continuously with strain.

necking ($d\sigma/d\varepsilon = \sigma$) is satisfied only at very large strains. A linear true stress-true strain curve is thus associated with a large elongation.

A metallographic examination of the specimens deformed at 77°K showed profuse deformation twinning. Figure 36 shows the volume fraction of twins as a function of strain for two specimens deformed at 77°K. One was deformed at 2.7×10^{-4} sec^{-1} and the other at three orders of magnitude faster strain rate. Notice that the twinning rate of the slowly deformed specimen is nearly twice that of the rapidly deformed specimen. It should be borne in mind that the former exhibited nearly five times greater elongation than the latter.

The importance of twinning in the low temperature deformation of titanium can be better appreciated with the aid of photomicrographs. Figures 37 and 38 show microstructures of specimens deformed to 10 percent and 40 percent strain, respectively, at a rate of 2.7×10^{-4} sec^{-1}. Note that at 10 percent strain twins have been nucleated homogeneously in the structure. At 40 percent strain, the entire structure is loaded with twins and it is sometimes even difficult to delineate the grain boundaries. Now compare the microstructures of Figs. 37 and 38 with those of Figs. 39 and 40 obtained with specimens deformed at the faster rate, 2.7×10^{-1} sec^{-1}. These again correspond to the same strain levels as those in Figs. 37 and 38. While

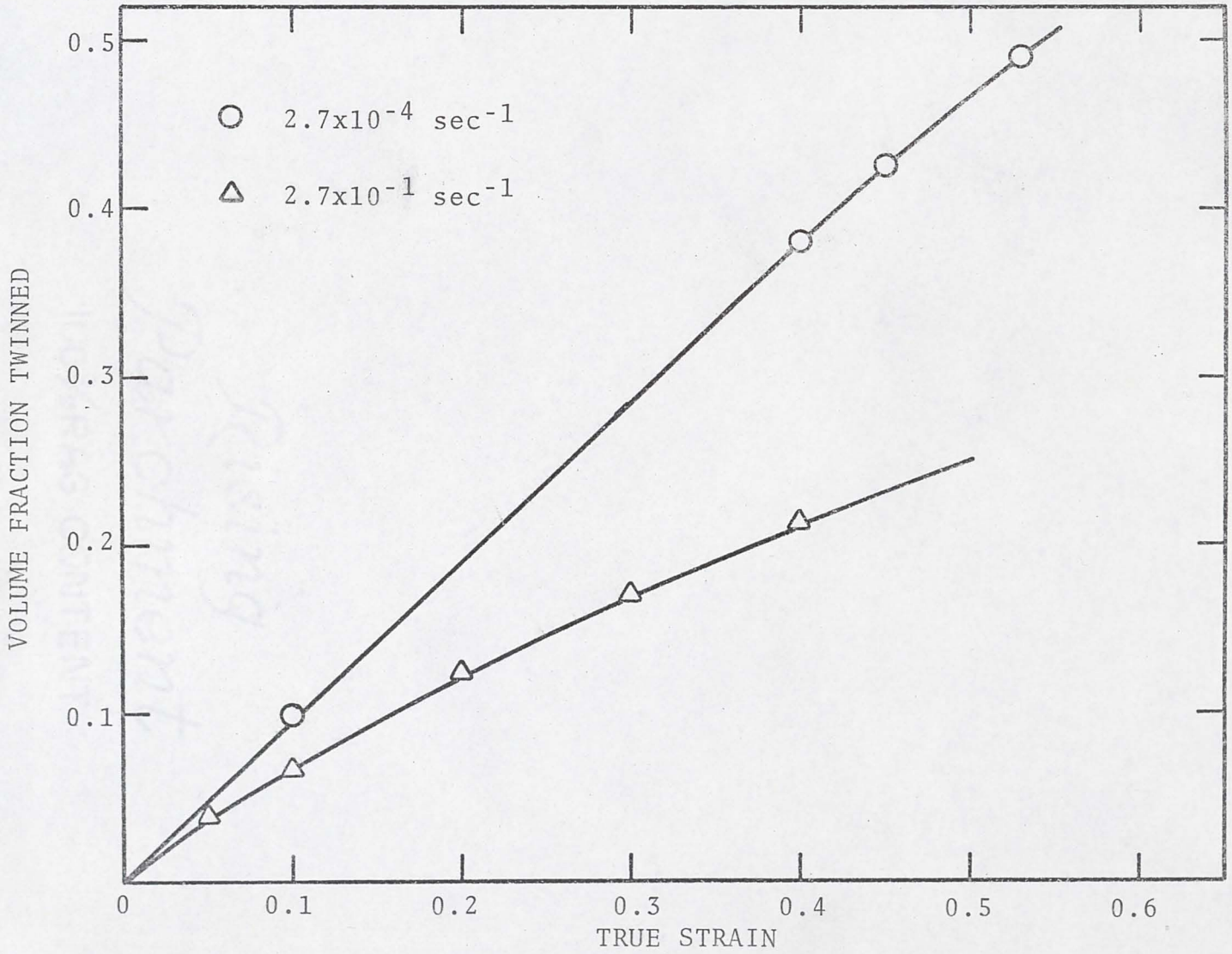

Fig. 36. The volume fraction of twins as a function of strain in titanium specimens deformed at 77°K and at two different strain rates.

Fig. 37. Microstructure of a titanium specimen deformed 10 percent at 77°K. Strain rate 2.7×10^{-4} sec^{-1}. Magnification 250 times.

Fig. 38. Microstructure of a titanium specimen deformed 40 percent at 77°K. Strain rate 2.7×10^{-4} sec^{-1}. Magnification 250 times.

Fig. 39. Microstructure of a titanium specimen deformed 10 percent at 77°K. Strain rate 2.7×10^{-1} sec^{-1}. Magnification 250 times.

Fig. 40. Microstructure of a titanium specimen deformed 40 percent at 77°K. (This larger strain was observed in the necked area of the specimen.) Strain rate 2.7×10^{-1} sec^{-1}. Magnification 250 times.

there is no appreciable difference in twin density at low strain, there is definitely much less twinning activity at 40 percent strain in the specimen deformed at the faster rate.

3.9. Strain Rate Change Tests

In general, the flow stress of metals increases with an increase in deformation speed. But the manner in which the flow stress varies, upon an instantaneous change in rate, would depend on both the temperature as well as the strain rate employed. Often, a change in deformation speed results in the flow stress varying smoothly and continuously to a value characteristic of the new rate. Such a behavior is shown schematically in Fig. 41(a) and will be referred to as "ideal." On the other hand, as shown in Fig. 41(b), it is also possible to observe yield drops on an increase in deformation rate as well as negative yield drops with a decrease in crosshead speed.

Figures 42 and 43 show true stress-true strain plots for commercial purity titanium deformed in tension. In these tests, the strain rate was varied by either one or two orders of magnitude. Note that ideal behavior is obtained at the two lowest temperatures (300° and 373°K) and also at the two highest temperatures (873° and 973°K). Transient flow stress maxima and minima are observed at intermediate

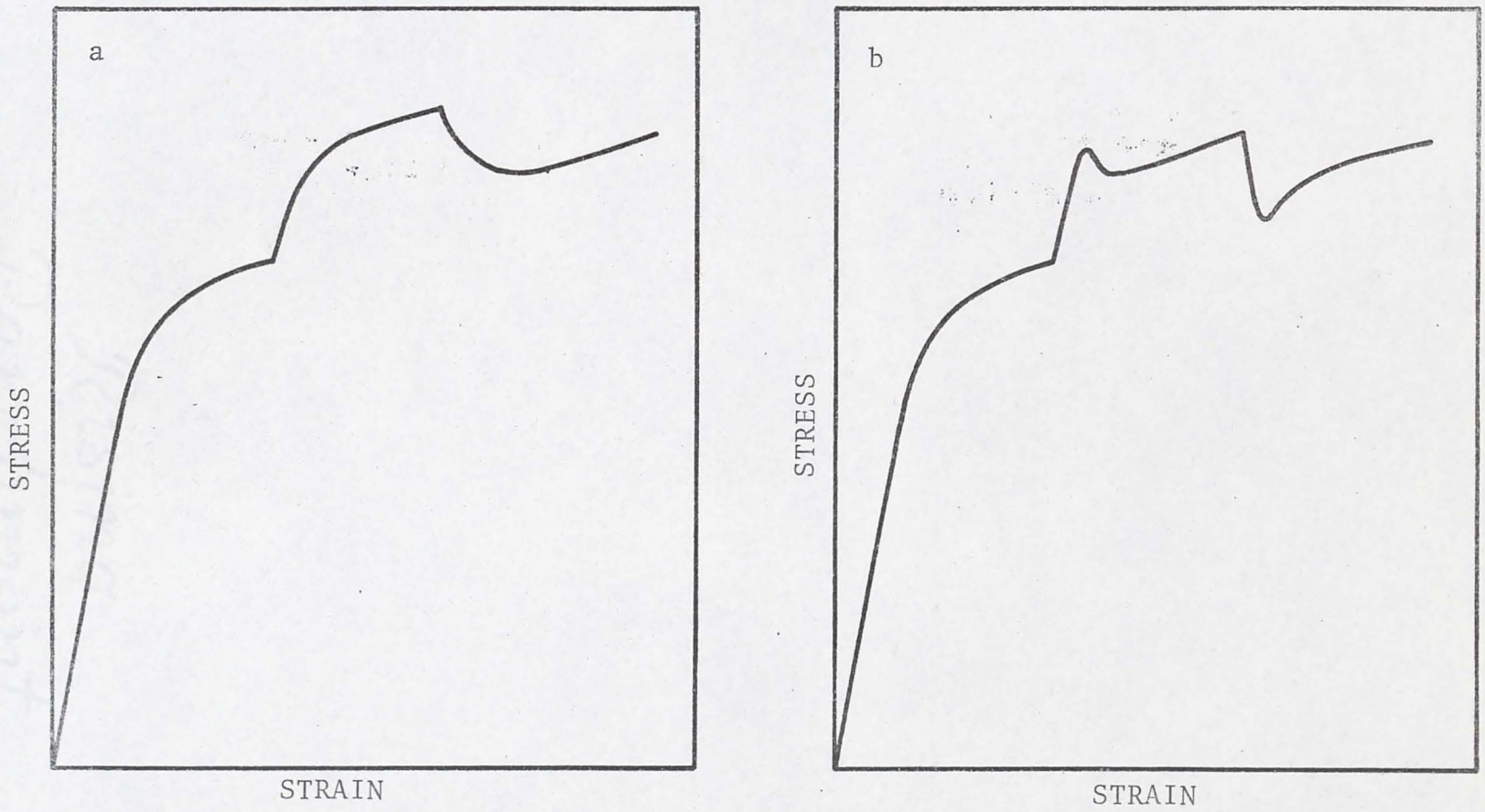

Fig. 41. Schematic stress-strain curves corresponding to change of strain rate: a) ideal case, and b) transient maxima and minima.

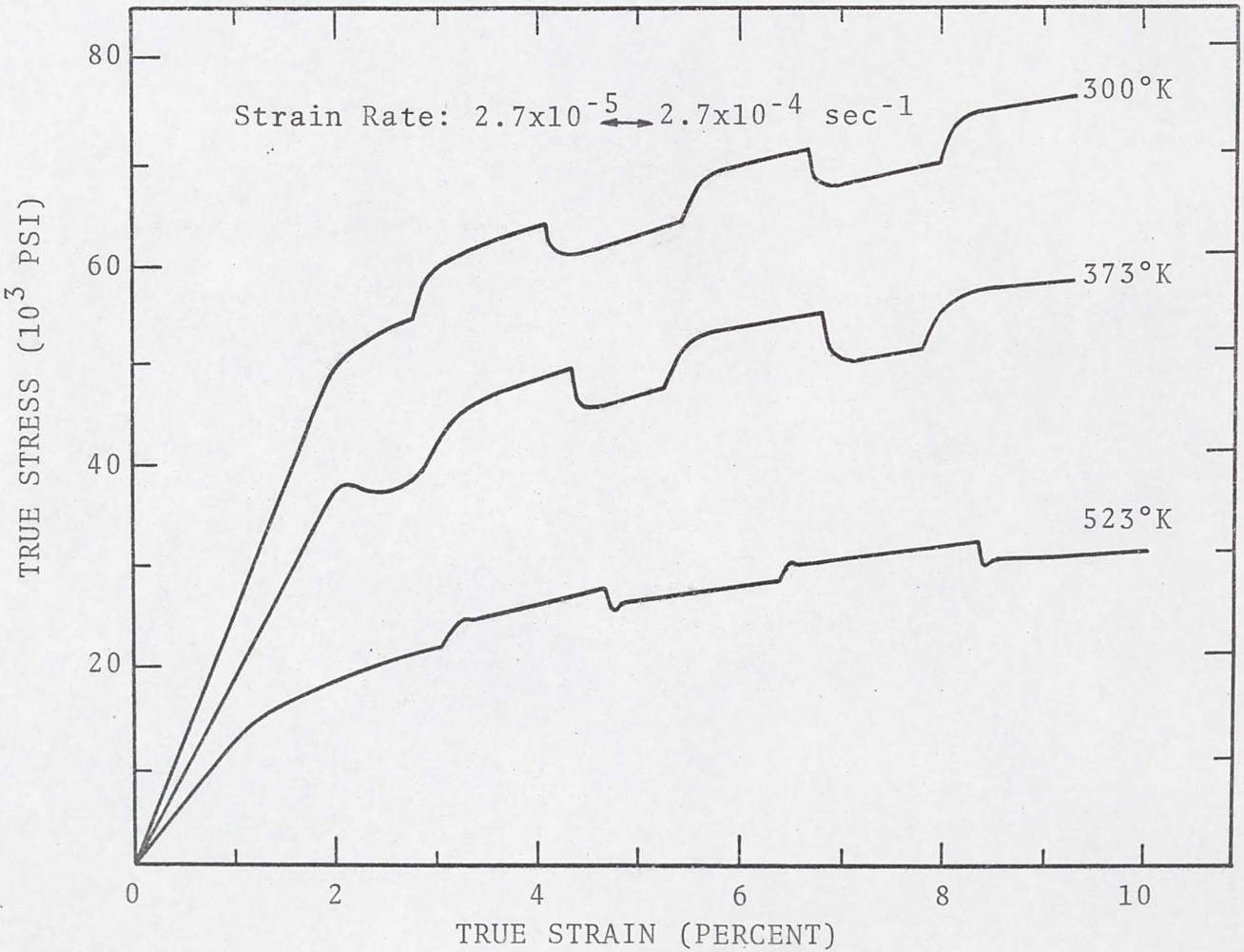

Fig. 42. Experimental strain rate cycling stress-strain curves of titanium.

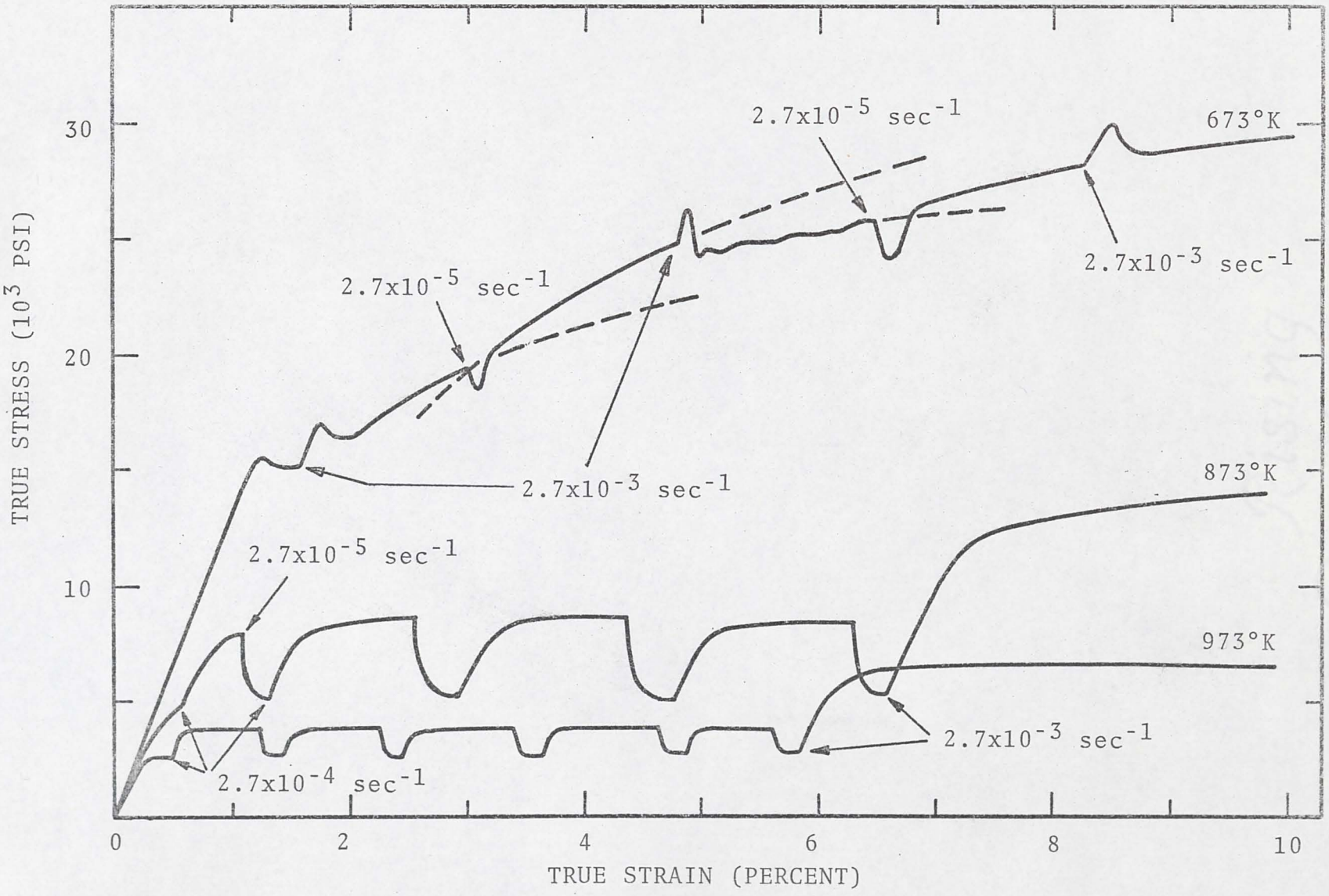

Fig. 43. Experimental strain rate cycling stress-strain curves of titanium.

temperatures (523° and 673°K). Similar transient flow stress peaks were also observed by Orava, Stone and Conrad[12] in commercial titanium in a temperature range centered around 200°K.

Yield drops upon change in strain rate have also been observed in single crystals of copper,[56-58] aluminum,[56] silver,[56,57] lead[57] and polycrystalline copper,[57], aluminum[56,57] and iron.[57] Bolling et al.[57] postulated that the transient effects of the present type may result from the effect of speed changes upon the testing machine. However, it is significant that in titanium, they were observed only at those temperatures where deformation behavior was anomalous. In order to test the hypothesis of Bolling et al., strain rate change tests were performed on aluminum 6061-T6, which exhibits similar yield drop effects at room temperature. The specimen was strained at 300°K at slow rates (2.7×10^{-5} and 2.7×10^{-4} sec^{-1}) and rate changes were accomplished by an electronic switching mechanism. Both load and specimen elongation were simultaneously recorded as a function of time. The latter was measured by attaching a strain gage extensometer directly to the specimen.

The upper curve in Fig. 44 shows the Instron load-time plot. The lower curve is the corresponding strain recorder plot showing how the specimen elongation varied with time. Notice that whenever the crosshead speed was changed, the slopes in the specimen elongation versus time

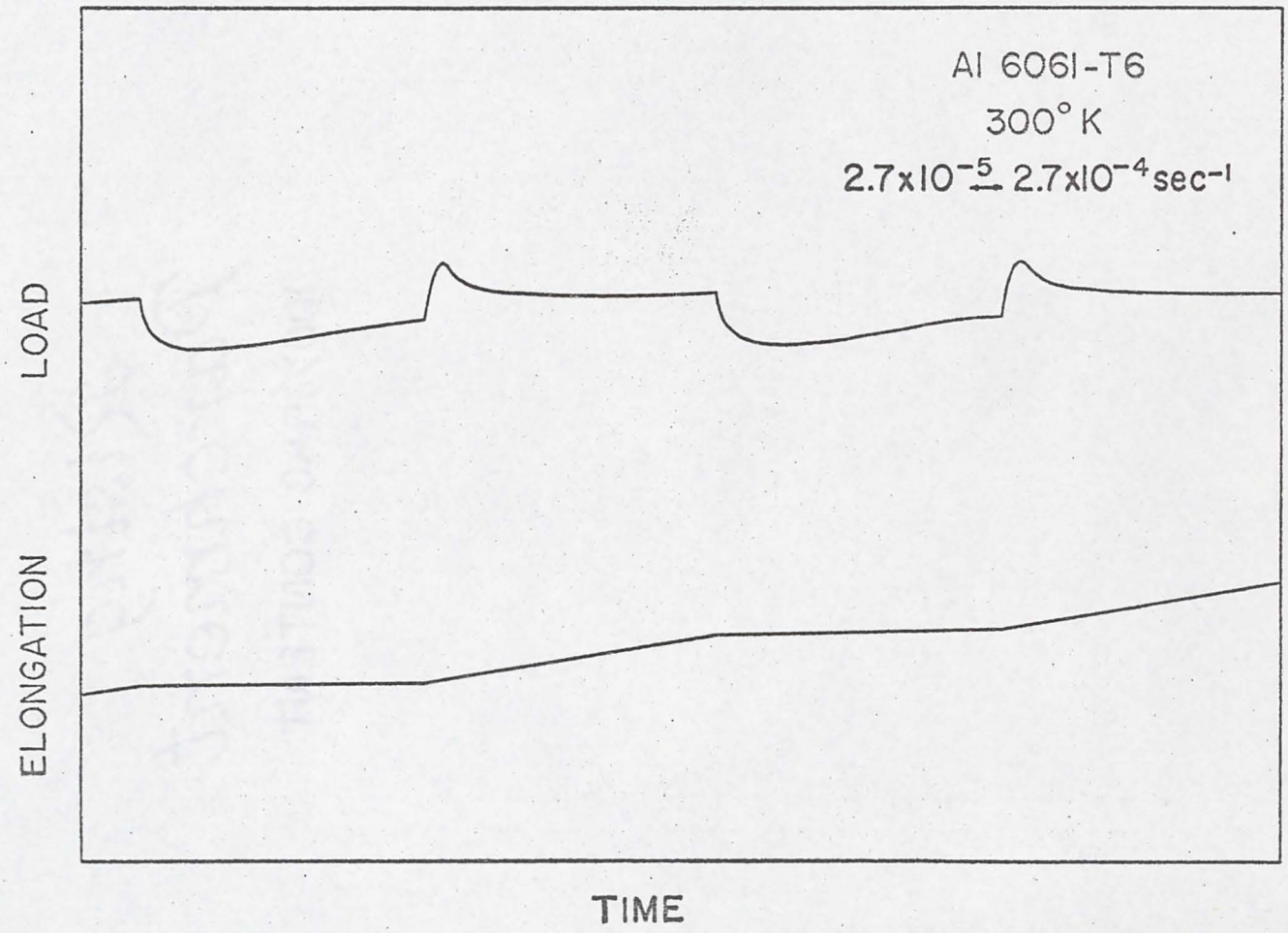

Fig. 44. Corresponding room temperature load-time and elongation-time curves for Al 6061-T6.

curve changed sharply, implying that the new deformation rate was achieved in the specimen in a time interval much smaller than that associated with the transient flow stress maxima and minima. One is thus led to believe that the yield drop effects are actually characteristic of the materials at temperatures at which they are observed. If this inference is true, it should be possible to predict the shape of the stress-strain curves from dislocation dynamics. The phenomenon will be analyzed from this point of view.

The strain rate sensitivity of the flow stress was determined from strain rate change experiments using Eq. (12). The resulting variation of strain rate sensitivity with temperature is shown in Fig. 45. Note that the strain rate sensitivity, instead of increasing linearly as in Carreker's platinum data shown in Fig. 2, deviates at two temperature intervals, one centered about 250°K and the other centered about 700°K. The general shape of the n-T curve is very similar to that obtained by Ramaswami and Craig[59] and by Ramachandran and Reed-Hill[42] for zirconium, and Orava et al.[12] for titanium. Attention is called to the nearly zero value for the strain rate sensitivity parameter between about 673° and 773°K. This is exactly the temperature interval where other anomalies like athermal flow stress, rate dependent work hardening and ductility minima are observed. Its significance will be discussed in the next chapter.

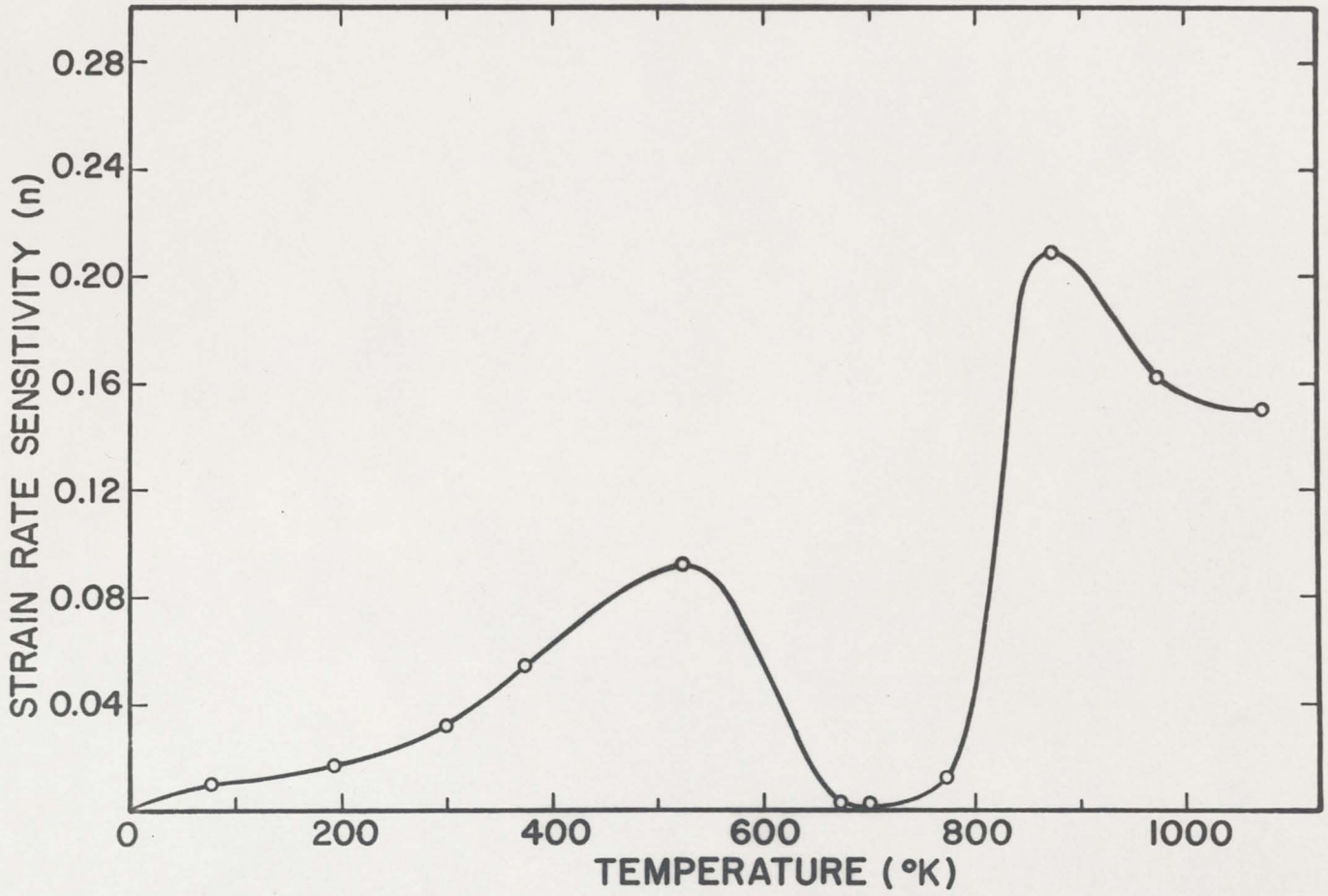

Fig. 45. The variation of the strain rate sensitivity of titanium with temperature.

CHAPTER IV

DISCUSSION

4.1. Athermal Flow Stress

We shall first consider the temperature dependence of the yield stress. In Fig. 10 it was observed that when the logarithm of the yield stress was plotted as a function of the absolute temperature, a linear relationship implied by Eq. (5) is not obtained. Instead, two positive deviations were observed. These were centered at about 300° and 700°K, respectively, at a strain rate of 2.7 x 10^{-5} sec^{-1}. On normal cartesian coordinates, the higher temperature deviation of Fig. 10 appears in part as a nearly temperature independent yield stress (Fig. 9). There is also negligible strain rate dependence in this interval. These two attributes are certainly in agreement with the concept of an athermal stress. However, this view may be questionable in the case of titanium. This is because the temperature interval in which the yield stress plateaus are observed are regions in which the stress-strain curves are serrated. Furthermore, the plateau stress itself may be a manifestation of dynamic strain aging. This can be demonstrated from a simple calculation.

There is a large body of experimental evidence[24,60] to the effect that the long-range flow stress component is related to the total dislocation density, ρ, through the relation

$$\tau_\ell = \alpha\mu b\rho^{1/2} \qquad (17)$$

where μ is the shear modulus, b is the Burgers vector, and α is a constant that takes into consideration the dislocation arrangement. Assuming a dislocation density of 10^9 cm^{-2} at a strain of 0.002 from Jones and Conrad's[61] data on commercial titanium, a μ of 4×10^6 psi at about 650°K and an α of 0.5, we get for τ_ℓ a value of 1,800 psi at a temperature inside the plateau region. Assuming a Taylor factor of 2.78,[38] the tensile yield stress in the plateau region should be 5,000 psi. The observed value was 15,000 psi. This large discrepancy between the observed value and that calculated on the assumption of a simple athermal flow stress clearly brings out the inconsistency in the latter concept. It also shows that there must be another component to the flow stress in this temperature interval. In this regard, it is interesting to note that a number of investigators[62-64] have pointed out that the flow stress in the plateau region may be the result of the combination of a drag stress due to dislocation interaction with impurity atoms and a normal thermally activated component. The following quotation is from Tyson.[44] "In the plateau region

and above (700°K) the components of the flow stress are more difficult to identify. Clearly, there must be an athermal component of the flow stress due to the dislocations present. However, the presence of strain aging complicates the interpretation; it appears that the interstitial impurities are sufficiently mobile at this temperature to produce dynamic aging effects."

4.2. The Effect of Dynamic Strain Aging on the Work Hardening Rate

The present results on commercial purity titanium are in agreement with those of Rosi and Perkins[14] in that its deformation behavior is complex in the temperature range, 500° to 850°K. Apart from the low strain rate sensitivity, the serrated stress-strain curves, the temperature and strain rate independent yield stress, the other important findings in this temperature range are

1. the effect of strain rate on the shapes of the stress-strain curve
2. the strain rate dependent work hardening maxima
3. the ductility minima.

Peaks in flow stress and high work hardening rates have been observed in commercial metals of all the three basic crystal structures (ferritic steel,[65-67] austenitic steel,[68] nickel containing carbon[69] or hydrogen[70-73] and zirconium[42]) and have been shown to be manifestations of dynamic strain

aging. In other words, in the temperature range where work hardening maxima are observed, one must consider the diffusion controlled interactions of solute atoms with moving dislocations.

Transmission electron microscope studies in steel,[24,36,38] vanadium[74] and nickel-hydrogen alloy[71] have revealed that there is a much greater increase in dislocation density for a given strain in the dynamic strain aging region than at other temperatures. It is possible that the dislocations might become pinned by solute atoms and fresh dislocations have to be created in order to allow deformation to proceed. There are other viewpoints that the increased strength may result from an increased frictional drag on moving dislocations by Snoek ordering and Cottrell atmospheres.[35]

If the increased work hardening rate in the dynamic strain aging region is due to a rapid increase in dislocation density with strain, this can be brought about either by activation of additional dislocation sources or by a decrease in the rate of dynamic recovery or by both.

Let us now consider the rate dependence of work hardening. Little attention has been paid to this subject in the past. This is probably because the investigators have associated serrated flow to be the most important aspect of dynamic strain aging. While serrations are weaker in titanium, the rate dependent work hardening is very pronounced. This was shown in Figs. 22, 24 and 25. In particular, the

data of Fig. 25 showed that at 760°K the work hardening rate showed a maximum at an intermediate strain rate of 2.7×10^{-4} sec^{-1}. This behavior can be rationalized in terms of the relative values of the diffusivity of the interstitial atoms and the dislocation velocity. At very low strain rates and dislocation velocities, there is enough time for solute atoms to go to equilibrium positions and form atmospheres. The dislocations would then carry the atmosphere along with them. On the other hand, at high strain rates, the solute atoms cannot be expected to catch up with the fast moving dislocations and will essentially act as fixed barriers to the moving dislocations. At the intermediate dislocation velocities, a maximum drag of solute atoms can occur. Since a coupling between dislocation velocity and diffusivity is involved, it is reasonable to expect the work hardening rate maximum to shift to a different strain rate when the deformation temperature is changed.

It is of interest to compare the work hardening rates observed in the dynamic strain aging region in commercial purity titanium with those in mild steel. There is, however, a difficulty in comparing the steel and titanium data because in steel the Lüders extension is normally larger than in titanium. For example, some of Brindley and Barnby's[36] mild steel specimens of 20μ grain size showed as high as 3 percent Lüders extension as compared to less than 0.5

percent in the present commercial purity titanium specimen. In order to calculate $1/E(\Delta\sigma/\Delta\varepsilon)$ values for their specimens, it was necessary to extrapolate some of their curves back to a strain of 0.5 percent. The results are shown in Fig. 46. While it is recognized that the data in this diagram are qualitative because of this extrapolation, this figure implies that the rate dependent work hardening phenomenon in steel involves a peak of about a 15 percent greater height than that of the titanium peak. If the height of the work hardening rate maximum is a measure of the significance of dynamic strain aging, this diagram shows that strain aging effects in titanium are nearly comparable to those in steel.

Another work hardening rate curve for mild steel with a ten times coarser grain size, also derived from Brindley and Barnby data,[36] is shown in Fig. 46. A comparison of the two curves for steel suggests a strong effect of grain size on the magnitude of the work hardening rate maximum in steel.

4.3. Apparent Activation Energies of Dynamic Strain Aging

The effect of strain rate on dynamic strain aging may be most conveniently described in terms of activation energies obtained from Arrhenius plots. Cottrell[75] was the first to demonstrate that Manjoine's data[33] for the initial appearance of serrations in mild steel can be represented

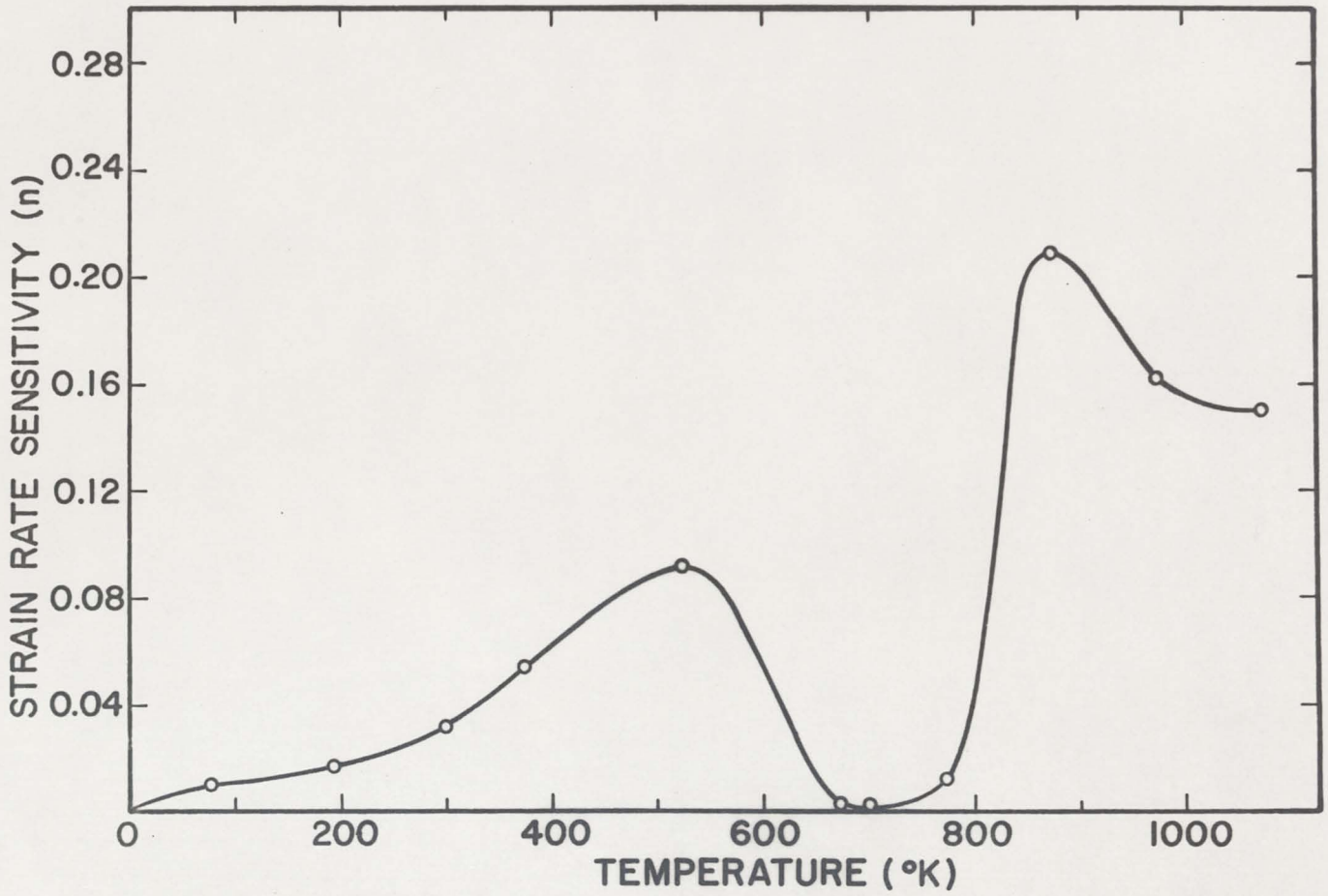

Fig. 45. The variation of the strain rate sensitivity of titanium with temperature.

by an Arrehenius relation between strain rate and temperature, $\dot{\varepsilon} = \dot{\varepsilon}_o \exp(-Q/RT)$ with Q = 18,200 cal/mole, which agrees closely with that for the diffusion of carbon or nitrogen in alpha iron.

To gain a better understanding of the dynamic strain aging phenomenon in titanium, the nature of the stress-strain curve was examined closely at various temperatures and strain rates. In Fig. 47 the logarithm of the strain rate is plotted against the reciprocal of absolute temperature for various shapes of the stress-strain curves. Straight lines could be drawn through points of similar stress-strain behavior. It was assumed that along each straight line, a single thermally activated mechanism operates and that the activation energy for the process can be obtained from the slope of the straight lines.

Figure 47 is divided into three regions, I, II and III. In regions I and III the stress-strain curves were smooth. In region II serrations were observed. The thick line separating regions I and II represents the beginning of serrations and the apparent activation energy for the process was computed to be 41,000 cal/mole. The activation energy for the complete disappearance of serrations was found to be 47,500 cal/mole.

In the case of iron, it was pointed out that the activation energy for the start of the serrations was close to that for diffusion of carbon or nitrogen in iron. The

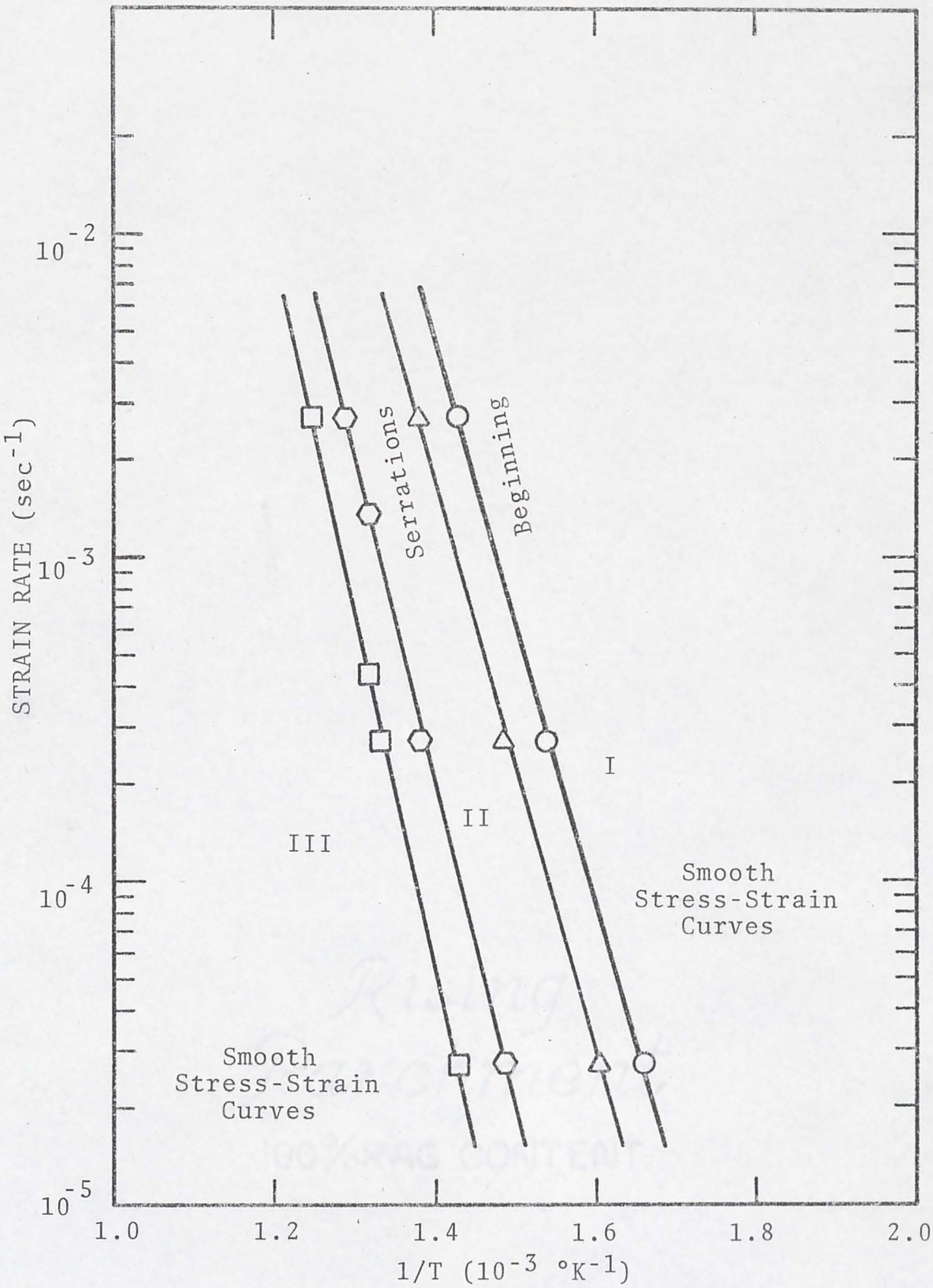

Fig. 47. Linear relation between log $\dot{\varepsilon}$ and 1/T for various degrees of serrations on the stress-strain curves of commercial purity titanium.

solubilities of carbon and nitrogen in iron are also small in the dynamic strain aging region (10^{-4} and 10^{-2} at. %, respectively, at 473°K).[66] This shows that very small amounts of carbon and nitrogen in solution are sufficient to show strain aging effects in iron.

There are four interstitials to be considered in commercial purity titanium. These are oxygen, nitrogen, carbon and hydrogen. Oxygen and nitrogen have extensive solubility in alpha titanium[76] (33 at. % oxygen and 9 at. % nitrogen at 873°K). Carbon and hydrogen have, however, a limited solubility (0.45 at. % carbon at 873°K and 8 at. % hydrogen at 573°K). The activation energy for diffusion of hydrogen in alpha titanium is only 12,000 cal/mole.[77] Hydrogen, therefore, cannot be responsible for the dynamic strain aging effects at high temperatures. However, the inflection in $\ell n\sigma$ - T curve (Fig. 10) near 300°K could be due to hydrogen. Of the three remaining elements, nitrogen has an activation energy of 45,250 ± 2,250 cal/mole[78] for diffusion in alpha titanium. The values for carbon and oxygen from internal friction peak measurements are 48,500 ± 3,000 and 58,000 cal/mole, respectively.[79] Among these, only nitrogen and carbon have activation energy values that are close to the values obtained in the present study. Miller and Browne[79] have shown that the presence of a substitutional atom like zirconium can produce marked changes in the characteristics of the internal friction peaks and

reduce the activation energy of a simple binary alloy. For example, the activation energy for the Ti-0.2 at. percent O-10 at. percent Zr alloy was reduced to 40,800 cal/mole from the 58,000 cal/mole value reported for the Ti-O alloy. Since substitutional iron atoms are present in the present material, and their effect on the internal friction peak is not known, the apparent activation energies obtained in the present study cannot be used with confidence to determine the element responsible for dynamic strain aging.

Let us now turn our attention to the appearance and disappearance of serrations. Sleeswick[80,81] and Wilcox and Rosenfield[82] consider the serrations to result directly from the negative strain rate dependence of the flow stress ($\frac{\partial \ln \sigma}{\partial \ln \dot{\varepsilon}} < 0$). The argument advanced in favor of this view is that if flow can take place at a lower stress when the strain rate is higher, then deformation must be unstable and will tend to occur locally at higher strain rates. This argument is questionable as far as the titanium data are concerned. A sudden increase in strain rate, in the event of a local yielding, does not drop the flow stress to that corresponding to the faster strain rate, but only decreases the work hardening rate without altering the general level of the flow stress. In fact, an increase in strain rate may momentarily increase the flow stress (transient maximum) as shown in Fig. 43 of a differential strain rate test in the dynamic strain aging region (673°K curve).

It would therefore be more appropriate to say that serrations appear in titanium stress-strain curves when $\frac{d(\Delta\sigma/\Delta\varepsilon)}{d \ln \dot{\varepsilon}}$ is negative. Attention is drawn to the fact that the stress-strain curves again become smooth at strain rates close to the work hardening rate maximum shown in Fig. 25, although here $\frac{d(\Delta\sigma/\Delta\varepsilon)}{d \ln \dot{\varepsilon}}$ is negative.

4.4. The Role of Dynamic Strain Aging on Ductility Minima

The present results show that commercial purity titanium exhibits ductility loss in the dynamic strain aging region. This is similar to the blue brittle effect in steel. As in the case of steel, the minimum ductility temperature in titanium depends on the deformation rate. At normal crosshead speeds (0.02 in/min) it occurs near 750°K. While this minimum has been reported by several investigators,[18,83] the phenomenon has not been analyzed.

Figure 29 showed that both the uniform and the necking strain decrease in the blue brittle region in titanium. The decrease in the reduction in area is, however, not as pronounced as that in the elongation. In fact, the lowest reduction in area value was 55 percent (Fig. 31). This fact and the Scanning Electron Microscope study of the fractured surfaces clearly imply that the phenomenon in question is not true embrittlement. On the other hand, it is a necking phenomenon. Not only the uniform strain is small, but once

necking starts, it becomes catastrophic and localized. The reduced necking strain (strain associated with the neck) can be rationalized in terms of the effect of dynamic strain aging on the work hardening rate. This will be treated in another section.

The loss of uniform elongation will now be considered. The onset of necking during a tensile test should occur when the work hardening rate decreases to a sufficiently low level.[84] The rate of work hardening in the early stages of the stress-strain curves is abnormally high in the dynamic strain aging region, but it decreases rapidly with strain. This is shown in Fig. 48 where the slope ($d\sigma/d\varepsilon$) of the stress-strain curve is plotted as a function of strain for two specimens, one deformed at 700°K (dynamic strain aging region), and the other at 473°K where aging effects are insignificant. Similar work hardening characteristics have been reported for steel in the blue brittle region.[65,85] A clue to the rapid decrease in the work hardening rate with increasing strain may be obtained from the shape of the serrations observed in titanium in the dynamic strain aging region. Assume that each rising portion of the serration in the titanium curve of Fig. 16 is associated with a smooth propagation of a Lüders band. The fact that the load rises above the general level of the curve implies that the propagation of the band is made difficult,probably due to aging. With increasing strain, however, the apparent slope of each

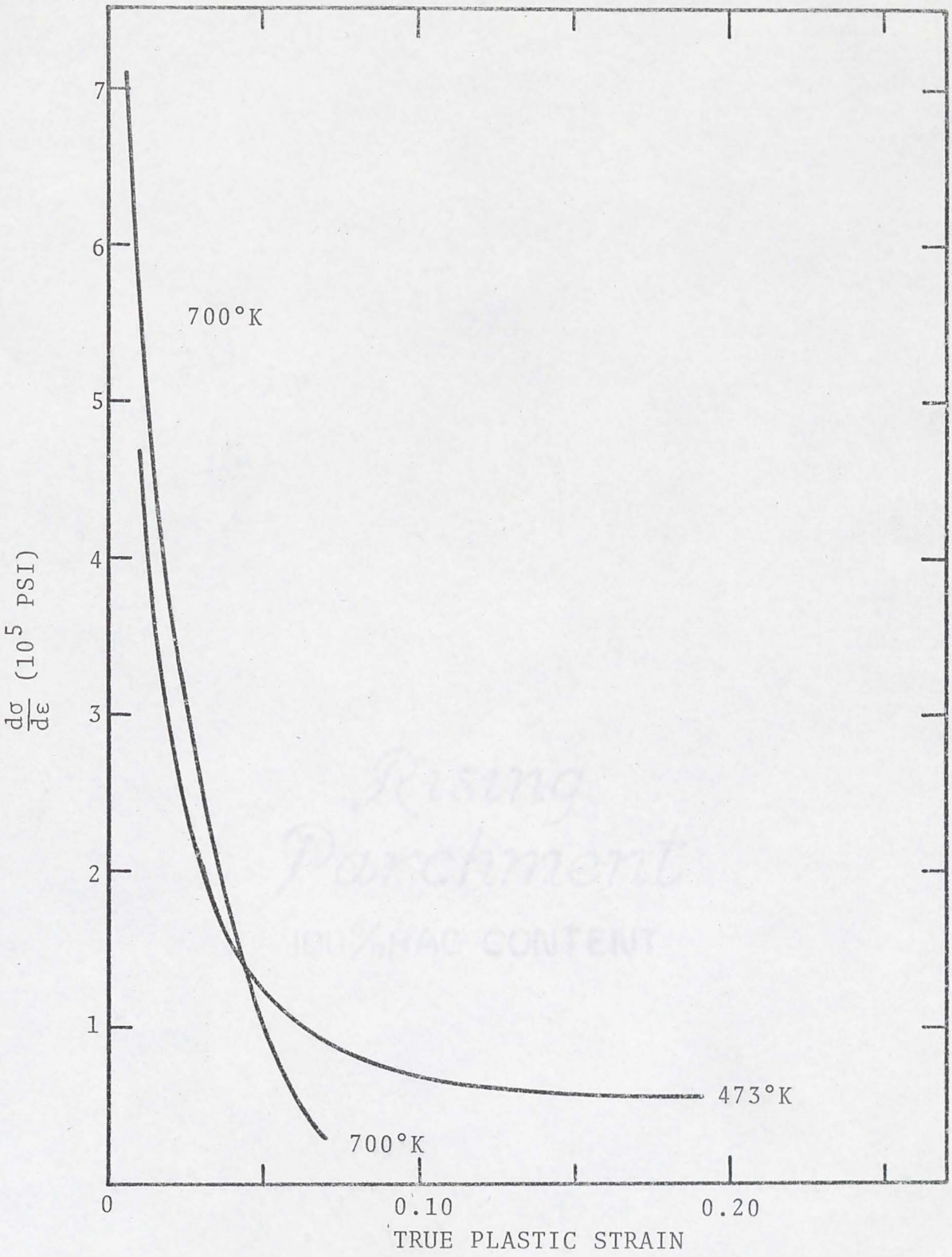

Fig. 48. This figure compares the variation of the work hardening rate with strain for two titanium specimens, one deformed at 700°K (the "blue brittle" temperature) and the other at 473°K where strain aging effects are negligible.

serration (Fig. 16) decreases. This suggests that locking becomes less severe with increasing strain. Apparently the solute atoms are continuously used up in pinning the dislocation, thereby increasing the mobility of the dislocations. This is consistent with Glen's model,[65] which postulates a depletion of the solute from the matrix as the former pins the dislocations.

4.5. The Influence of Strain Rate Dependent Work Hardening on the Necking Strain

In the last section it was shown that the "blue brittle" effect in titanium is a necking phenomenon. At the ductility minimum temperature, the neck in a tensile specimen is very sharply defined [Fig. 28(a)] and all the necking strain is concentrated in a small region. However, just above the blue brittle temperature, the neck becomes diffuse and spreads over the entire gage length of the specimen. The strain associated with the diffuse neck is large and the total elongation is well above 100 percent. See Figs. 28(b) and 29.

Extremely large necking strains are also observed in superplasticity.[34,86,87] However, the experimental conditions normally encountered in superplasticity are not the same as those existing in titanium just above the blue brittle temperature. We shall now consider the differences. First, in the temperature range of interest, the strain

rate sensitivity parameter, n, of titanium is only about 0.01 (Fig. 45). Superplastic effects are considered to occur in metals when n is over thirty times greater than this value or above 0.30.[87,88] In this regard, the elongation of a titanium specimen deformed just above the blue brittle temperature (say 773°K, $\dot{\varepsilon} = 2.7 \times 10^{-5}$ sec^{-1}) should be compared with that predicted by one of the correlations between total elongation and n, made in the studies of superplasticity. That of Lee and Backofen,[88] for several titanium and zirconium alloys shows too much scatter below n = 0.10 to be applicable. However, the more extensive correlation of Woodford[89] shows a smaller scatter of data even to values of n much below 0.10. This is shown in Fig. 49. From this figure, one would predict a total elongation of 6 percent for an n of 0.01. The observed elongation was 120 percent, or twenty times larger than would be expected if the metal conformed to a simple superplastic type of behavior.

Furthermore, Avery and Stuart[87] point out that superplastic deformation involves a zero work hardening rate. Morrison[90] also points out that superplastic alloys are characterized by a flow stress that is sensitive to strain rate but relatively insensitive to strain. All this means that the flow stress in superplasticity is only a function of the strain rate. On the other hand, in the dynamic strain aging region between about 500° and 850°K, the flow stress

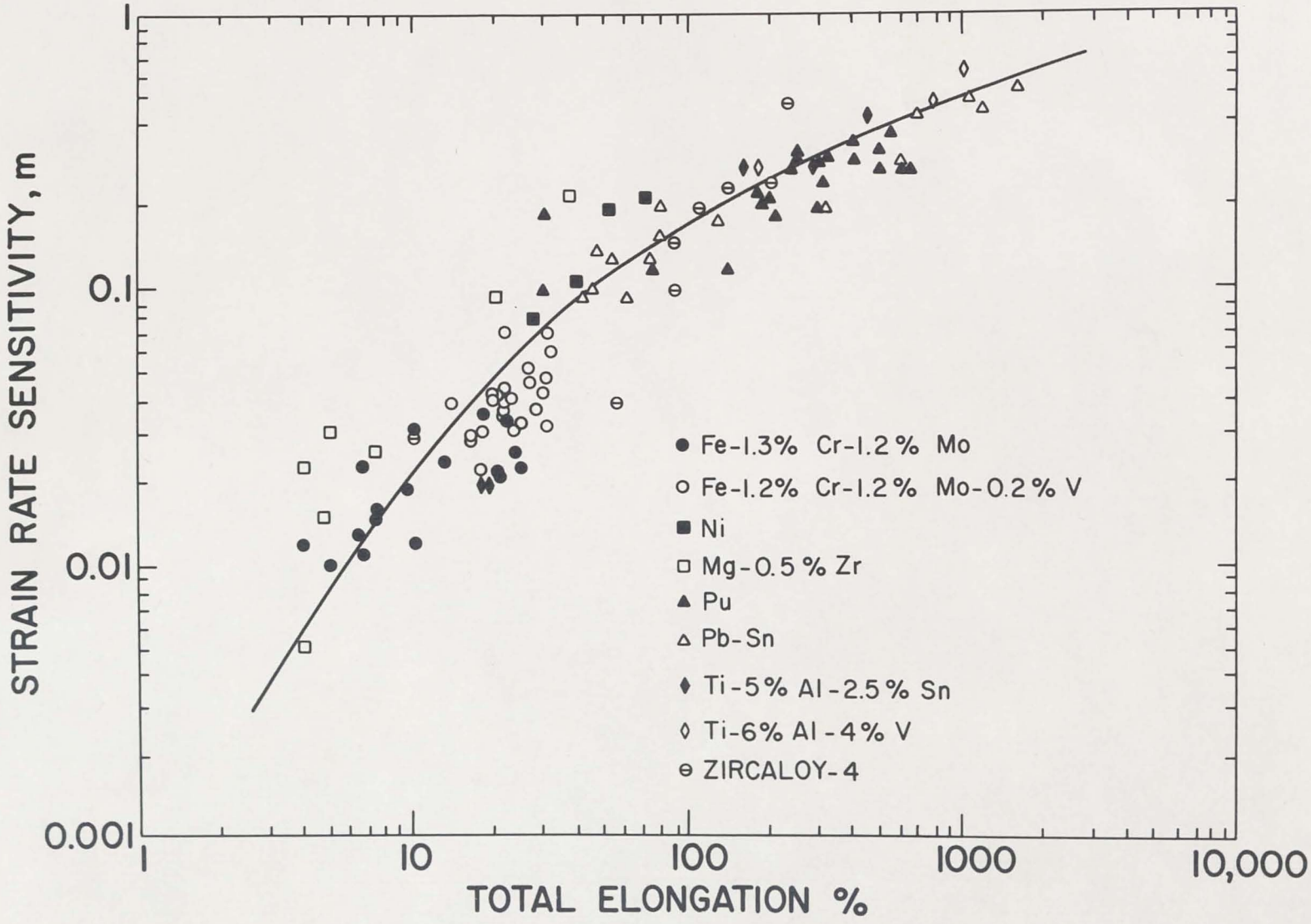

Fig. 49. Correlation between strain rate sensitivity and total elongation for a number of metals and alloys. Data from Woodford.[89]

is primarily determined by the work hardening. Not only is $d\sigma/d\varepsilon$ not zero but, as shown in Fig. 22, the work hardening rate is very large and passes through a rate dependent maximum. A strong dependence of the flow stress on the work hardening rate implies that, unlike superplastic deformation, the flow stress is a function of strain. It can be concluded that the conditions existing just above the "blue brittle" temperature in titanium are not equivalent to those associated with superplasticity.

Now consider the growth of a neck in a tensile specimen. Many years ago, Nadai and Manjoine[34] pointed out that a diffuse or extended neck as in a specimen deformed just above the blue brittle temperature, could only be rationalized in terms of a flow stress that is rate dependent. When a specimen work hardens but does not show a rate dependence of flow stress, the deformation would be concentrated in a region where necking starts. This is because the work hardening rate is not sufficient to offset the increase in stress due to reduction in cross-section. On the other hand, when the flow stress becomes strain rate dependent, the entire gage section may deform, although the smaller cross-sections may deform at a higher strain rate. This may induce the flow stress to increase in regions of smaller cross-section and further local deformation would stop.

There are two ways by which the flow stress may exhibit its rate dependence. Superplastic investigations have focussed their attention on $d\sigma/d\dot{\varepsilon}$ or the direct effect of strain rate on the flow stress. This is usually expressed as a power law

$$\sigma = p\dot{\varepsilon}^{n} \tag{18}$$

where p is a constant, n is the strain rate sensitivity, and σ and $\dot{\varepsilon}$ have their usual meanings.

Attention is now called to a different form of rate dependence, that is due to an effect of strain rate on the work hardening rate. This can also result in a variation of the flow stress with strain rate as the specimen is strained.

Since the work hardening rate is $d\sigma/d\varepsilon$, its dependence on the strain rate is $\partial^2\sigma/\partial\dot{\varepsilon}\partial\varepsilon$ or a second order derivative. If the flow stress is a function of one second order derivative, it may also be affected significantly by other second order derivatives. One should therefore examine the Taylor expansion for a function of two variables. Thus, at constant temperature,

$$\sigma(\varepsilon,\dot{\varepsilon}) = \sigma(\varepsilon_o,\dot{\varepsilon}_o) + (\frac{\partial\sigma}{\partial\varepsilon})d\varepsilon + (\frac{\partial\sigma}{\partial\dot{\varepsilon}})d\dot{\varepsilon} + \frac{1}{2}[(\frac{\partial^2\sigma}{\partial\varepsilon^2})d\varepsilon^2$$

$$+ 2(\frac{\partial^2\sigma}{\partial\dot{\varepsilon}\partial\varepsilon})d\dot{\varepsilon}d\varepsilon + (\frac{\partial^2\sigma}{\partial\dot{\varepsilon}^2})d\dot{\varepsilon}^2] + \ldots \tag{19}$$

In the case of necking, an approximation can be made that simplifies this relationship. It has been demonstrated[65,91] that at constant deformation rate, once necking has started, the true stress-true strain curve becomes approximately linear. Rosi and Perkins[14] have particularly demonstrated this for titanium. This implies that $\partial^2\sigma/\partial\varepsilon^2$ is nearly zero. Of the remaining terms, $\partial\sigma/\partial\varepsilon$ represents the work hardening. As indicated by Nadai and Manjoine,[34] this term cannot be responsible for the development of elongated necks. It is also experimentally observed that in the temperature range of interest, $d\sigma/d\dot{\varepsilon}$ is small and its variation with strain rate in the interval from 2.7×10^{-5} to 2.7×10^{-3} sec^{-1} is also small. Thus, it can be assumed that the effect of $\partial^2\sigma/\partial\dot{\varepsilon}^2$ is negligible. Of the remaining two terms, $\partial^2\sigma/\partial\dot{\varepsilon}\partial\varepsilon$ can be shown to be the more important in producing the diffuse neck above the blue brittle temperature in titanium with the aid of a simple strain rate change experiment. This experiment, as shown in Fig. 50(a), involved a tenfold increase in strain rate made at a strain approaching that required to start necking. This increase in rate should be roughly equivalent to that occurring during the period of necking in the various cross-sections of the specimen located between the center of the neck and the ends of the gage section. Note that, as a result of the rate change, the flow stress increased instantaneously by about 600 psi. This increase in flow stress,

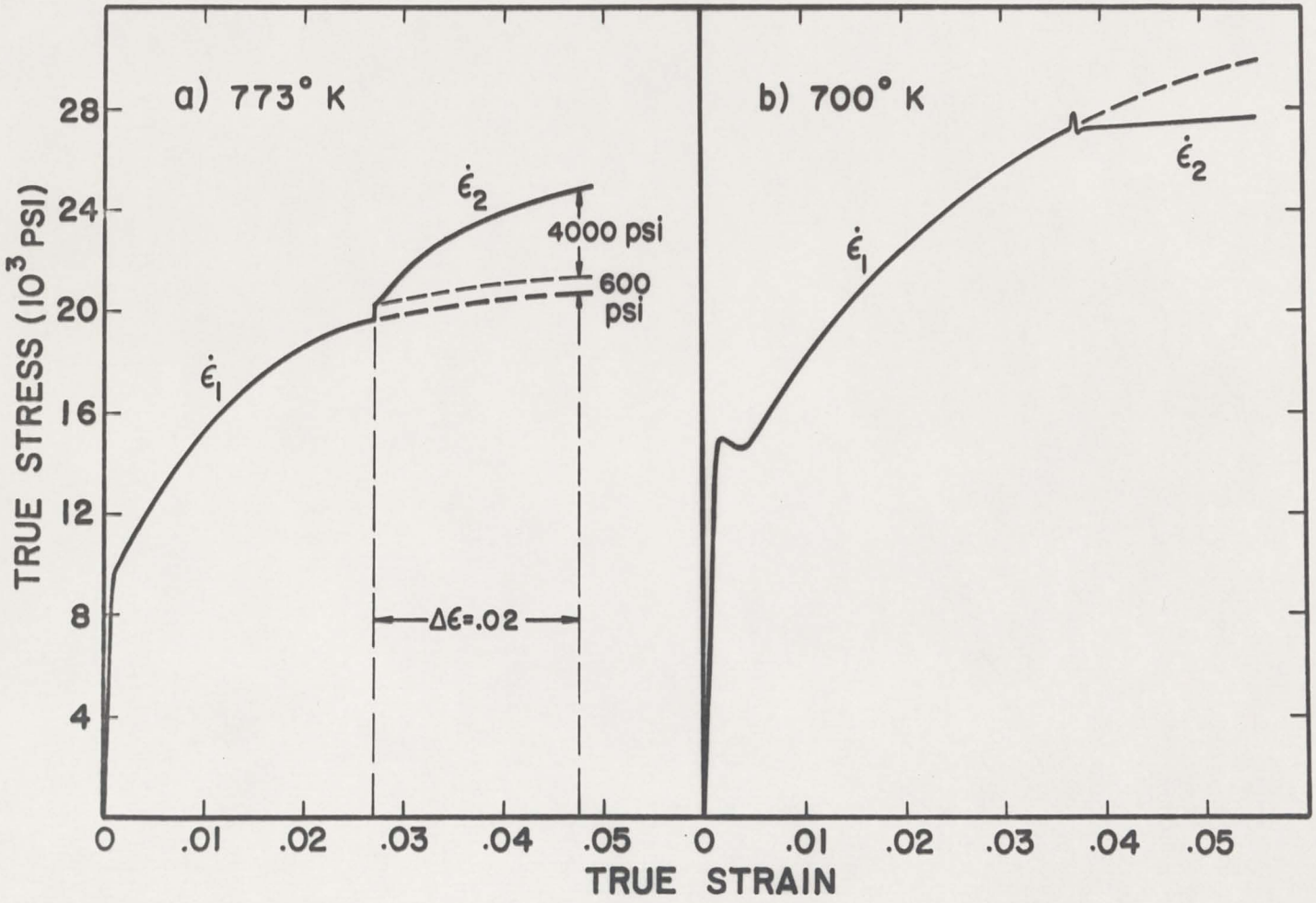

Fig. 50. True stress-true strain curves for strain rate change tests. $\dot{\varepsilon}_1 = 2.7 \times 10^{-5}$ sec^{-1}; $\dot{\varepsilon}_2 = 10\ \dot{\varepsilon}_1$; a) 773°K, b) 700°K.

which is due to $\partial\sigma/\partial\dot{\varepsilon}$, may be considered to be independent of strain, since Orava, Stone and Conrad[12] have shown that in commercial purity titanium, the increment in flow stress due to a strain rate change, is nearly constant during a tensile test. On the other hand, the effect of the rate change on the flow stress due to the change in the slope of the stress-strain curve can be seen by considering a small strain increment such as that between 2.75 and 4.75 percent. As a result of the increased slope of the stress-strain curve, the flow stress rises by 4,000 psi in this interval. This is nearly seven times larger than the instantaneous increase in flow stress. Diameter measurements near the fractured end of the specimen have shown that the strain there was nearly 200 pct. During the development of this large necking strain, the rise in flow stress due to work hardening could be many times larger than the 4,000 psi obtained for a 2 percent strain interval. This in turn further strengthens the conclusion that the rate dependent work hardening is the controlling factor in determining the necking strain in titanium just above the blue brittle temperature.

By a similar argument, the small necking strain and the resulting sharp and localized neck [Fig. 28(a)] at the blue brittle temperature can also be rationalized in terms of the rate dependence of work hardening. Thus, Fig. 24 implies that an order of magnitude increase in strain rate

at 700°K should decrease the work hardening rate. A direct strain rate change experiment at this temperature confirmed the above prediction [see Fig. 50(b)].

Finally, it should be pointed out that above 850°K the work hardening as well as its rate dependence become negligibly small. The large necking strain in this interval is therefore undoubtedly due to the fact that the strain rate sensitivity becomes large at elevated temperatures as shown in Fig. 45. In this temperature range, the diffuse neck is therefore probably due to the same causes that produce this type of neck in superplastic materials.

4.6. Deformation at 77°K

In section 3.7 quantitative microstructural evidence was presented that showed the ability of titanium to twin readily at 77°K. It was also pointed out that a significant feature of the titanium stress-strain curves in Fig.35 is that the work hardening rate remains nearly constant to large strains. These strains are about twice those observed at room temperature before necking commences. It is thus apparent that there is a close correlation between deformation twinning and the shape of the stress-strain curve.

There are three ways by which twinning might act to increase the work hardening rate at large strains. First, when a twin forms, there is always a lattice reorientation inside the twin. In a longitudinal titanium specimen this

reorientation should result in a less favorable Schmid factor for prism slip. Second, at all strains twinning tends to reduce the effective grain size of the metal. This should result in a continuous increase in flow stress due to a dynamic Petch effect.[55] Third, at large strains, the grains become so fragmented by twinning that the mean free path across a crystalline area becomes small enough to impede the formation of a cell structure. In other words, twinning could impede dynamic recovery.

Consider first the reorientation hardening. It has been experimentally observed[92] that when titanium has a texture with basal planes closely aligned parallel to the stress axis, twinning occurs primarily on $\{11\bar{2}2\}$ and $\{11\bar{2}4\}$ planes. With the formation of each $\{11\bar{2}2\}$ or $\{11\bar{2}4\}$ twin, the basal plane in the twin is rotated to where it makes an angle of about 65° and 76°, respectively, with the basal plane of the original grain. Rotations of this magnitude of the basal plane relative to the stress axis in the longitudinal tensile specimens have a drastic effect on the Schmid factors for prism slip. In a $\{11\bar{2}2\}$ twin the Schmid factor should be decreased by a factor of about 4 to 5 and in a $\{11\bar{2}4\}$ twin the decrease should be even larger. If it is assumed that twinning does not alter the flow stress for prism slip, then we may conclude that prism slip inside the twins is probably not a factor in the plastic deformation of the aggregate. It is probable, however, that other deformation

modes act inside the twins, as demonstrated by the fact that $\{11\bar{2}2\}$ twins always undergo extensive second order twinning.[92] These second order twins may be seen in many of the twins in Figs. 37 and 39. At the present time, it is not possible to estimate the stress level required to operate these other deformation modes and we can only conclude that reorientation hardening may be a significant effect.

The significance of the Petch effect can be roughly evaluated with the fracture stress-grain size data of Coleman and Hardie.[28] These authors showed that reducing the grain size of alpha zirconium from 64μ to 4μ increased the fracture stress at 77°K by about 42,000 psi. Since twinning is not of major significance in longitudinal zirconium specimens used by Coleman and Hardie,[28] we can conclude that a reduction in the effective grain size (as in twinning) could have a measurable effect on the flow stress.

Further insight into the role of twinning in low temperature deformation is afforded by the stress-strain behavior of a transverse specimen of zirconium. Figure 51 shows the 77°K true stress-true plastic strain curves for two zirconium specimens cut from the same plate in the longitudinal and transverse direction. In the longitudinal specimen the texture favors prism slip. In the transverse specimen, many grains are unfavorably oriented for prism slip and hence plastic deformation in these grains requires

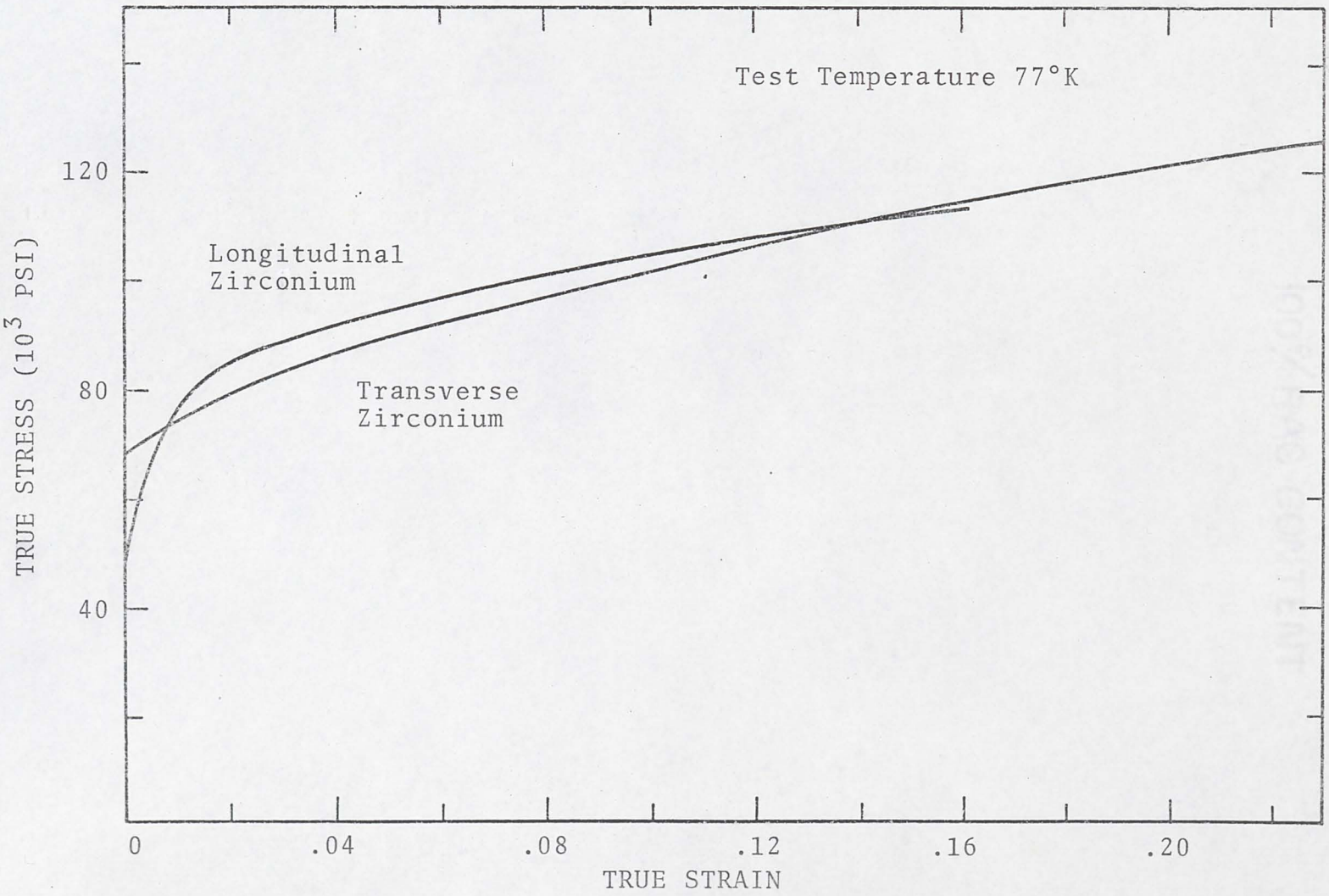

Fig. 51. True stress-true strain curves for longitudinal and transverse zirconium specimens. (R. E. Reed-Hill, Deformation Twinning, AIME Met. Conf. Series, Vol. 25, Gordon and Breach Science Publishers, New York, 1964, pp. 295-320.)

twinning. It can be seen that the stress-strain curve for the transverse specimen is nearly linear and that it has a larger uniform strain than the longitudinal one. The microstructure of the transverse specimen showed profuse twinning (Fig. 52), whereas the longitudinal specimen had a low density of twinning.

The preceding discussion demonstrates the close connection between deformation twinning and the stress-strain behavior in specimens deformed at normal strain rates. A question that remains unanswered is why the twinning rate should decrease in the specimen deformed at the fastest rate, 2.7×10^{-1} sec^{-1}. It is quite possible that, apart from temperature and stress level, a certain minimum time is necessary for the twins to nucleate and probably to grow. If this assumption is true, the twin density should be even lower in specimens deformed under impact conditions. This should result in greatly reduced ductility and may even partially account for the significant loss in impact strength observed in titanium alloys at low temperatures.

4.7. An Investigation of the Shape of the Stress-Strain Curves After a Strain Rate Change

Strain rate changes during a tensile test of commercial purity alpha titanium do not have the same effect on the shape of the stress-strain diagram at all temperatures. As can be seen in Figs. 42 and 43, only within rather limited

Fig. 52. Microstructure of a transverse zirconium specimen deformed 29 percent at 77°K. Magnification 300 times. (R. E. Reed-Hill, Deformation Twinning, AIME Met. Conf. Series, Vol. 25, Gordon and Breach Science Publishers, New York, 1964, pp. 295-320.)

temperature ranges does the flow stress change smoothly and continuously to a value characteristic of the new strain rate. In the dynamic strain aging region a rate increase produces a small transient flow stress maximum similar in appearance to a yield point, while equivalent minimum can be observed upon a decrease in strain rate. In this section these different shapes of the stress-strain curves will be analyzed by the theory of dislocation dynamics.

Following Johnston and Gilman,[21] the total crosshead displacement in a tensile test is composed of two parts,

$$\Delta y = \Delta y_{el(system)} + \Delta y_{pl(specimen)} \tag{20}$$

or

$$\Delta y_{el(system)} = \Delta y - \Delta y_{pl(specimen)} \tag{21}$$

The elastic displacement, $\Delta y_{el(system)}$ is related to the incremental load, ΔF, by the expression:

$$\Delta y_{el(system)} = \Delta F/K \tag{22}$$

where K is the effective spring constant. The total crosshead displacement is $\Delta y = S_c \Delta t$, where S_c is the crosshead speed and Δt is the time interval for which the displacement is measured. Also, $\Delta y_{pl(specimen)} = \ell_o \dot{\varepsilon}_{pl} \Delta t$, where ℓ_o is the initial gage length of the specimen and $\dot{\varepsilon}_{pl}$ is the plastic strain rate.

For infinitesimal changes, Eq. (21) becomes:

$$\dot{F} = K[S_c - \ell_o \dot{\varepsilon}_{pl}] \tag{23}$$

The plastic strain rate may be expressed by the well known Orowan equation, $\dot{\varepsilon}_{pl} = sb\rho_m v$, where s is the Schmid factor, b is the Burgers vector, ρ_m is the mobile dislocation density and v is the average dislocation velocity. In absence of any known dislocation velocity measurements on titanium, the average velocity, v, of the dislocation will be assumed to follow a power law. It is assumed that the flow stress, τ, in a nearly pure metal is composed of two parts, τ_s, the short-range component which is believed to be thermally activated, and τ_i, the internal stress component which is long-range in nature and depends on the internal structure and the shear modulus. It is postulated that only τ_s, the effective stress, acts on the dislocation. The power law thus becomes:

$$v = \left[\frac{\tau_s}{D}\right]^{m^*} = \left[\frac{\tau - \tau_i}{D}\right]^{m^*} \qquad (24)$$

where τ is the total shear stress, τ_i is the internal stress, D is a constant for the material, and m* is assumed to be a constant that depends only on temperature.

In terms of tensile load,

$$v = \left[\frac{F - F_i}{aD'}\right]^{m^*} \qquad (25)$$

where a is the specimen cross-section and D' is a constant related to D through the Schmid factor.

Substituting for $\dot{\varepsilon}_{pl}$ in Eq. (23),

$$\dot{F} = K \left[S_c - sb\rho_m \ell_o \left(\frac{(F-F_i)}{aD'} \right)^{m^*} \right] \qquad (26)$$

The above equation may be integrated in a computer if the time dependence of the mobile dislocation density, ρ_m, and of the internal force component, F_i, is known.

The load-time curve in a tensile test for alpha titanium is found to be roughly linear for any 1.5 percent strain interval after an initial plastic strain of about 1 percent. This strain interval is about that required to produce steady state conditions after a rate change. It can be shown that the thermally activated part of the flow stress, τ_s, does not vary appreciably in this strain interval since it is not a strong function of dislocation density.[1] From the above, it follows that the internal force component would vary roughly linearly with time.

$$F_i = F_{i_o} + \dot{F}_i t \qquad (27)$$

where F_{i_o} is the internal force at the instant the strain rate is changed and $\dot{F}_i$ is a measure of work hardening.

The time dependence of ρ_m will now be considered. Dislocation density measurements by Jones and Conrad[61] on alpha titanium at room temperature indicate a linear dependence with strain. However, these measurements give the total density and not the mobile fraction. There appears to be

no way by which the latter can be measured. In the absence of any experimental information, it will be assumed that the mobile density also varies linearly with strain.

$$\rho_m = \rho_{m_o} + \alpha\varepsilon \tag{28}$$

where ρ_{m_o} is the mobile density at the instant the strain rate is changed.

Taking the time derivative on both sides,

$$d\rho_m/dt = \alpha\dot{\varepsilon} \tag{29}$$

For a constant strain rate, the above equation would imply that ρ_m varies linearly with time.

$$\rho_m = \rho_{m_o}(1 + \gamma t) \tag{30}$$

where $$\gamma\rho_{m_o} = d\rho_m/dt = \alpha\dot{\varepsilon} \tag{31}$$

The parameter γ which appears in subsequent equations is thus related to the rate at which mobile dislocations multiply.

Substituting for ρ_m and F_i in Eq. (26),

$$\dot{F} = K\left[S_c - sb\ell_o\rho_{m_o}(1+\gamma t)\left(\frac{F-(F_{i_o}+\dot{F}_i t)}{aD'}\right)^{m^*}\right] \tag{32}$$

It is possible to eliminate some of the constants in the above equation by applying the initial conditions when the

deformation speed is changed. These are as follows:

$$\text{At} \quad t = o,\ F = F_o;\ S_c = S_{c_o};\ F_i = F_{i_o} \text{ and } \dot{F} = \dot{F}_o$$

For a strain rate change by a factor P, it can be shown that Eq. (32) reduces to the following:

$$\dot{F} = K\left[PS_{c_o} - (S_{c_o} - \frac{\dot{F}_o}{K})(1+\gamma t)\left(\frac{F-(F_{i_o}+\dot{F}_i t)}{F_o - F_{i_o}}\right)^{m^*}\right] \quad (33)$$

It may be noticed that D does not appear in the above equation. The parameters K, $\dot{F}_o$ and $\dot{F}_i$ may be estimated directly from the Instron chart. It is possible to estimate γ from dislocation density measurements but the mobile and total dislocation densities need not necessarily have the same functional dependence with strain. Stress relaxation experiments can give a measure of the internal force component, F_{i_o}, as long as the mobile dislocation density remains constant during the relaxation process.[93] Finally, in that which follows, m* is considered to be an adjustable parameter which can be varied until a close fit with the experimental curve is obtained.

The integration of Eq. (33) was carried out in an IBM 360 computer. Table II summarizes the parameters used for that part of the load-time curves obtained after increasing the crosshead speed by a factor of 10. Consider first those for the elevated temperatures (873°, 973° and 1073°K) where

Table II

Parameters of Equation 33 for
Strain Rate Increase

	300°K	523°K	873°K	973°K	1073°K
m*	9.0	4.6	4.45	5.5	5.6
F_{i_o} (lb.)	1,580	800	20	10	10
$\dot{F}_i$ (lb.min^{-1})	50	22	9	4.25	3.25
γ(min^{-1})	0.5	5.0	0	0	0
α(in.$^{-2}$)	1.45x10^{12}	1.45x10^{13}	0	0	0
m	27	10.9	6.7	5.5	5.3

the deformation behavior is believed to be the simplest. At these high temperatures, the work hardening rate, $\dot{F}_i$, is very small,and consistent with this low work hardening rate is the assumption that both the total as well as the mobile dislocation density are nearly constant, or γ is zero. The other parameters were estimated as discussed earlier. The value of m* was adjusted until a good fit between the theoretical and experimental curves was obtained.

Consider the parameters for 300°K. This temperature falls in a region where the effects associated with dynamic strain aging are present only to a rather small degree. From Jones and Conrad's[61] data on dislocation density, α was estimated as 1.45×10^{12} in^{-2}. Assuming that the mobile density varies with strain in the same way as the total density and is a constant fraction (0.40) of the latter, γ was estimated as shown in Table II. The value of m* obtained by close fit with the experimental curve is also shown in Table II.

Similar computations were performed for decreases in strain rate. The parameters used for these calculations are summarized in Table III. The values of α are negative, consistent with the postulate that the mobile density decreases with decreasing deformation rate. It should be noted that the units for work hardening rate, $\dot{F}_i$, are $lb.min^{-1}$. The chart speed was not decreased simultaneously with that of the crosshead. Therefore, for the same work

Table III

Parameters of Equation 33 for
Strain Rate Decrease

	300°K	523°K	873°K	973°K	1073°K
m^*	9.6	5.4	4.0	5.3	5.3
F_{i_o} (lb.)	1,600	822	20	10	10
$\dot{F}_i$ (lb.min^{-1})	5.0	0.4	0.9	0.425	0.325
γ (min^{-1})	-0.05	-0.5	0	0	0
α (in.$^{-2}$)	-1.45×10^{12}	-1.45×10^{13}	0	0	0

hardening rates at both strain rates, the actual values of $\dot{F}_i$ at the lower strain rate should be one-tenth of those at the faster strain rate. These are shown in Table III.

Let us now consider the 523°K curve, where a small yield point was observed upon an increase in strain rate and an inverse or negative yield point upon a decrease in strain rate. A better insight into the nature of this type of phenomenon is afforded by the stress-strain curve corresponding to 673°K shown in Fig. 43. This diagram clearly indicates that the transient yield phenomena can occur without any change in the basic level of the flow stress. That is, at 673°K as soon as the transients are completed, the flow stress returns to approximately the value it had before the rate was changed. There is also another feature of the 673°K curve that is more evident than in the 523°K curve. In both cases there is an inverse strain rate dependence of the work hardening rate. In other words, increasing the strain rate results in a decrease in the work hardening rate. That this is true at 673°K can be seen in Fig. 43 where the average slope of the stress-strain curve following the transient region can be seen to drop sharply after a rate increase. It is believed that both of these effects, the transient yield phenomena and the inverse strain rate dependence of the work hardening,are related and both are aspects of dynamic strain aging. The coupling between the two phenomena can be rationalized rather simply; namely

that, with increasing strain rate and dislocation velocity, the probability of a moving dislocation becoming pinned should decrease. This should result in both an increase in the number of mobile dislocations, accounting for the small yield point, as well as in a lowering of the rate of accumulation of dislocations, accounting for the decrease in the work hardening rate.

Further support for the assumption that the transients are associated with sudden changes in the mobile dislocation density immediately after a rate change can be obtained by the following. On increasing the strain rate at 673°K (Fig. 43), there is an instantaneous increase in the slope of the stress-strain curve. The most reasonable assumption is that this rapid rise in flow stress can only be due to a sudden change in τ_s, the thermally activated flow stress component. If this were not true, one would have to assume an almost instantaneous change in the long-range component, τ_ℓ. Since τ_ℓ is not dependent on dislocation velocity, this would imply an instantaneous macroscopic increase in dislocation density which is inconsistent with dislocation dynamics. On the other hand, a sudden increase in flow stress with an increase in strain rate is characteristic of τ_s which strongly depends on dislocation velocity. Consequently, we can rationalize the peaks as follows. It is assumed that under the conditions of the test in Fig. 43 a mobile dislocation density is developed that is

characteristic of both the strain and strain rate and is larger at a higher strain rate. This suggests that during the strain interval associated with the transients, the mobile density increases from a value characteristic of the lower strain rate to one characteristic of higher strain rate. There is strong evidence to assume that the major change in mobile density occurs during the transient period and the change thereafter is small. Several factors support this viewpoint. First, consider Fig. 53. This shows a set of curves corresponding to various values of the dislocation multiplication factor, α. The effect of work hardening has been included in these curves. They clearly demonstrate that yield points occur only for large rates of dislocation multiplication and these become more pronounced with increasing α. Also note that if one assumes an α sufficient to give a yield point,the flow stress continues to fall after the yield point and the computed curves do not correspond to the experimental ones. Only if the rapid multiplication of dislocations is assumed to stop after the transient period is over is it possible to make the computed curves agree with the experimental ones.

With regard to the magnitude of the mobile dislocation multiplication rate after the transient period, it is reasonable to assume that it is again proportional to the rate of build-up of the total dislocation density. Since the work hardening rate at 523°K is nearly equal to that at

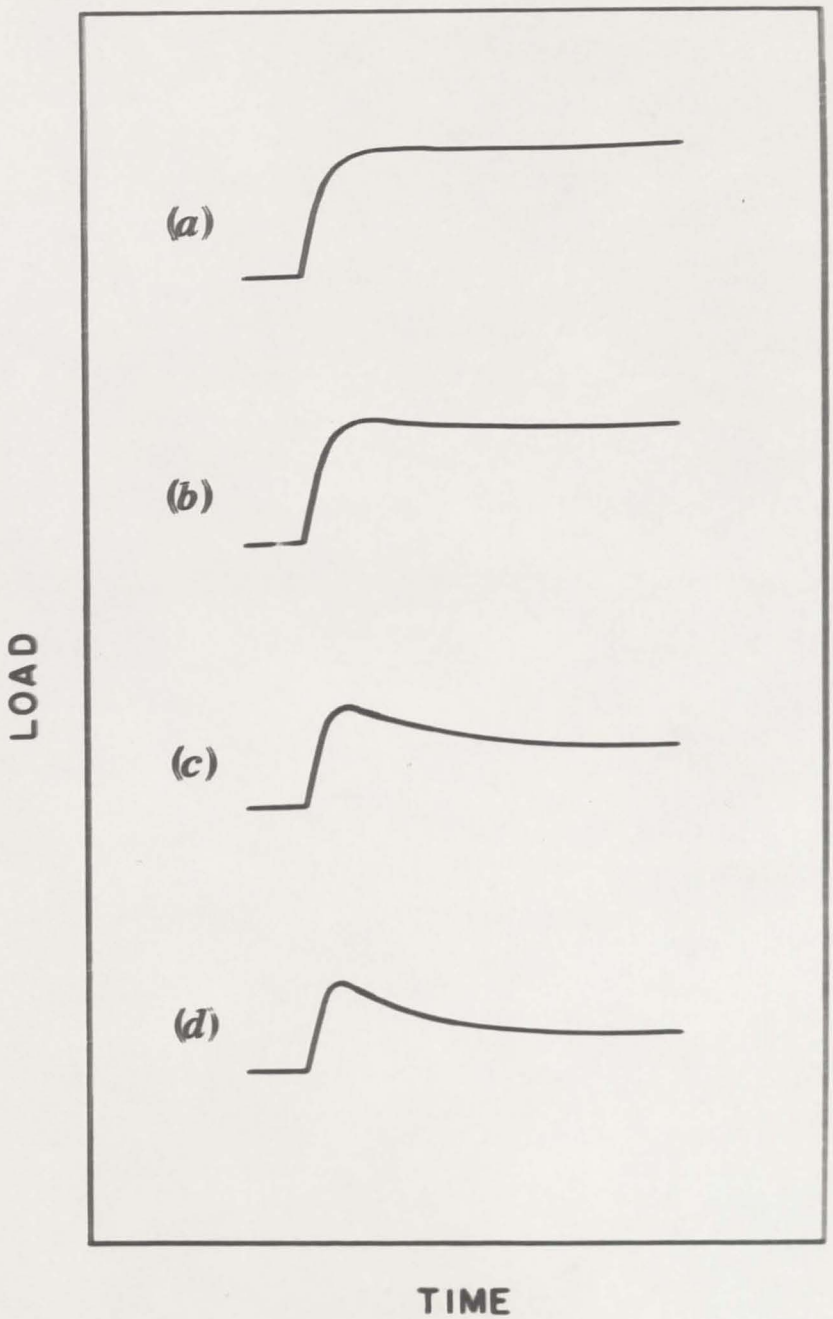

Fig. 53. Effect of mobile dislocation multiplication rate, α at 523°K on the shape of the load-time curves of titanium with a strain rate change. a) $\alpha = 1.45 \times 10^{12}$ inch^{-2}; b) $\alpha = 2.90 \times 10^{12}$; c) $\alpha = 1.45 \times 10^{13}$; d) $\alpha = 2.90 \times 10^{13}$.

300°K (Fig. 24), one might, therefore, expect that after the transient period, α would be roughly the same at 300° and 523°K. In making the 523°K calculations, however, it was assumed that α was zero after the transient period in order to simplify the calculations. This was justified on the basis that this small value of α has very little effect on the stress-strain curve after nearly steady state conditions are attained as is the case after the transient is completed.

The exact nature of functional dependence of ρ_m with time in the transient interval is not known. One could, however, assume to a first approximation that the mobile density varies linearly in this interval and that it is constant at the end of this period. With the above postulate, and using reasonable estimates of α, F_{i_o} and $\dot{F}_i$, the value of m* was obtained by the best fit with the experimental curve.

The results of the present analysis are given in Figs. 54 and 55. The solid curves are the experimental load-time curves, whereas the dots represent the predicted data. The calculations indicated that the value of m* strongly depends on the internal force component, F_{i_o}. In order to get accurate values for m*, it is necessary to know the other parameters, namely α, F_{i_o} and $\dot{F}_i$, accurately. In general, knowing any three parameters, the fourth may be estimated from strain rate cycling experiments.

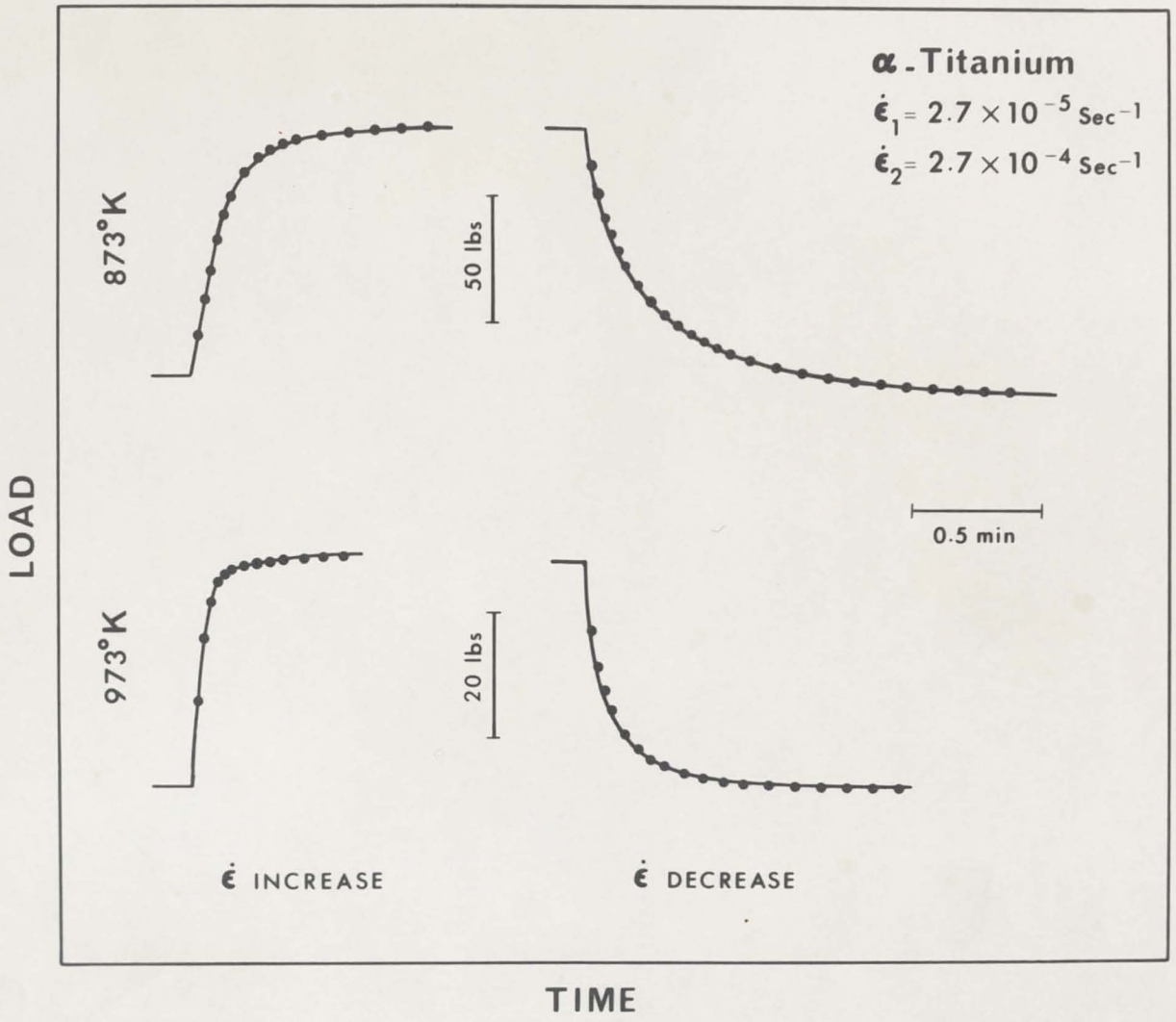

Fig. 54. Experimental and predicted load-time curves for titanium corresponding to strain rate changes.

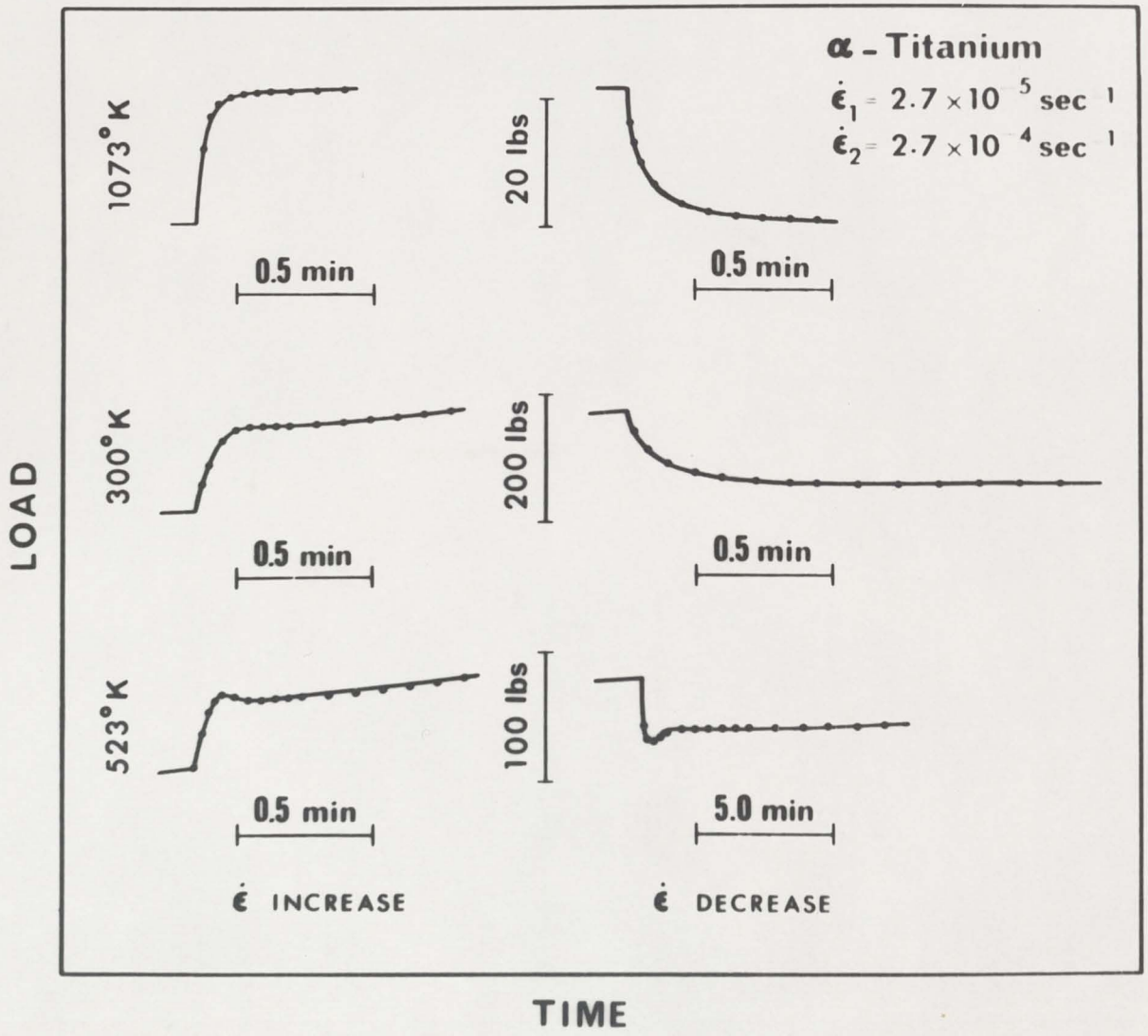

Fig. 55. Experimental and predicted load-time curves for titanium corresponding to strain rate changes.

Tables II and III give the m* values at different temperatures for alpha titanium obtained by the present analysis. Also included in Table II are the values obtained by the strain rate cycling method assuming that $m = 1/n$, where n is the strain rate sensitivity parameter. The values obtained from analysis of the shape of the stress-strain curves are much smaller than those estimated from the latter method. This is not unexpected since the present analysis considers only the effective stress acting on the dislocations. It is felt that the method of obtaining m* from analysis of the shape of the stress-strain curve is more meaningful than the strain rate cycling method since the assumption of constant mobile density inherent in the latter method need not be made in the former.

The preceding discussion demonstrates that information of a significant nature may be obtained from an analysis of the shapes of the load-time curves obtained after a strain rate change. Figure 56 shows schematically the load-time curves that might be expected under various conditions of the test. Curve A in Fig. 56 would imply absence of work hardening with no change in the mobile dislocation density. In curve B work hardening is superimposed. Curve C implies that only the mobile density changes, whereas in curve D work hardening is also superimposed on the former.

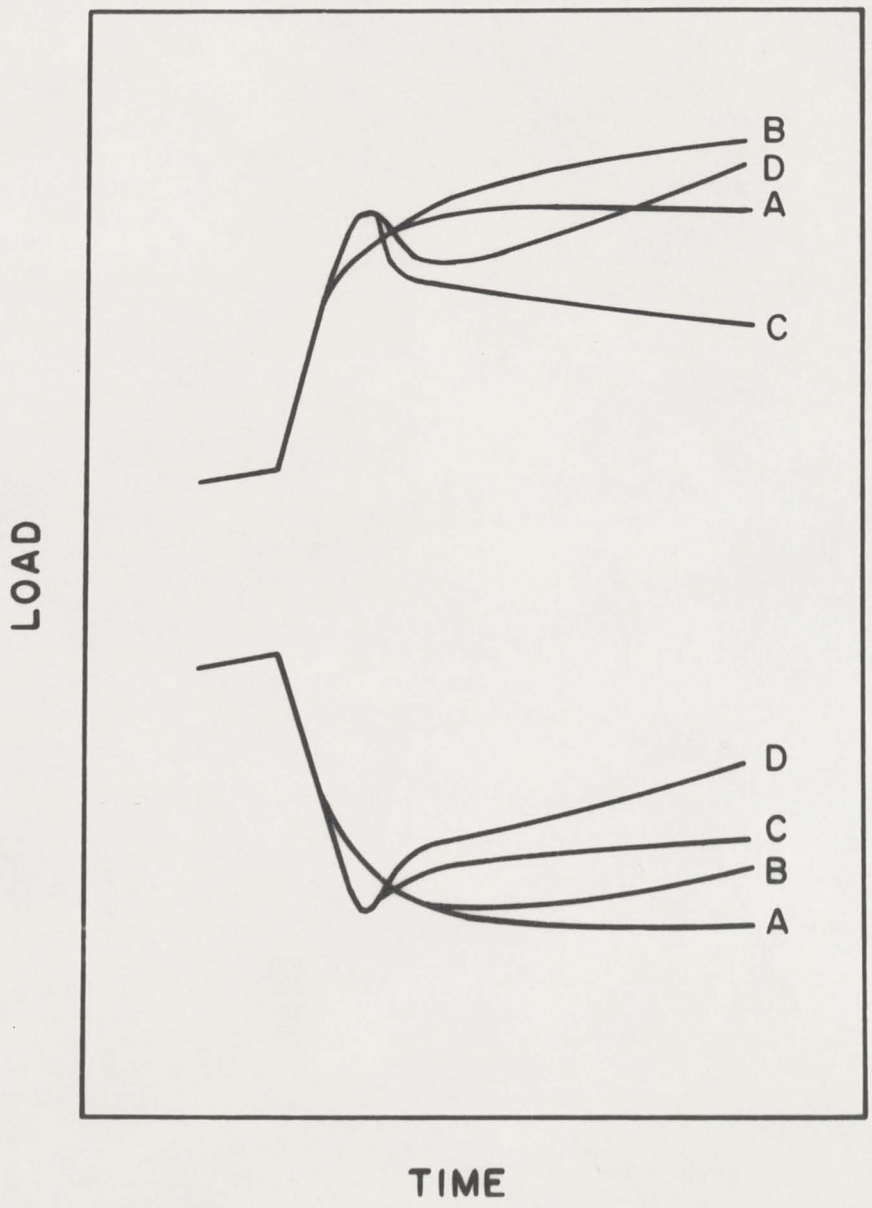

Fig. 56. Schematic diagram showing some possible shapes of load-time curves on changing the strain rate.

CHAPTER V

CONCLUSIONS

1. The stress-strain behavior of commercial purity titanium is markedly affected by deformation twinning and dynamic strain aging.

2. Below 200°K deformation twinning enhances the ductility of the metal by increasing the work hardening rate at large strains so that the true stress-true strain curve is linear and Considere's criterion for necking is satisfied only at large strains.

3. There are three ways by which deformation twinning could accomplish the above result. These are by lattice reorientation inside the twins, by reducing the effective grain size (Petch effect), and by making dynamic recovery more difficult. At the present time, it is not possible to state definitively which of these effects is most significant.

4. A semi-logarithmic plot of yield stress against temperature shows two deviations from linearity, centered at about 300° and 700°K. Dynamic strain aging phenomena are observed in these two temperature intervals. The lower temperature region may be associated with the interaction between hydrogen atoms and dislocations. The upper tem

temperature interval is probably associated with oxygen, nitrogen or carbon.

5. The pronounced minimum in elongation that occurs in titanium in the dynamic strain aging region is similar to the "blue brittle" effect in steel. As in the case of steel, the temperature of the minimum elongation depends on the deformation rate. At normal strain rates (10^{-4} sec^{-1}) it occurs near 750°K, but moves by about 50°K for each order of magnitude increase in strain rate. The minimum in elongation is not accompanied by a drastic loss in reduction in area.

6. The "blue brittle" effect in titanium is a necking phenomenon. At the ductility minimum temperature necking occurs at small strains and,once it starts, it develops catastrophically. The neck in the tensile specimen deformed at the "blue brittle" temperature is thus very sharply defined.

7. Above the "blue brittle" temperature the tensile elongation rises very rapidly. The large elongation in this region is due to the development of a diffuse neck.

8. Strain rate dependent work hardening rate maxima have been observed in the dynamic strain aging region (between 600° and 850°K). Both the "blue brittle" effect and the pronounced increase in tensile elongation just above the "blue brittle" temperature in titanium can be rationalized in terms of the strain rate dependent work hardening.

9. Above 850°K the work hardening as well as its rate dependence is small but the strain rate sensitivity of the flow stress is large. The large tensile elongation in this interval is probably caused by the same conditions as those that result in superplasticity.

10. A modified Johnston-Gilman analysis has shown that the transients observed in the stress-strain curves upon a strain rate change can be rationalized on the assumption that the mobile dislocation density increases more rapidly with increasing strain rate and similarly decreases with decreasing strain rate during a time interval at which transients are observed.

BIBLIOGRAPHY

1. R. E. Reed-Hill, "An Analysis of the Components of the Flow Stress in Titanium," Technical Report to the Air Force Materials Laboratories, Wright-Patterson Air Force Base, November 8, 1967.

2. S. N. Monteiro, M. S. Thesis, University of Florida, 1968.

3. F. D. Rosi, C. A. Dubé and B. H. Alexander, Trans. AIME, 197 (1953) 257-265.

4. E. A. Anderson, D. C. Jillson and S. R. Dunbar, Trans. AIME, 197 (1953) 1191-1197.

5. A. T. Churchman, Nature (London), 171 (1953) 706.

6. F. D. Rosi, F. C. Perkins and L. L. Seigle, Journal of Metals, 8 (1956) 115.

7. C. J. McHargue and J. P. Hammond, Acta Metallurgica, 1 (1953) 700.

8. T. R. Cass, The Science, Technology and Application of Titanium, R. Jaffee and N. Promisel, eds., Pergamon Press, Oxford, 1970, p. 459.

9. J. C. Williams and M. J. Blackburn, Phys. Stat. Sol., 25 (1968) K1.

10. Y. Lii, V. Ramachandran and R. E. Reed-Hill, Met. Trans., 1 (1970) 447-453.

11. E. B. Kula and T. S. DeSisto, American Society of Testing Materials, Special Technical Publication 387, 1966.

12. R. N. Orava, G. Stone and H. Conrad, Trans. ASM, 59, (1966) 171-184.

13. A. M. Garde and R. E. Reed-Hill, "The Importance of Mechanical Twinning in the Stress-Strain Behavior of Swaged High Purity Fine Grained Titanium at Sub-ambient Temperatures," accepted for publication in the Met. Trans.

14. F. D. Rosi and F. C. Perkins, Trans. ASM, 45 (1953) 972-981.

15. R. J. Wasilewski, Trans. ASM, 56 (1963) 221-235.

16. W. R. Kiessel and M. J. Sinnott, Trans. AIME, 197 (1953) 331.

17. N. G. Turner and W. T. Roberts, J. Less Common Metals, 16 (1968) 37-44.

18. J. W. Suiter, J. Inst. Metals, 83 (1954-55) 460-464.

19. J. D. Baird, Metals and Materials, 5 [2] (1971) Review 149.

20. S. N. Monteiro, A. T. Santhanam and R. E. Reed-Hill, The Science, Technology and Application of Titanium, R. Jaffee and N. Promisel, eds., Pergamon Press, Oxford, 1970, p. 503.

21. W. G. Johnston and J. J. Gilman, J. Appl. Phys., 30 (1959) 129-144.

22. W. G. Johnston, J. Appl. Phys., 33 (1962) 2716-2730.

23. G. T. Hahn, Acta Met., 10 (1962) 727-738.

24. D. J. Dingley and D. McLean, Acta Met., 15 (1967) 885-901.

25. R. P. Carreker, Jr., J. Appl. Phys., 21 (1950) 1289-1296.

26. T. Yokobori, Phys. Rev., 88 (1952) 1423.

27. N. J. Petch, Phil. Mag., 1 (1958) 1089-1097.

28. C. E. Coleman and D. Hardie, J. Inst. Metals, 94 (1966) 387-391.

29. D. H. Baldwin and R. E. Reed-Hill, Trans. Met. Soc. AIME, 242 (1968) 661-669.

30. C. E. Stromeyer, Minutes of Proc. of Inst. of Civil Engr., 80 (1885) 114.

31. J. D. Lubahn, Trans. ASM, 44 (1952) 643-666.

32. A. H. Cottrell, Dislocations and Plastic Flow in Crystals, Oxford University Press, 1953.

33. M. J. Manjoine, Trans. ASME, 66 (1944) A211-A218.

34. A. Nadai and M. J. Manjoine, Trans. ASME, 63 (1941) A77-A91.

35. J. D. Baird and A. Jamieson, J. Iron Steel Inst., 204 (1966) 793-803.

36. B. J. Brindley and J. T. Barnby, Acta Met., 14 (1966) 1765-1780.

37. E. T. Wessel, L. L. France and R. T. Begley, "The Flow and Fracture Characteristics of Electron-Beam Melted Columbium," Columbium Metallurgy, Interscience Publishers, New York, 1961, pp. 459-502.

38. A. S. Keh, Y. Nakada and W. C. Leslie, Dislocation Dynamics, A. R. Rosenfield et al., eds., McGraw-Hill, New York, 1968, p. 381.

39. A. Portevin and F. Le Chatelier, Compt. Rend., 176 (1923) 507-510.

40. C. F. Elam, Proc. Roy. Soc., A165 (1938) 568.

41. E. Schmidtman, L. Elsing and H. Schenck, Arch. Eisenhüttenwesen, 36 (1965) 415.

42. V. Ramachandran and R. E. Reed-Hill, Met. Trans., 1 (1970) 2105-2109.

43. C. R. Simcoe and D. E. Thomas, "The Tensile Properties of Zirconium Alloys at Fabrication Temperatures and Strain Rates," WAPD-51, Westinghouse Atomic Power Division, Pittsburgh, Pa., 1952.

44. W. R. Tyson, The Science, Technology and Application of Titanium, R. Jaffee and N. Promisel, eds., Pergamon Press, Oxford, 1970, pp. 479-487.

45. M. Ohmori and Y. Yoshinaga, J. Japan Inst. Metals, 30 (1966) 58-63.

46. B. J. Brindley and P. J. Worthington, "Yield Point Phenomena in Substitutional Alloys," Central Electricity Research Laboratory, Note No. RD/L/M 265, Feb., 1970.

47. P. R. Cetlin, unpublished data, Department of Metallurgical and Materials Engineering, University of Florida, Gainesville, Florida.

48. J. H. Hollomon, Trans. AIME, 162 (1945) 268-290.

49. R. E. Reed-Hill, "Plastic Deformation in Titanium and its Relation to Dynamic Recovery, Work Hardening and the Cottrell-Stokes Law," Second Technical Report to the Air Force Materials Laboratories, Wright-Patterson Air Force Base, October 10, 1969.

50. J. T. Michalak, Acta Met., 13 (1965) 213-222.

51. D. L. Davidson, U. S. Lindholm and L. M. Yeakley, Acta Met., 14 (1966) 703-710.

52. R. P. Carreker, Jr., and W. R. Hibbard, Jr., Acta Met., 1 (1953) 654-663.

53. H. C. Rogers, Trans. AIME, 218 (1960) 498.

54. N. R. Risebrough and E. Teghtsoonian, Canad. J. Phys., 45 (1967) 591-605.

55. R. E. Reed-Hill, "Tensile Properties of Alpha Zirconium," sent for publication to Review of High Temperature Materials, Freund Publishing House, Holon, Israel.

56. Z. S. Basinski, Phil. Mag., 4 (1959) 393-432.

57. G. F. Bolling, L. E. Hays and H. W. Wiedersich, Acta Met., 9 (1961) 622-624.

58. H. Conrad, Acta Met., 6 (1958) 339-350.

59. B. Ramaswami and G. B. Craig, Trans. Met. Soc. AIME, 239 (1967) 1226-1231.

60. R. L. Jones, F. W. Cooke and H. Conrad, The Franklin Institute Research Laboratories Technical Report SA-C1887-1 (July 1, 1966, to December 31, 1966), Wright Field Air Force Contract No. AF33(615)-3864.

61. R. L. Jones and H. Conrad, Trans. TMS-AIME, 245 (1969) 779-789.

62. F. R. N. Nabarro, Theory of Crystal Dislocations, Oxford Press, London, 1967, p. 431.

63. G. T. Hahn, C. N. Reid and A. Gilbert, Acta Met., 10 (1962) 747-749.

64. J. P. Hirth and J. Lothe, Theory of Dislocations, McGraw-Hill Book Co., New York, 1968, pp. 613-616.

65. J. Glen, J. Iron and Steel Inst., 186 (1957) 21-28.

66. J. D. Baird, Iron and Steel, 36 (1963) 450-466.

67. D. A. Woodford and R. M. Goldhoff, Mater. Sci. Eng., 5 (1969/70) 303-324.

68. C. F. Jenkins and G. V. Smith, TMS-AIME, 245 (1969) 2149-2156.

69. V. F. Sukhorava and R. P. Kharlova, Physics of Metals and Metallography, 10 [6] (1960) 143-146.

70. T. Boniszewski and G. C. Smith, Acta Met., 11 (1963) 165-178.

71. B. A. Wilcox and G. C. Smith, Acta Met., 12 (1964) 371-376.

72. A. H. Windle and G. C. Smith, Met. Sci. Jour., 2 (1968) 187-191.

73. A. H. Windle and G. C. Smith, Met. Sci, Jour., 4 (1970) 136-144.

74. J. W. Edington and R. E. Smallman, Acta Met., 12 (1964) 1313-1328.

75. A. H. Cottrell, Phil. Mag., 74 (1953) 829-832.

76. M. Hansen and K. Anderko, Constitution of Binary Alloys, McGraw-Hill, New York, 1958, pp. 383, 800, 990 and 1069.

77. R. J. Wasilewski and G. L. Kehl, Metallurgia, Manchr., 50 (1954) 225.

78. R. J. Wasilewski and G. L. Kehl, J. Inst. Met., 83 (1954-55) 94.

79. D. R. Miller and K. M. Browne, The Science, Technology and Application of Titanium, R. Jaffee and N. Promisel, eds., Pergamon Press, Oxford, 1970.

80. A. W. Sleeswick, Acta Met., 6 (1958) 598.

81. A. W. Sleeswick, Acta Met., 8 (1960) 130.

82. B. A. Wilcox and A. R. Rosenfield, Mater. Sci. Eng., 1 (1966) 201.

83. T. Yamane and J. Ueda, Trans. Japan Inst. Metals, 7 (1966) 91-95.

84. G. E. Dieter, Ductility, Am. Soc. Met., 1967, p. 1.

85. B. J. Brindley, Acta Met., 18 (1970) 325-329.

86. W. A. Backofen, I. R. Turner and D. H. Avery, Trans. ASM, 57 (1964) 980-990.

87. D. H. Avery and J. M. Stuart, Surfaces and Interfaces II, J. J. Burke et al., eds., Syracuse University Press, Syracuse, New York, 1968, pp. 371-392.

88. D. Lee and W. A. Backofen, Trans. AIME, 239 (1967) 1034-1040.

89. D. A. Woodford, Trans. ASM, 62 (1969) 291-293.

90. W. B. Morrison, Trans. AIME, 242 (1968) 2221-2227.

91. C. W. MacGregor, J. Franklin Inst., 238 (1944) 111-135.

92. R. E. Reed-Hill and W. A. Slippy, Jr., "Advanced Techniques for Material Investigation and Fabrication," Science of Advanced Materials and Process Engineering Proceedings, 1968, Vol. 14, p. 1-1-1.

93. J. C. M. Li, Canad. J. Phys., 45 (1967) 493-509.

BIOGRAPHICAL SKETCH

A. T. Santhanam was born May 5, 1943, in Tirupapuliyur, Tamil Nadu, India. He was graduated from St. Joseph's High School at Tirupapuliyur in 1957. In 1964, he received the degree of Bachelor of Technology with a major in Metallurgy from the Indian Institute of Technology, Madras. From July, 1964, to August, 1965, he was employed as a Senior Technical Assistant in the Department of Metallurgy at the Indian Institute of Technology, Madras. In September, 1965, he obtained the K. C. Mahindra Travel Scholarship and came to the United States for graduate studies. He received the degree of Master of Science with a major in Metallurgical Engineering from the University of Minnesota in September, 1967. From September, 1967, until the present time he has pursued his doctoral studies at the University of Florida. During this period he was supported by a contract from the United States Atomic Energy Commission.

A. T. Santhanam is married to the former Mohana Krishnamachar. He is a member of the American Institute of Mining, Metallurgical and Petroleum Engineers, American Society for Metals, Alpha Sigma Mu and Sigma Xi.

I certify that I have read this study and that in my opinion it conforms to acceptable standards of scholarly presentation and is fully adequate, in scope and quality, as a dissertation for the degree of Doctor of Philosophy.

R. E. Reed-Hill

R. E. Reed-Hill, Chairman
Professor of Metallurgical and Materials Engineering

I certify that I have read this study and that in my opinion it conforms to acceptable standards of scholarly presentation and is fully adequate, in scope and quality, as a dissertation for the degree of Doctor of Philosophy.

D. L. Baldwin for J. J. Hren

J. J. Hren
Associate Professor of Metallurgical and Materials Engineering

I certify that I have read this study and that in my opinion it conforms to acceptable standards of scholarly presentation and is fully adequate, in scope and quality, as a dissertation for the degree of Doctor of Philosophy.

C. S. Hartley

C. S. Hartley
Associate Professor of Engineering Science and Mechanics

I certify that I have read this study and that in my opinion it conforms to acceptable standards of scholarly presentation and is fully adequate, in scope and quality, as a dissertation for the degree of Doctor of Philosophy.

E. H. Hadlock

E. H. Hadlock
Professor of Mathematics

This dissertation was submitted to the Dean of the College of Engineering and to the Graduate Council, and was accepted as partial fulfillment of the requirements for the degree of Doctor of Philosophy.

August, 1971

Dean, College of Engineering

Dean, Graduate School